Targeting the 5' untranslated region of *SMN2* as a therapeutic strategy for spinal muscular atrophy

Audrey Marie Winkelsas

St John's College

University of Oxford

2020

A thesis submitted for the degree of DPhil in Biomedical Sciences

through the Nuffield Department of Medicine

in partnership with the

National Institutes of Health Oxford-Cambridge Scholars Program

under the supervision of

Dr. Kenneth Fischbeck

Neurogenetics Branch, National Institute of Neurological Disorders and Stroke,

National Institutes of Health, Bethesda, Maryland, United States of America

and

Professor Matthew Wood

Department of Paediatrics, University of Oxford, Oxford, United Kingdom

DECLARATION

Unless otherwise stated, all the work presented in this thesis is the work of the author. This work has not been submitted for any other degrees at any other University or educational institute.

TABLE OF CONTENTS

ABSTRACT

Nucleic acid therapeutics allow sequence-based targeting of disease genes, such as the genes involved in spinal muscular atrophy (SMA) pathogenesis. SMA is a neuromuscular disorder caused by mutations in the survival motor neuron 1 gene (*SMN1*). All patients have at least one copy of a paralog, *SMN2*, but a C-to-T transition in this gene results in exon 7 skipping in a majority of transcripts. As a result, only 10 to 20 percent of *SMN2* transcripts encode the fully functional SMN protein. Nusinersen, an FDA-approved therapeutic for SMA, is an antisense oligonucleotide (ASO) that promotes exon 7 inclusion in the *SMN2* transcript. The ceiling effect associated with splice-switching approaches makes complementary therapeutic strategies necessary. Increasing the total pool of *SMN2* transcripts and increasing the translational efficiency of these transcripts are strategies that can be used in combination with splice correction. I sought to determine whether the 5' untranslated region (5'UTR) of *SMN2* contains an element that reduces its expression that can be targeted as a means of increasing SMN levels. I found that ASOs targeting the 5' end of *SMN2* increase SMN mRNA and protein levels, and that this effect is due to ASO-mediated inhibition of *SMN2* mRNA decay. Moreover, using the 5'UTR ASO in combination with a splice-switching oligonucleotide (SSO) increases SMN levels above those attained with the SSO alone. I show that the effect of this 5'UTR ASO is human-specific. These results add to the current understanding of SMN regulation and point toward a new therapeutic target for SMA.

ACKNOWLEDGMENTS

First and foremost, I would like to express my deepest appreciation to my supervisors, Kenneth Fischbeck and Matthew Wood. I am fortunate to have been given this opportunity to spend the last four years in such inspiring research environments, and for their mentorship during my training. I am most grateful for their resolute confidence in me and for their unwavering support of my endeavors.

I would like to thank Christopher Grunseich for his sincere care about my personal and professional well-being. I would also like to thank Carlo Rinaldi and Suzan Hammond for their day-to-day mentorship while in Oxford.

I am grateful for other mentors, including Roy Parker, Markus Hafner, Gideon Dreyfuss, Vivian Cheung, and Kevin Talbot, for the time and insight they have shared in helpful discussions.

Thank you to the leadership of the National Institutes of Health Oxford-Cambridge Scholars Program (NIH OxCam), past and present, and to Randi Balletta and the International Biomedical Research Alliance for the many enriching experiences they have offered.

I would like to thank the following people for their assistance in this project: George Harmison, for many, many hours of cell culture and other research support; Katarzyna Chwalenia, for general laboratory assistance, including her assistance in handling mouse tissues and cell culture; Suzan Hammond, for sharing with me her expert knowledge of the SMA mouse model and for performing injections and tissue harvests; Kory Johnson, for processing the sequencing data; Corey Ruhno, for kindly sharing his custom reference genome with us; Sukrat Arya, for treating his motor neuron-like cells with our ASO; and

Yan Li, Director of the National Institute of Neurological Disorders and Stroke (NINDS) Protein/Peptide Sequencing Facility for running the mass spectrometry.

This work was supported by intramural research funds from NINDS, as well as funding from the Gwendolyn Strong Foundation and the Wellcome Trust.

As an NIH OxCam student, I am fortunate to have had many great lab mates and classmates. A special thanks goes to Naemeh Pourshafie who is a fantastic friend and who taught me to confidently and unashamedly pursue my goals. I also am indebted to Larissa Goli for reminding me to keep life balanced, and for the truly unforgettable experiences we shared. Thank you to many others who supported me scientifically and personally throughout this journey, especially Crystal Lee, Apurva Sarathy, Britt Hanson, Robert Guber, Jill Hakim, Yotam Blech-Hermoni, Veronique Bolduc, Loïc Roux, Nina Ahlskog, and Josh Bernstock. Thank you also to the students I have had the opportunity to interact with, including Vedika Rajasekaran and Clara D'Ambra.

Most importantly, I would like to thank my parents, Keely and Layne Winkelsas, and my brother, Bryan Winkelsas, for the sacrifices they have made in order for me to follow my dreams. My mother deserves the highest praise for being my "hands" at the bench, where she spent many late nights and tolerated my perpetual critiques. Without her support inside and outside of the lab, none of this would have been possible. Finally, I would like to dedicate this thesis to my grandmother, Vina Springer, who was an advocate for spinal muscular atrophy awareness and who was my biggest fan from the beginning.

LIST OF ABBREVIATIONS

2’F	2′-fluoro
2’MOE	2′-O-(2-methoxyethyl)
2’OMe	2′-O-methyl
3’UTR	3’ untranslated region
5’UTR	5’ untranslated region
Δ7	delta 7, exon 7-skipped
AAV	adeno-associated virus
ActD	actinomycin D
ANOVA	Analysis of variance
AS	Angelman syndrome
ASO	antisense oligonucleotide
AU-rich	Adenylate-uridylate-rich
BBB	blood-brain barrier
bp	base pair
Cas9	CRISPR associated protein 9
cDNA	complementary DNA
CNS	central nervous system
CRISPR	clustered regularly interspaced short palindromic repeats
CSF	cerebrospinal fluid
C_t	cycle threshold
Da	dalton
dCas9	deactivated Cas9
DMEM	Dulbecco’s Modified Eagle Medium
DNA	deoxyribonucleic acid

eGFP	enhanced green fluorescent protein
EU	5-ethynyl uridine
FBS	fetal bovine serum
FDA	US Food and Drug Administration
FL	full-length
FXS	Fragile X syndrome
GC content	guanine-cytosine content
GEO	Gene Expression Omnibus database repository
HDAC	histone deacetylase
HEK293T	Human embryonic kidney 293T
HRP	horseradish peroxidase enzyme
IGV	Integrative Genomics Viewer
iPSCs	induced pluripotent stem cells
ISS-N1	intronic splicing silencer N1
kb	kilobase
kDa	kilodalton
LNA	locked nucleic acid
lncRNA	long non-coding RNA
MEFs	mouse embryonic fibroblasts
mRNA	messenger RNA
NCALD	neurocalcin delta gene
NHLBI	National Heart, Lung, and Blood Institute
NIH OxCam	National Institutes of Health Oxford-Cambridge Scholars Program
NINDS	National Institute of Neurological Disorders and Stroke

nM	nanomolar
nt	nucleotide
NTC	non-targeting control
PAH	phenylalanine hydroxylase gene
PBS	phosphate-buffered saline
PCR	polymerase chain reaction
Phe	phenylalanine
PKU	Phenylketonuria
PLS3	plastin 3 gene
PMO	phosphorodiamidate morpholino oligomer
PND	post-natal day
poly(A)	polyadenylation
pORF	primary open reading frame
pPMO	PMO conjugated to a cell-penetrating peptide
PS	phosphorothioate
PTC	premature termination codon
PVDF	polyvinylidene fluoride or polyvinylidene difluoride
RACE	rapid amplification of cDNA ends
RIPA	radioimmunoprecipitation assay buffer
RISC	RNA-induced silencing complex
RNA	ribonucleic acid
RNA-seq	RNA-sequencing
RPE65	retinoid Isomerohydrolase
RT-PCR	reverse transcription polymerase chain reaction
RT-qPCR	quantitative reverse transcription polymerase chain reaction

scAAV9	self-complementary adeno-associated virus 9
SEM	standard error of the mean
shRNA	short hairpin RNA
siRNA	small interfering RNA
SMA	spinal muscular atrophy
SMN	survival motor neuron protein
SMN1	survival motor neuron 1 gene
SMN2	survival motor neuron 2 gene
SMN-AS1	*SMN* antisense strand
snRNP	small nuclear ribonucleoprotein
SSO	splice-switching oligonucleotide
T_a	annealing temperature
TBST	Tris-buffered saline and 0.1% Tween
TPM	Transcripts Per Kilobase Million
UBE3A-ATS	*UBE3A* antisense transcript
uORF	upstream open reading frame
U snRNA	uridine-rich, small nuclear RNA
UTR	untranslated region
WHO	World Health Organization

LIST OF FIGURES

CHAPTER 1

CHAPTER 2

CHAPTER 3

SUPPLEMENTARY MATERIAL

LIST OF TABLES

Chapter 1

INTRODUCTION

1.1 CLINICAL MANIFESTATIONS OF SPINAL MUSCULAR ATROPHY

Spinal muscular atrophy (SMA) is an autosomal recessive neuromuscular disorder caused by the degeneration of alpha motor neurons in the anterior horn of the spinal cord. Denervation results in symmetrical muscle weakness, often within weeks or months of birth. With an incidence of approximately 1 in 10,000 live births, there are 4 types of SMA into which patients are classified based on age of disease onset and motor milestones reached (Markowitz et al. 2012). The pattern of muscle weakness is the same in all 4 types: greater in proximal muscles than in distal muscles, and more prominent in the legs than in the arms (Crawford and Pardo 1996).

SMA type 1 (also known as Werdnig-Hoffmann disease in recognition of the two neurologists who first described SMA at the end of the nineteenth century) accounts for approximately 60 percent of cases (Werdnig 1891). Comprising the most severely affected individuals, patients with SMA type 1 are symptomatic by 6 months of age (often sooner) and never attain the ability to sit without support (Munsat and Davies 1992; Thomas and Dubowitz 1994; Wang et al. 2007). Historically, infants diagnosed with SMA type 1 rarely survived beyond their second birthday. In SMA type 2, age of onset is between 7 and 18 months and, by definition, patients in this group reach the motor milestone of maintaining a sitting position independently but are never able to walk. Those with SMA type 3 have disease onset in childhood and attain the ability to walk, even if at present they are non-ambulatory. At the mildest end of the clinical spectrum are those patients with adult onset, or type 4, SMA. Some patients fall at the margins and do not fit clearly into one particular category of this stratification system (Table 1).

Other clinical features include weakness of bulbar and intercostal muscles, which often lead to respiratory complications for patients with SMA types 1 and 2. Scoliosis and contractures are prevalent in SMA types 1 and 2, and, to a lesser degree, SMA type 3. Close monitoring and proactive management of these and other symptoms according to published standards of care for SMA can increase survival and improve quality of life (Wang et al. 2007; Finkel et al. 2018; Mercuri et al. 2018).

Compared to other neurodegenerative diseases, SMA follows a unique clinical course (Crawford and Pardo 1996). After a period of normal development, there is a steep decline in muscle power at disease onset. This is then followed by long plateau periods with no or minimal additional loss of strength (Russman et al. 1992). Of note, while disease progression is slow, in almost no instance in the natural history of SMA is there an increase in motor function score after disease onset, even in the presence of respiratory and nutritional support (De Sanctis et al. 2016). It was not until the advent of gene-based therapeutics, to be discussed later in this chapter, that improvements in the SMA phenotype emerged.

Table 1.1 SMA clinical classifications and phenotypes

SMA type	Age of onset	Highest motor milestone	Natural history
Type I	0-6 months	Never sits without support	Severe weakness and hypotonia; weak cry and cough; swallowing and feeding difficulties; tongue fasciculations; intercostal muscle weakness combined with relative sparing of diaphragm leads to paradoxical breathing and chest wall collapse; survival < 2 years without nutritional and respiratory intervention
Type II	7-18 months	Sits without support	Diaphragmatic breathing; difficulty with coughing and secretion clearance; bulbar weakness and swallowing difficulties in some patients; fine tremors in fingers/hands; kyphoscoliosis and joint contractures develop
Type III	> 18 months, < 21 years	Walks unaided	May lose ability to walk in childhood, adolescence, or adulthood; scoliosis develops in some patients; bulbar and respiratory problems are less common than in above types; muscle aching is common
Type IV	> 21 years	Walks unaided	Mild motor impairment; respiratory and gastrointestinal problems absent

1.2 GENETICS OF SPINAL MUSCULAR ATROPHY

Early in the hunt for the genetic basis of SMA, it was unclear if the clinical heterogeneity between patients may be due to mutations in different genes. However, an argument in favor of SMA being a monogenic disease is that this striking variation in severity can be seen even between siblings, as described by Dubowitz a couple of decades earlier (Dubowitz 1964). In 1990, a series of studies were published that used linkage analysis to map the SMA locus to chromosome 5q (Brzustowicz et al. 1990; Melki et al. 1990). A follow-up paper concluded that “acute SMA” (type 1) and “chronic SMA” (types 2 and 3) are caused by defects at the same chromosomal position (Gilliam et al. 1990). Further mapping of the disease gene was hindered by the complexity of chromosome 5q13, which was found to contain repeated sequences, deletions, and rearrangements (Francis et al. 1993; Kleyn et al. 1993; Melki et al. 1994).

In a landmark paper published in 1995, Judith Melki’s group reported the identification of the SMA-determining gene (Lefebvre et al. 1995). This paper described a 20 kb gene that produces a 1.7 kb transcript and encodes a 294 amino acid protein. They aptly named this the survival motor neuron (*SMN*) gene, since its loss of function leads to the death of alpha motor neurons in SMA. 93 percent of SMA patient samples tested showed deletions of *SMN* exons 7 and 8 on both chromosomes. Nearly 6 percent of the remaining patients were missing exon 7 on both chromosomes but retained exon 8. Two of the three patients who were not homozygous for large-scale deletions involving *SMN* had intronic mutations in splice sites, and the third patient had a missense mutation. Other mutations were soon thereafter identified in SMA patients heterozygous for the exon 7 deletion and novel mutations that cause loss of SMN function are still

identified (Parsons et al. 1998; Xu et al. 2020). These cases continue to account for only about 5 percent of SMA diagnoses.

As noted, it was evident from early mapping studies that the region on chromosome 5q containing the SMA locus is unstable and prone to deletions, duplications, and rearrangements. The *SMN* gene is part of a 500 kb inverted duplication event (Lefebvre et al. 1995). The two *SMN* genes, designated the telomeric and centromeric copies (and later named *SMN1* and *SMN2*, respectively), differ by 5 nucleotides which allow for the genes to be distinguished molecularly. It is deletions and mutations involving the telomeric gene (*SMN1*) that cause SMA. In rare instances, there is gene conversion in which *SMN1* sequence is fused to *SMN2* sequence (Van Der Steege et al. 1996). These chimeric genes may explain the approximately 6 percent of patients who are missing *SMN1* exon 7 but retain exon 8.

Of the 5 nonpolymorphic nucleotide differences between *SMN1* and *SMN2*, only one is functionally relevant. The C-to-T transition in exon 7 is a silent mutation that does not change the encoded amino acid sequence but does result in alternative splicing by disrupting an exonic splicing enhancer (Lorson et al. 1999; Monani et al. 1999; Cartegni et al. 2006). As a result, only 10 to 20 percent of the mRNA produced by *SMN2* contains exon 7 and encodes the full-length SMN protein. There is no difference in stability between the *SMN* transcripts with and without exon 7 (Heier et al. 2007). However, the protein encoded by the exon 7 skipped transcript, known as SMNΔ7, is unstable and has reduced ability to self-oligomerize as compared to the full-length protein (Lorson et al. 1998; Burnett et al. 2009).

All individuals with SMA have at least one copy of the centromeric (*SMN2*) gene, each copy producing low levels of SMN protein (Figure 1.1). This is because a complete absence of SMN protein results in embryonic lethality. *SMN2* copy number is a genetic modifier of SMA phenotype, with an inverse correlation between copy number and disease severity (Parsons et al. 1998; Stabley et al. 2015). Greater than 80 percent of patients diagnosed with SMA type 1 based upon clinical presentation have 1 or 2 copies of *SMN2* (Feldkötter et al. 2002; Mailman et al. 2002; Calucho et al. 2018). Individuals with SMA type 2 most often have 3 copies of *SMN2* and those with SMA type 3 usually have 3 or 4 copies of *SMN2*. Five copies of *SMN2* is protective and can prevent disease manifestation in some instances (Prior et al. 2004; Wirth et al. 2006).

While higher *SMN2* copy numbers are associated with a milder disease course, it should be emphasized that the genotype-phenotype correlation is not absolute. In the studies referenced above, some individuals with 3 copies of *SMN2* have an age of onset and motor function consistent with SMA type 1, while other individuals with 3 copies of *SMN2* have symptoms characteristic of SMA types 2 or 3. Rarely, even patients presenting with SMA type 3 are found to have only 2 copies of *SMN2* (Calucho et al. 2018). Several other genetic modifiers have been identified. Two proposed modifiers, *PLS3* and *NCALD*, are involved in endocytosis regulation, but the protective effects of their altered expression remain controversial (Hosseinibarkooie et al. 2016; Riessland et al. 2017). Several sequence variants in *SMN2* have been described to modify the phenotype, demonstrating that not all *SMN2* genes are functionally equivalent (Prior et al. 2009; Wu et al. 2017; Ruhno et al. 2019). In summary, *SMN2* copy

number is only modestly predictive of disease severity. It is nonetheless useful for stratifying patients in clinical trials.

The association between *SMN2* copy number and disease severity relates to SMN dosage. In theory, since each *SMN2* gene produces small amounts of SMN, a higher number of *SMN2* genes means cells have a better ability to compensate for loss of *SMN1*. Indeed, levels of full-length *SMN2* transcripts are significantly higher in individuals with SMA type 3 than type 2, and higher in SMA type 2 than type 1 (Crawford et al. 2012). Interestingly, levels of full-length *SMN2* transcripts do not correlate to *SMN2* copy number, suggesting that differences in *SMN2* transcription, splicing, stability, or other RNA processing events may account for the inability to definitively predict SMA type from copy number (Harada et al. 2002; Crawford et al. 2012).

Taken together, these findings indicate that methods of increasing expression of the *SMN2* gene are therapeutic strategies for SMA.

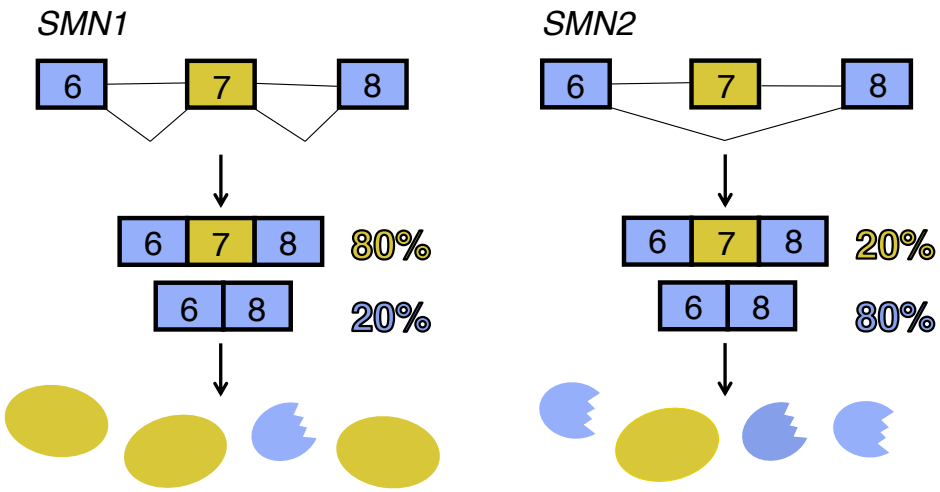

Figure 1.1 *SMN2* is less efficient than *SMN1* at producing the SMN protein. A C-to-T transition in exon 7 results in the skipping of this exon in 80% of *SMN2* transcripts. Yellow ovals represent the full-length protein (encoded by transcripts with exon 7). Blue, truncated ovals represent the Δ7 protein (encoded by transcripts without exon 7). SMA is caused by homozygous mutation of the *SMN1* gene but retention of the *SMN2* gene.

1.3 SMN PROTEIN FUNCTION

The SMA-determining gene, *SMN1*, encodes the ubiquitously expressed survival motor neuron protein (SMN) (Figure 1.2). The best characterized function of SMN is in small nuclear ribonucleoprotein (snRNP) assembly. Splicing plays a critical role in the regulation of gene expression. The spliceosome, which is responsible for the removal of intronic sequence from pre-mRNA, is made up of snRNPs. snRNPs are themselves composed of seven Sm proteins arranged in a ring around a short, uridine-rich, small nuclear RNA (U snRNA). The SMN protein, in association with Gemins 2-8 and Unr-interacting protein (unrip), directly binds and facilitates the interaction between these protein and RNA components of spliceosomal snRNPs (Kolb et al. 2007). When SMN is immunodepleted from cell extracts, Sm cores do not assemble on U snRNAs (Pellizzoni et al. 2002). Likewise, SMA patient cells, which are SMN-deficient, have reduced snRNP assembly capacity (Wan et al. 2005). In addition to facilitating efficient assembly, the SMN complex ensures that Sm cores only assemble on appropriate RNA targets and prevents their binding to other cellular RNA species, such as ribosomal RNAs (Pellizzoni et al. 2002). Impaired spliceosome biogenesis is likely the cause of the RNA splicing defects observed in a subset of genes in SMA (Zhang et al. 2008; Jangi et al. 2017). It is possible that mis-splicing events for (a) particular gene(s) involved in motor neuron health contribute to the selective vulnerability of this cell type to SMN-deficiency (Lotti et al. 2012; Sleigh et al. 2014).

The spliceosome biogenesis orchestrated by SMN occurs in the cytoplasm and nucleus. It has been shown that SMN also localizes to neuronal processes and growth cones (Zhang et al. 2003). Compared to control motor neurons,

SMN-deficient motor neurons have significantly lower levels of poly(A) mRNA in axons (Fallini et al. 2016). These two findings support the hypothesis that SMN plays a role in the axonal transport of mRNA. SMN, through interactions with RNA-binding proteins like HuD, IMP1, hnRNP Q, and hnRNP R, may be responsible for the assembly of mRNA transport complexes in neurons (Rossoll et al. 2003; Akten et al. 2011; Fallini et al. 2016). Indeed, RNA immunoprecipitation of SMN in mouse motor neuron-like cells reveals that SMN-containing complexes bind to mRNA, a subset of which are known to localize to axons (Rage et al. 2013). Several transcripts which are bound by SMN, including *β-actin*, *GAP43,* and *Anxa2*, do not translocate into the distal part of axons or growth cones in SMN-deficient motor neurons. As a result, β-actin and GAP43 protein do not accumulate in growth cones of these cells (Rossoll et al. 2003; Fallini et al. 2016). This is a developing area of research, but data to date suggest that SMN is necessary for the proper axonal localization of select mRNAs and, subsequently, their local translation. This function, uniquely applicable to neurons, may at least partially explain the cell-type specific vulnerability in SMA.

There is evidence for the involvement of SMN in a number of other cellular processes, as highlighted in Figure 1.3.

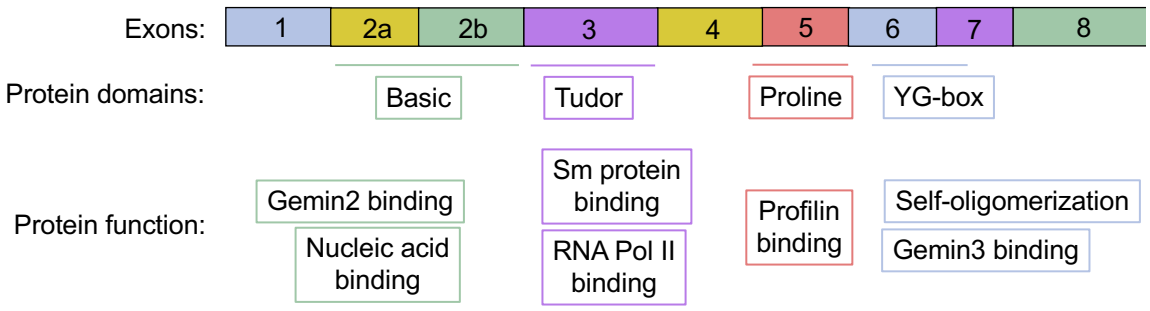

Figure 1.2 SMN domains and function. Figure adapted from (Singh et al. 2017). The SMN Tudor domain is involved in binding to Sm proteins and to the C-terminal domain of RNA polymerase II. The YG-box is involved in SMN self-oligomerization and binding to Gemin3.

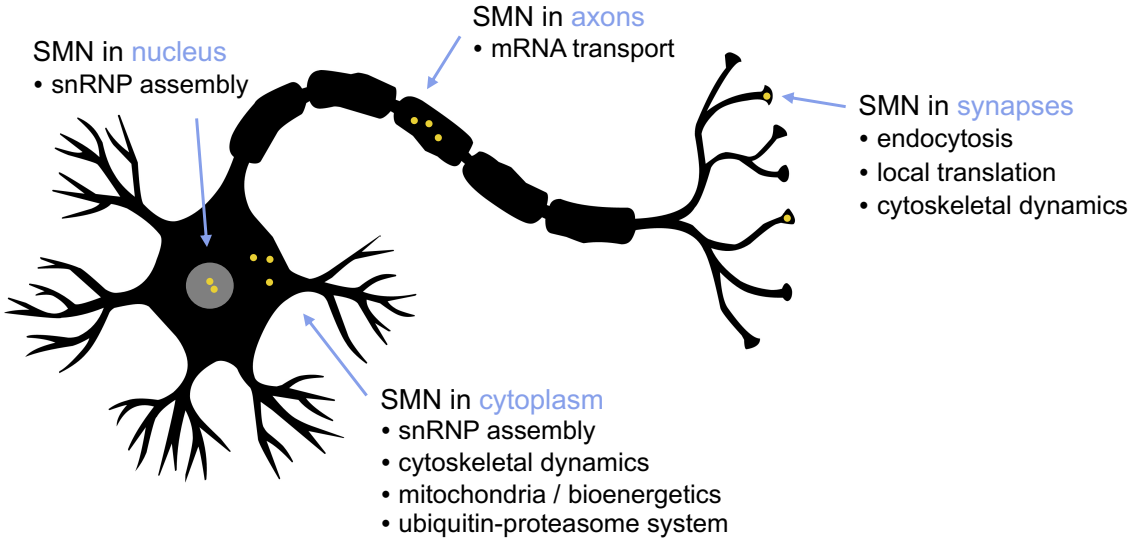

Figure 1.3 SMN is involved in many cellular processes and localizes in both the nucleus and cytoplasm. Figure adapted from (Bowerman et al. 2017).

1.4 NUCLEIC ACID THERAPEUTICS FOR NEUROLOGICAL DISEASE

Nucleic acid therapeutics can be used to increase the expression and function of disease genes, like *SMN2*, or to decrease the expression of toxic gene products. There are now more than 6500 hereditary diseases with known genetic cause (https://omim.org/), and many of them are amenable to this approach to treatment. To put our work in the broader context, we discuss the uses and limitations of four major classes of nucleic acid therapeutics (antisense oligonucleotides, small interfering RNAs, gene-replacement therapies, and gene editing) and highlight their applications in neurological disorders (Figure 1.4).

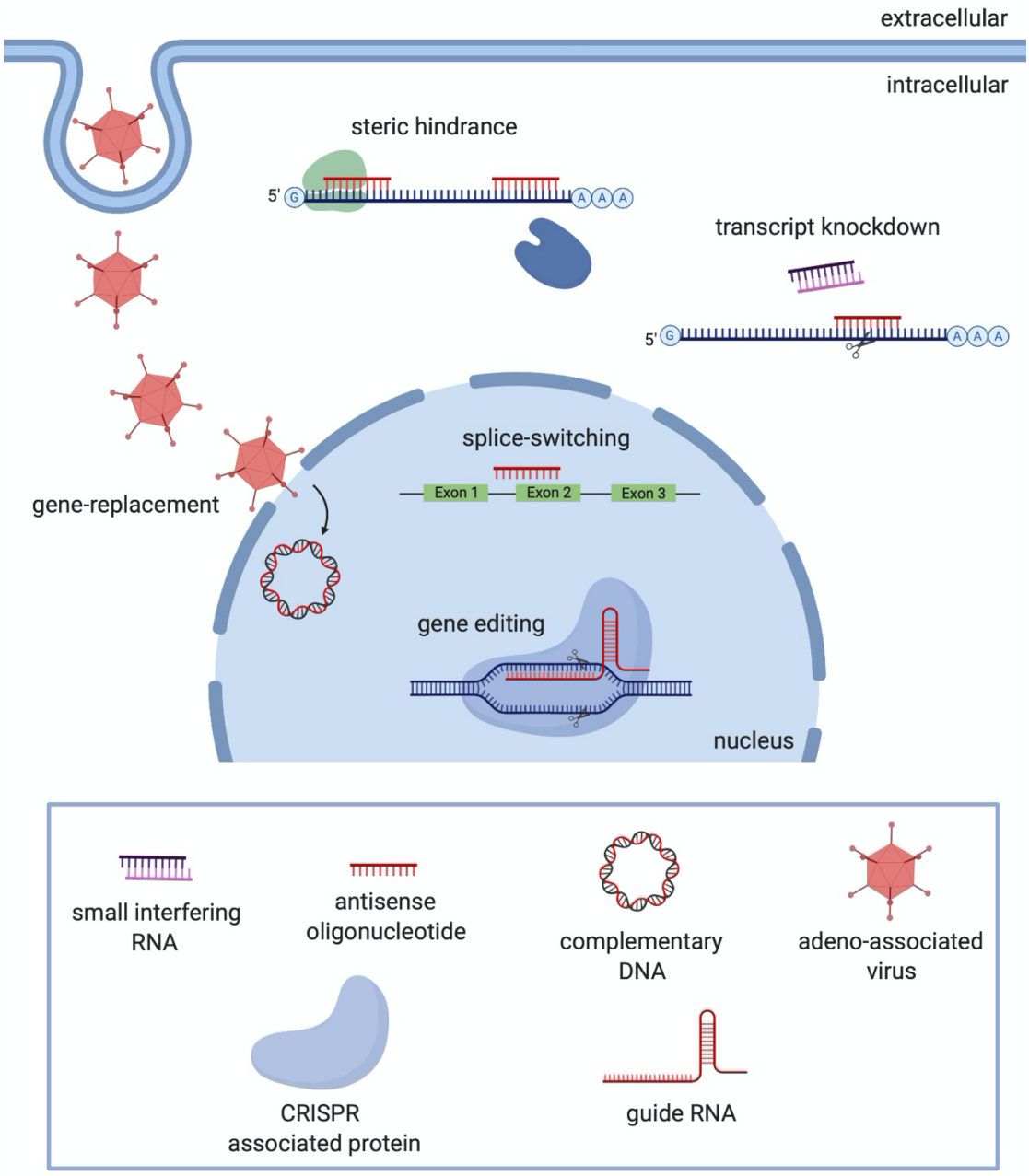

Figure 1.4 Nucleic acid therapeutics for the treatment of neurological disease.

1.4.1 ANTISENSE OLIGONUCLEOTIDES AND SMALL INTERFERING RNA

An antisense oligonucleotide (ASO) is a synthetic nucleic acid strand designed to hybridize to an RNA target via Watson-Crick base pairing and to modulate gene expression. After binding to the RNA, an ASO can act through one of two major mechanisms: sterically blocking the binding of *trans*-acting factors (e.g., RNA-binding proteins and non-coding RNAs) or promoting the endonucleolytic cleavage of the target. The mechanism of action is determined by factors such as the site on the transcript to which the ASO is directed and the chemical nature of the ASO's backbone and sugar moieties. Thus, ASOs can be used for a variety of purposes, such as altering the splicing of pre-mRNA, promoting the use of alternative polyadenylation signals, inhibiting translation initiation, degrading mRNA, and disrupting RNA structure (Bennett et al. 2019). This list is not exhaustive, and the number of tractable targets in the transcriptome is continually expanding as our knowledge of ASO mechanisms grows, as ASO technology advances, and as novel applications are reported.

To develop therapeutic agents, a variety of chemical modifications are available to improve ASO binding affinity, stability, cellular uptake, and biodistribution (Shen and Corey 2018). For example, phosphorothioate linkage, the most widely used linkage modification, increases ASO resistance to nucleases and improves ASO bioavailability and cellular uptake (Eckstein 2014). On the ribose moiety, substituting a 2′-O-methyl (2'OMe), 2′-O-methoxyethyl (2'MOE), or 2′-fluoro (2'F) group for the 2'-hydroxyl group also increases nuclease resistance as well as the affinity of binding between the ASO and its target RNA. Locked nucleic acids (LNAs) have even higher binding affinity, allowing efficacy when the ASO is as short as 12-nt in length and creating lower

tolerance for mismatches (Straarup et al. 2010). Oftentimes, two ASOs that have the same nucleotide sequence but different chemical modifications have different efficacy and toxicity (Duygu et al. 2019; Shen et al. 2019; Sheng et al. 2020). Optimization of sequence and backbone chemistry is best determined empirically. Taken together, different combinations of sequence and backbone modifications can be evaluated when designing ASOs for new targets in order to maximize potency, reduce toxicity, and ultimately increase chances of clinical success.

In most cases, ASOs to be used in the treatment of neurological disorders will need to reach their RNA targets in the central nervous system (CNS). Clinically, this requires direct administration into the CNS (as opposed to systemic delivery) since ASOs are not sufficiently blood-brain barrier (BBB) penetrant. ASOs in saline injected intrathecally can be seen inside lumbar spinal cord motor neurons as early as 30 minutes post-injection, and are diffusely distributed in CNS parenchyma by 24 hours post-injection (Mazur et al. 2019). Although only about 20% of injected ASO is delivered to brain tissue due to cerebrospinal fluid (CSF) turnover, the molecular activity may persist for several weeks to several months (Bennett et al. 2019). In the case of nusinersen, an ASO for the treatment of spinal muscular atrophy (SMA), the long term pharmacodynamic effect led to a dosing schedule with maintenance doses every four months (Finkel et al. 2017). Alternative delivery methods that allow CNS uptake following systemic administration are an important area of research. Peptide-conjugated ASOs, antibody-conjugated ASOs, extracellular vesicles, and nanomaterial-based drug delivery systems for crossing the BBB are under investigation (Hammond et al. 2016; Yang et al. 2017; Furtado et al. 2018).

Machine learning has the potential to expedite this process, and has already been demonstrated to aid in the identification of effective cell-penetrating peptides and to predict toxicity (Hagedorn et al. 2013; Wolfe et al. 2018).

1.4.2 A CASE OF TRANSCRIPT KNOCKDOWN: ANGELMAN SYNDROME

Angelman syndrome (AS) is a neurodevelopmental disorder characterized clinically by seizures, minimal expressive speech, mild microcephaly, ataxia, hypotonia, and motor delay (Buiting et al. 2016). It is caused by a deficiency of ubiquitin-protein ligase E3A (encoded by *UBE3A*) in neurons. Although *UBE3A* is biallelically expressed in non-neuronal cell types, the paternal allele is silenced by a long non-coding RNA in neurons, causing them to rely exclusively on *UBE3A* transcribed from the maternal allele. When the maternally inherited *UBE3A* is nonfunctional due to mutations or epigenetic defects, Angelman syndrome occurs.

One strategy to increase levels of the E3 ubiquitin ligase in neurons is knocking down the long non-coding RNA, referred to as the *UBE3A* antisense transcript (*UBE3A-ATS*), that represses the *UBE3A* paternal allele. Indeed, an ASO developed by Meng et al. is able to knock down *UBE3A-ATS* and, as a result, increases levels of ubiquitin-protein ligase E3A *in vitro* and *in vivo* (Meng et al. 2015). The ASO used in this study consisted of ten 2'- deoxynucleotides flanked by five 2'MOE modified nucleotides on each end. This ASO composition, commonly referred to as a 'gapmer' because it contains a central DNA 'gap', promotes RNase H-mediated degradation of the *UBE3A-ATS*. Although there was significant *UBE3A* induction in an Angelman syndrome mouse model, only partial phenotypic correction was achieved (Meng et al. 2015). This finding may

indicate, among other possibilities, that earlier treatment is required for complete rescue. The therapeutic “window of opportunity” is an important consideration in study.

A Phase 1/2, open-label, non-randomized, dose-escalating study was recently initiated (NCT04259281, ClinicalTrials.gov) for ASO-mediated knockdown of *UBE3A-ATS* in children with AS. Safety and pharmacokinetics will be monitored after four intrathecal injections (given every 4 weeks).

An alternative to ASO-mediated transcript knockdown is gene silencing with double-stranded, small interfering RNAs (siRNAs). During siRNA-mediated knockdown, one strand of the siRNA is loaded into the cellular RNA-induced silencing complex (RISC), and, through complementary base-pairing, this assembly recognizes and cleaves target mRNAs. Many of the same chemical modifications used to increase the potency and stability of ASOs can be introduced into synthetic siRNAs. The auxiliary challenge with siRNAs is that being double-stranded impedes their cellular uptake, and the phosphorothioate modification, known to improve oligonucleotide uptake, can limit siRNA efficacy (Lima et al. 2012; Alterman et al. 2019). At this time, siRNAs are very effective at targeting mRNAs in the liver, but overcoming delivery challenges associated with other organ systems is an active area of research (Wittrup and Lieberman 2015). The first FDA-approved siRNA, patisiran, is a liver-directed siRNA developed by Alnylam for the treatment of hereditary transthyretin-mediated amyloidosis (Adams et al. 2018). Other design strategies are emerging, such as single-stranded siRNAs, ligand-conjugated siRNAs, and divalent siRNAs, which greatly enhance cellular uptake and hold promise for applying siRNAs to the treatment of CNS diseases (Lima et al. 2012; Alterman et al. 2019; Setten et al. 2019).

1.4.3 GENE-REPLACEMENT THERAPY AND GENE EDITING

The development of adeno-associated virus (AAV) vectors has led to leveraging these viruses as vehicles for the delivery of human transgenes. DNA sequences of up to about 5 kb (including the transgene and its regulatory elements) can be packaged into AAV capsids (Wang et al. 2019). The capsid proteins determine which cell types the viruses infect and release their circularized DNA contents which remain episomal. Safe and effective gene replacement has recently been achieved with AAV vectors for RPE65-associated retinal dystrophy and SMA (Mendell et al. 2017; Russell et al. 2017) and these treatments now have regulatory approval. This approach, which offers the advantage of lasting benefit with a single administration, is now being pursued for a number of other hereditary neurologic disorders caused by mutations that cause loss of gene function.

1.4.4 A CASE OF GENE THERAPY: PHENYLKETONURIA

Phenylketonuria (PKU) is a metabolic disorder most often due to mutations in the phenylalanine hydroxylase gene (*PAH*), which encodes an enzyme that converts phenylalanine (Phe) to tyrosine. As a result, phenylalanine accumulates in the brain, which leads to intellectual disability and seizures. Currently, a low Phe diet is the standard of care, although adherence to the highly restrictive diet may be challenging. Although unmanaged PKU results in neurological problems, the target organ for treatment is the liver, where Phe is metabolized. Several studies have found that delivering *PAH* to the liver in mice, using either AAV or nonviral DNA vectors, is a viable treatment option.

A Phase 1/2, open-label, randomized controlled clinical trial has recently begun (NCT03952156, ClinicalTrials.gov). This dose-escalation study evaluates the safety and pharmacodynamic efficacy of *PAH* gene transfer in adults with PKU, as determined by treatment-related adverse events and by plasma Phe levels, respectively. The gene is delivered with AAVHSC15 which, like other AAV vectors including AAV9, is known to have extensive transduction in the liver as well as the CNS following intravenous administration (Ellsworth et al. 2019). This particular treatment strategy is problematic for children with PKU because as their liver grows, plasma Phe levels may again rise due to episomal dilution (Grisch-Chan et al. 2019). Also, it is unclear how well *PAH* expression will persist in the setting of hepatocyte proliferation induced by liver injury in adults. Neutralizing antibodies from AAV treatment may preclude re-dosing, and require switching to a different AAV if a second administration is needed. A permanent effect may require genomic integration of the delivered *PAH* DNA or of DNA base editors to correct the underlying mutation (Villiger et al. 2018; Richards et al. 2020).

Gene-replacement therapy is more challenging for large disease genes due to limitations in the packaging capacity of viral vectors, although there are strategies to overcome this such as using a dual vector approach or packaging truncated transgenes that encode only certain domains of the protein of interest (Duan 2018). Furthermore, while the non-integrating nature of AAV-mediated gene-replacement therapy is advantageous in terms of genotoxicity, its lack of permanency in dividing cells may limit its use.

Some of the limitations of gene-replacement therapy may be overcome by using AAV instead to deliver gene editing components. Gene editing uses

nucleases (e.g., zinc-finger nucleases or CRISPR/Cas9) and guide RNAs to induce DNA double strand breaks at specific genomic loci. Cells repair these breaks via endogenous non-homologous end joining or homology-directed repair pathways, and in so doing disrupt expression of the target gene or precisely change the DNA sequence. Preliminary work shows that it is possible to delete an entire chromosome using CRISPR, such as chromosome 21 in cells from individuals with Down syndrome (Zuo et al. 2017).

Recruitment is underway for a number of clinical trials implementing CRISPR technologies, primarily for *ex vivo* uses such as the infusion of edited hematopoietic stem and progenitor cells (HSPCs) for sickle cell disease or the infusion of edited chimeric antigen receptor (CAR) T cells for certain cancers (Li et al. 2020). *In vivo* delivery of CRISPR machinery in humans is now being evaluated in Leber congenital amaurosis (NCT03872479, ClinicalTrials.gov). In the case of SMA, preliminary evidence shows that CRISPR can be used to edit the *SMN2* C-to-T transition in exon 7 as a way to increase SMN protein levels (Zhou et al. 2018).

1.4.5 A CASE OF GENE EDITING: FRAGILE X SYNDROME

Fragile X syndrome (FXS) is the most common cause of inherited intellectual disability (Ramírez-Cheyne et al. 2019). Often, FXS has features of autism spectrum disorder. Caused by a trinucleotide repeat expansion in the 5'UTR of *FMR1*, FXS results from CGG repeat lengths over 200; 55-200 copies of the CGG repeat is associated with later onset fragile X ataxia-tremor syndrome (FXTAS) (Salcedo-Arellano et al. 2020). The CGG repeat expansion induces transcriptional silencing of *FMR1*, which can be partially ameliorated with a DNA

demethylating agent, 5-azacytidine (Chiurazzi et al. 1998; Coffee et al. 1999). Due to toxicity associated with 5-azacytidine, a more precise therapeutic approach with activity restricted to the *FMR1* locus is desired for safe clinical use in FXS.

The CRISPR system, using RNA-guided nucleases, offers the potential for genetic and epigenetic modification of *FMR1* with increased sequence-based specificity. One approach is to remove the pathogenic CGG repeats altogether. Indeed, excision of the *FMR1* CGG expansion by CRISPR/Cas9-mediated genome editing can significantly decrease promoter methylation and reactivate *FMR1* transcription (Park et al. 2015; Xie et al. 2016). An alternative strategy is to induce *FMR1* expression while leaving the mutated gene intact. This can be achieved via a catalytically deactivated Cas9 (dCas9) that does not induce DNA double strand breaks and instead enables epigenetic modifications. For example, Liu et al. fused the cytosine demethylation protein TET1 to dCas9. This fusion protein, when led by CGG repeat-targeting guide RNAs, directs TET1 to reverse hypermethylation at the *FMR1* locus and leads to increased FMRP levels in edited neurons *in vitro* and in those neurons transplanted into mouse brain (Liu et al. 2018). Similarly, a dCas9-VP16 transactivator fusion protein can increase *FMR1* mRNA levels in FXS cells (Haenfler et al. 2018).

These and other nucleic acid therapeutic strategies, including direct mRNA delivery (Uchida et al. 2020), can be considered for the treatment of many other diseases. The particular subset of strategies relevant for a given disease is determined by the nature of the mutation, such as whether it causes a loss of gene function, a gain of gene function, is in a haploinsufficient gene, etc. (Figure

1.5). Other considerations for drug development include unmet need, rationale, risk-benefit ratio, biomarkers, clinical trial readiness.

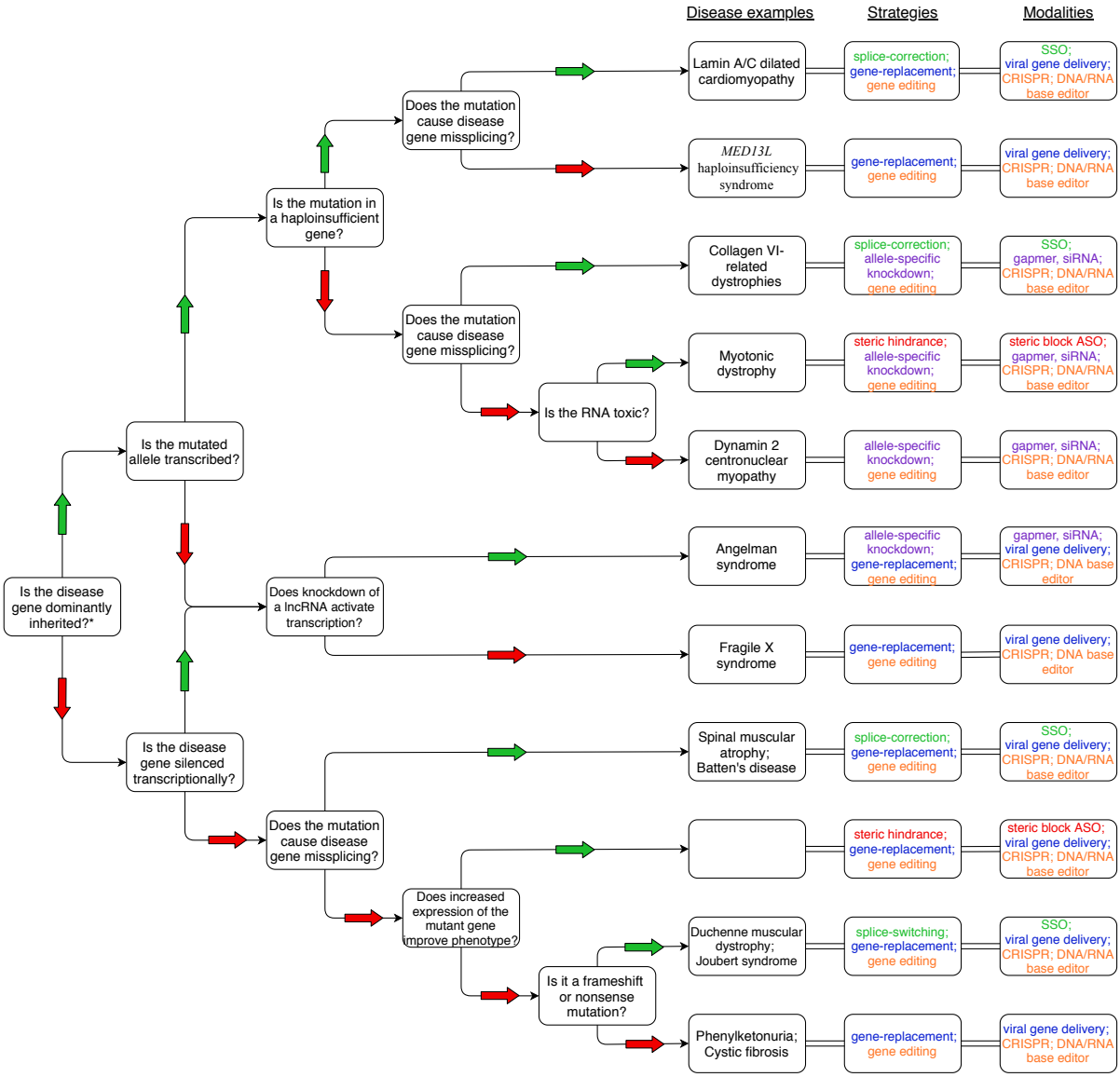

Figure 1.5 Stepwise approach to identifying nucleic acid therapeutic strategies to consider for commonly encountered mutations. Starting on the left, if the answer to the question is yes, follow the green arrow; if no, follow the red arrow. * = treat a Y-linked mutation as dominant for the purpose of this algorithm. lncRNA = long non-coding RNA. SSO = splice-switching oligonucleotide. Disease examples are provided for each path: lamin A/C dilated cardiomyopathy (Ito et al. 2017), *MED13L* haploinsufficiency syndrome (Cafiero et al. 2015), collagen VI–related dystrophies (Bolduc et al. 2014; Bolduc et al. 2019), myotonic dystrophy (Gao and Cooper 2013), dynamin 2 centronuclear myopathy, Angelman syndrome (Meng et al. 2015), Fragile X syndrome (Park et al. 2015; Xie et al. 2016), spinal muscular atrophy (Finkel et al. 2017), Batten's disease (Kim et al. 2019), Duchenne muscular dystrophy (Echevarría et al. 2018), Joubert syndrome (Ramsbottom et al. 2018), phenylketonuria (Grisch-Chan et al. 2019).

1.5 THERAPEUTICS FOR SMN RESTORATION

An FDA-approved therapeutic for SMA, nusinersen, is an ASO that increases the proportion of *SMN2* transcripts containing exon 7 (Finkel et al. 2017). As discussed above, the C-to-T transition in *SMN2* exon 7 disrupts the SF2/ASF binding motif, hereby nullifying its exonic splicing enhancer activity and causing exon skipping (Cartegni et al. 2006). Nusinersen sterically blocks the binding of hnRNP A1/A2 to a nearby intronic splicing silencer, which shifts the alternative splicing back toward exon 7 inclusion (Hua et al. 2008). In limited human autopsy data, nusinersen increases *SMN2* exon 7 inclusion by about 2.7-fold in the thoracic spinal cord (Finkel et al. 2016). In patients, this translates to increased motor function scores in at least half of trial participants (compared to zero percent in the sham control group) and reduced incidence of death or permanent ventilation (Finkel et al. 2016; Finkel et al. 2017). With intrathecal maintenance doses every 4 months, a majority of children experience clinically meaningful improvements in motor function over at least 3 years of treatment (Darras et al. 2019).

A second splice modifier, risdiplam, is a small molecule which has the advantage of being orally bioavailable (Ratni et al. 2018). The small molecule's central ring binds to an unpaired adenine in the 5' splice site of *SMN2* exon 7 and the small molecule's positively charged piperazine group forms an electrostatic interaction with the U1 snRNA (Campagne et al. 2019). Thus, the small molecule promotes exon 7 inclusion by facilitating the interaction between the 5' splice site and the U1 snRNA, and it does so with minimal off target effects.

Another FDA-approved therapeutic for SMA involves systemic delivery of a copy of *SMN1* cDNA with a self-complementary adeno-associated virus 9

(scAAV9-SMN, “AVXS-101”). Most infants in the study who were diagnosed with SMA type 1 and subsequently treated with scAAV9-SMN attained independent sitting (i.e., met the criteria for SMA type 2), and 2 out of 12 stood and walked independently (i.e., met the criteria for SMA type 3) (Mendell et al. 2017). In mice, delivery directly into the CSF can achieve the same degree of phenotypic correction as systemic administration but with a dose that is 10 times smaller (Meyer et al. 2015). This is advantageous since the dose required for systemic administration causes liver toxicity in some patients. Additionally, intrathecal delivery may allow for the treatment of those with neutralizing antibodies and older individuals, as well as reduce production (and thus treatment) costs. A clinical trial was initiated to assess intrathecally delivered scAAV9-SMN gene therapy, but it was subsequently suspended (NCT03381729, ClinicalTrials.gov).

1.6 POPULATION-BASED SCREENING FOR SMA

Evidence from pre-clinical studies, trials, and real-world data for each of these interventions indicates that treatment is most effective when initiated early, ideally before symptom onset. In an effort to achieve pre-symptomatic treatment, newborn screening (NBS) for SMA is being implemented by some governments. With disease-modifying treatments available and validated, cost-effective diagnostic tests, SMA satisfies the criteria for addition to NBS panels (Dangouloff et al. 2020). Many pilot programs have demonstrated the feasibility of implementing SMA NBS in clinical practice (Chien et al. 2017; Kraszewski et al. 2018; Boemer et al. 2019; Vill et al. 2019; Kariyawasam et al. 2020). qPCR assays for dried blood samples have been developed to detect the *SMN1* deletion that is common to approximately 95% of patients (Taylor et al. 2015;

Czibere et al. 2020; Pan et al. 2020). Findings from the aforementioned pilot program studies and additional surveys (Wood et al. 2014; Boardman et al. 2018) indicate that SMA NBS is viewed favorably by the general population.

An alternative approach to NBS is carrier screening of pregnant women followed by prenatal testing for cases in which both partners are carriers (Sugarman et al. 2012; Zhang et al. 2020). At present, this strategy is more costly and technically complex. Furthermore, carrier testing does not identify individuals with two copies of *SMN1* in *cis* and zero copies of *SMN1* on the second allele, nor does it account for SMA in offspring caused by mosaicism or *de novo* mutations (Dangouloff et al. 2020).

1.7 RATIONALE AND HYPOTHESIS OF THIS STUDY

Despite the success of the disease-modifying interventions discussed in section 1.5, alternative therapeutic strategies are still needed for SMA. At this time, gene-replacement therapy is only approved for infants up to the age of two years. Furthermore, targeting splicing as a means of increasing SMN levels has a ceiling effect determined by the abundance of *SMN2* transcripts in cells, and combinatorial therapies will be required to overcome this ceiling.

Outside of the exon 7 region, the rest of the *SMN2* transcript has remained relatively unstudied as an avenue for modulating SMN levels. Increasing the stability of *SMN2* mRNA or increasing the translational efficiency of these transcripts may facilitate the production of functional SMN protein from the relatively low levels of full-length *SMN2* mRNA. It was shown that anisomycin and celecoxib activation of the p38 pathway leads to a nuclear to cytoplasmic shuttling of the RNA binding protein HuR, and subsequently, an increase in levels

of SMN protein (Farooq et al. 2009; Farooq et al. 2013). Therapeutic compounds that act to increase the stability of *SMN2* transcripts specifically, as opposed to compounds that activate entire pathways, have not been reported.

Much of the mRNA life cycle, such as its transport, stability and translational efficiency, are regulated via the 5' and 3' untranslated regions (5'UTR and 3'UTR, respectively). After seeing inconsistent effect of 3'UTR elements on *SMN2* expression, we decided to focus on the 5'UTR, which is the topic of this thesis. We hypothesized that there is an element in the 5'UTR of *SMN2* that reduces *SMN2* expression, and that can be targeted to increase SMN levels. Here, we describe our identification of an ASO complementary to the 5' most end of the *SMN2* transcript that increases SMN levels by stabilizing *SMN2* mRNA, and we describe its activity in 3 SMA model systems.

1.8 SUMMARY

In summary, there are many factors that determine the severity of the SMA phenotype (Figure 1.6). These include the age of clinically detectable disease onset, *SMN2* copy number, *SMN2* sequence variants, and genetic modifiers outside of the *SMN* locus. It is likely the particular combination of these and other factors that contribute to the spectrum of disease manifestations observed in SMA patients. Nucleic acid therapeutics now offer an opportunity to tip the scale toward milder disease phenotype and lighten disease burden.

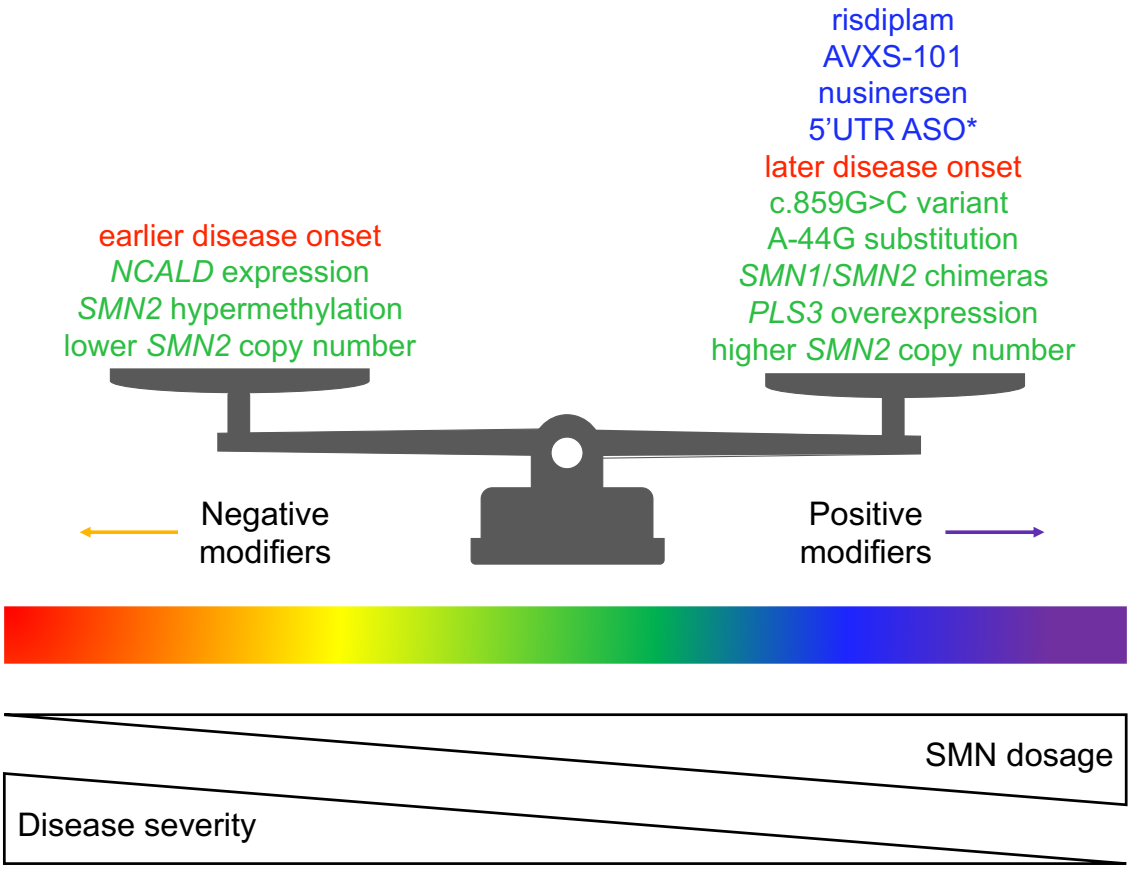

Figure 1.6 Factors that predict and influence SMA disease severity. SMN dosage is inversely correlated to disease severity. A number of other factors, shown on the scale, are associated with the range of SMA phenotypes. Factors in green are genetic modifiers, factors in red are phenotypic predictors, and factors in blue are interventions. * indicates that this modality is the subject of this thesis.

Chapter 2

AN ASO COMPLEMENTARY TO THE 5' UNTRANSLATED REGION OF *SMN2* INCREASES SMN LEVELS

2.1 ABSTRACT

Therapeutics that promote exon 7 inclusion in the *SMN2* transcript have been shown to increase motor function in infants with SMA. While successful, this approach has a ceiling effect that is determined by the abundance of *SMN2* transcripts in cells. Increasing the total pool of *SMN2* transcripts and increasing the translational efficiency of these transcripts are strategies that could be used in combination with splice correction. I sought to determine whether the 5'UTR of *SMN2* contains an element that reduces its expression, targeting of which could increase SMN levels. I identified ASOs complementary to the 5' end of *SMN2* that increase SMN protein levels in fibroblasts. Treatment with the 5'UTR ASO also increases levels of other proteins in the SMN complex. Using RNA labeling, I found that the 5'UTR ASO does not increase the transcription rate of *SMN2*. Consistent with this, by measuring the half-life of SMN transcripts in fibroblasts treated with the 5'UTR ASO, I found that the higher steady-state level of *SMN2* mRNA is due to its increased stability. I next tested the 5'UTR ASO in combination with a previously developed splice-switching oligonucleotide (SSO) (i.e., nusinersen). This combination of 5'UTR ASO and SSO increases SMN levels more than use of the SSO alone. These results add to the current understanding of *SMN2* turnover and point toward a new therapeutic target for SMA that can be pursued as a combinatorial therapy.

2.2 INTRODUCTION

Regulatory motifs in UTRs influence gene expression by controlling the stability, subcellular localization, and translational efficiency of transcripts. This occurs through a dynamic interplay between *cis*-acting elements (i.e., the primary sequence and secondary structures of UTRs) and *trans*-acting factors (i.e., RNA-binding proteins and non-coding RNAs). Examples of UTR features that may affect gene expression include UTR length and GC content, structural elements like stem-loops and G-quadruplexes, and the presence of upstream open reading frames (uORFs), internal ribosome entry sites, alternative polyadenylation signals, and AU-rich elements (Mignone et al. 2002; Chatterjee and Pal 2009). mRNAs in neurons tend to have longer 3'UTRs than mRNAs in other cell types. In addition, isoforms segregate in different neuronal compartments by length of the 3'UTR and by transcript half-life (Tushev et al. 2018).

Nearly half of all human transcripts contain uORFs, translation of which can reduce translation of the main protein coding sequence (primary ORF, pORF) through a variety of mechanisms (Calvo et al. 2009). If a uORF initiation codon is recognized, the translating ribosome may dissociate from the mRNA when it reaches the uORF stop codon (Figure 2.1B). Alternatively, the ribosome may stall upon reaching the uORF stop codon, creating a blockade to ribosomes that follow it (Figure 2.1C). Either case impedes further ribosome scanning and thus translation of the pORF may be reduced. A uORF stop codon can also reduce gene expression by inducing nonsense-mediated mRNA decay, akin to premature termination codons (Figure 2.1D). Hundreds of single nucleotide polymorphisms that create, destroy, or otherwise modify uORFs are known, and

numerous mutations have been identified that cause disease by a mechanism involving uORFs (Barbosa et al. 2013).

I set out to determine whether the steric hindrance capacity of ASOs could be leveraged to block the *SMN2* uORF translation. Situated so closely to the 5' cap, an ASO directed to this location may also work by blocking another inhibitory regulatory motif described above.

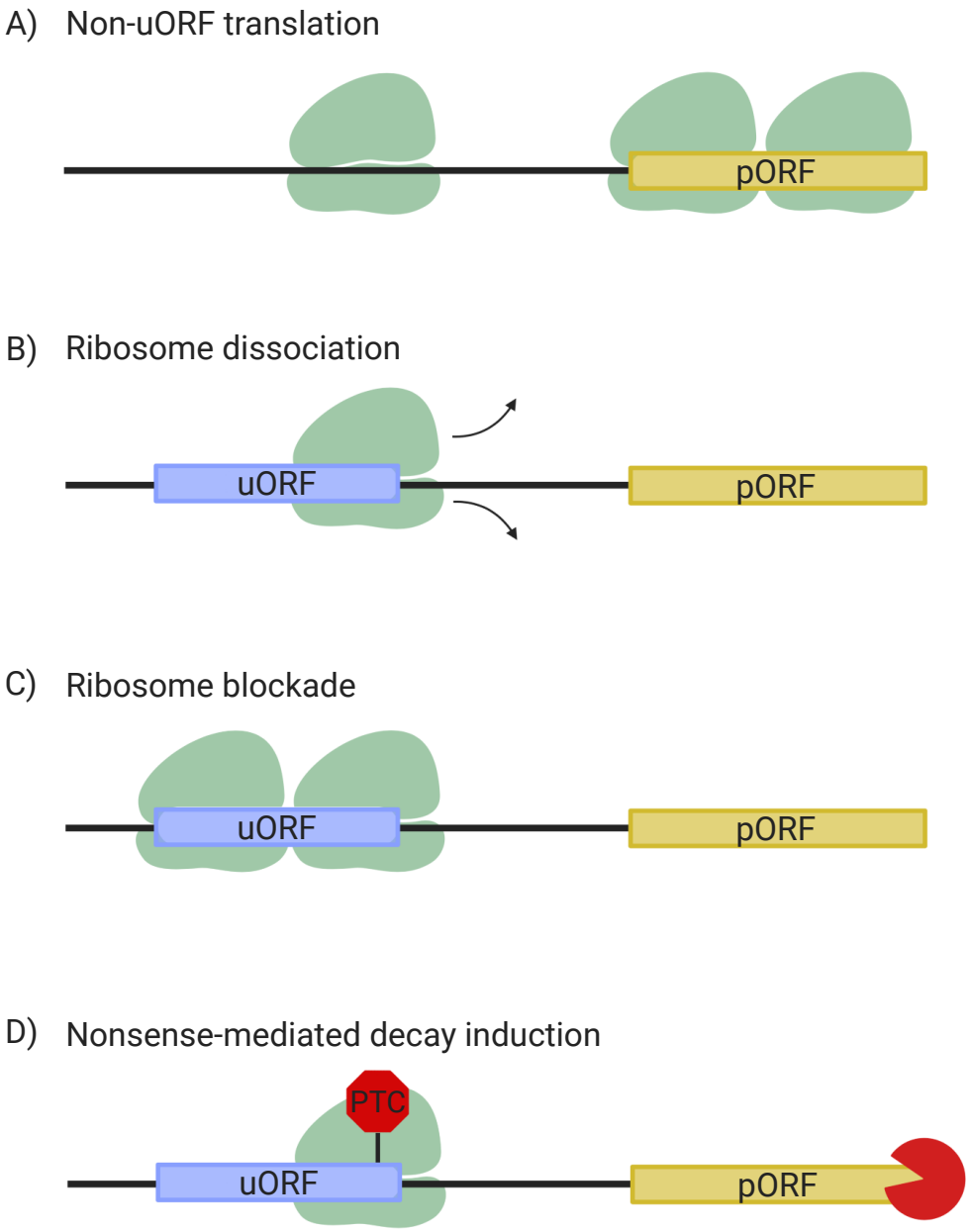

Figure 2.1 Mechanisms by which uORFs reduce pORF translation. When a ribosome encounters a uORF stop codon, there are a number of possible outcomes: B) the ribosome may dissociate from the mRNA; C) the ribosome may stall, leading to a blockade; D) the stop codon may be processed like a premature termination codon (PTC), subjecting the mRNA to nonsense-mediated decay. Each of these scenarios can result in reduced translation of the pORF relative to the level of translation when no uORF is present (A).

2.3 RESULTS

2.3.1 TILING ASOS ACROSS THE 5' END OF *SMN2*

Our interest in the 5'UTR of *SMN2* began when we noticed a start codon 157 nucleotides upstream of the canonical SMN translation initiation codon in the human sequence. Morpholinos were historically used to block translation initiation (Taylor et al. 1996; Satou et al. 2001). I therefore hypothesized that an ASO complementary to the region containing the upstream start codon would prevent translation initiation at this site, hereby diverting ribosomes to the primary ORF (pORF) and increasing SMN levels. Indeed, shortly after I initiated this study, it was shown that ASO-binding at start codons in 5' leader sequences can prevent translation initiation at upstream open reading frames (uORFs) and promote translation of pORFs (Liang et al. 2016). In addition, ASOs have been used to increase translation of mRNAs with other types of 5'UTR inhibitory elements, such as G-quadruplexes or hairpin structures (Rouleau et al. 2015; Liang et al. 2017).

I designed 2'OMe ASOs to tile in 2-nt increments along the beginning of the *SMN2* transcript that overlap the uORF (Figure 2.2A). Supplementary Table S1 shows characteristics such as the GC content and theoretical melting temperature for each ASO. Transfection of a subset of these 5'UTR ASOs into SMA patient fibroblasts resulted in increased SMN protein levels as compared to the level of SMN in untransfected patient cells or those treated with a non-targeting control (NTC) ASO (Figures 2.2B and 2.2C). Stepping 5' to 3' across the UTR, there is a downward trend in ASO effect on SMN expression, indicating that the critical target region is closest to the 5' terminal cap. I decided to use the 5'-most ASO (ASO #1) in the experiments that follow since it demonstrated the

largest biological effect, with an average 2.7-fold increase in SMN protein levels. I tested this 5' most ASO in a second SMA cell line (Supplementary Figure S1) to confirm that its effects are not cell line specific.

I also tested an ASO with the same sequence as ASO #1 but with 2'MOE modified bases. 2'MOE ASOs are known to undergo less non-specific protein binding, and are among the most widely used in clinical trials to date (Schoch and Miller 2017; Shen and Corey 2018). I found that treating SMA fibroblasts with the 2'MOE 5'UTR ASO also increases SMN protein levels (see Supplementary Figure S2 and future figures in this chapter).

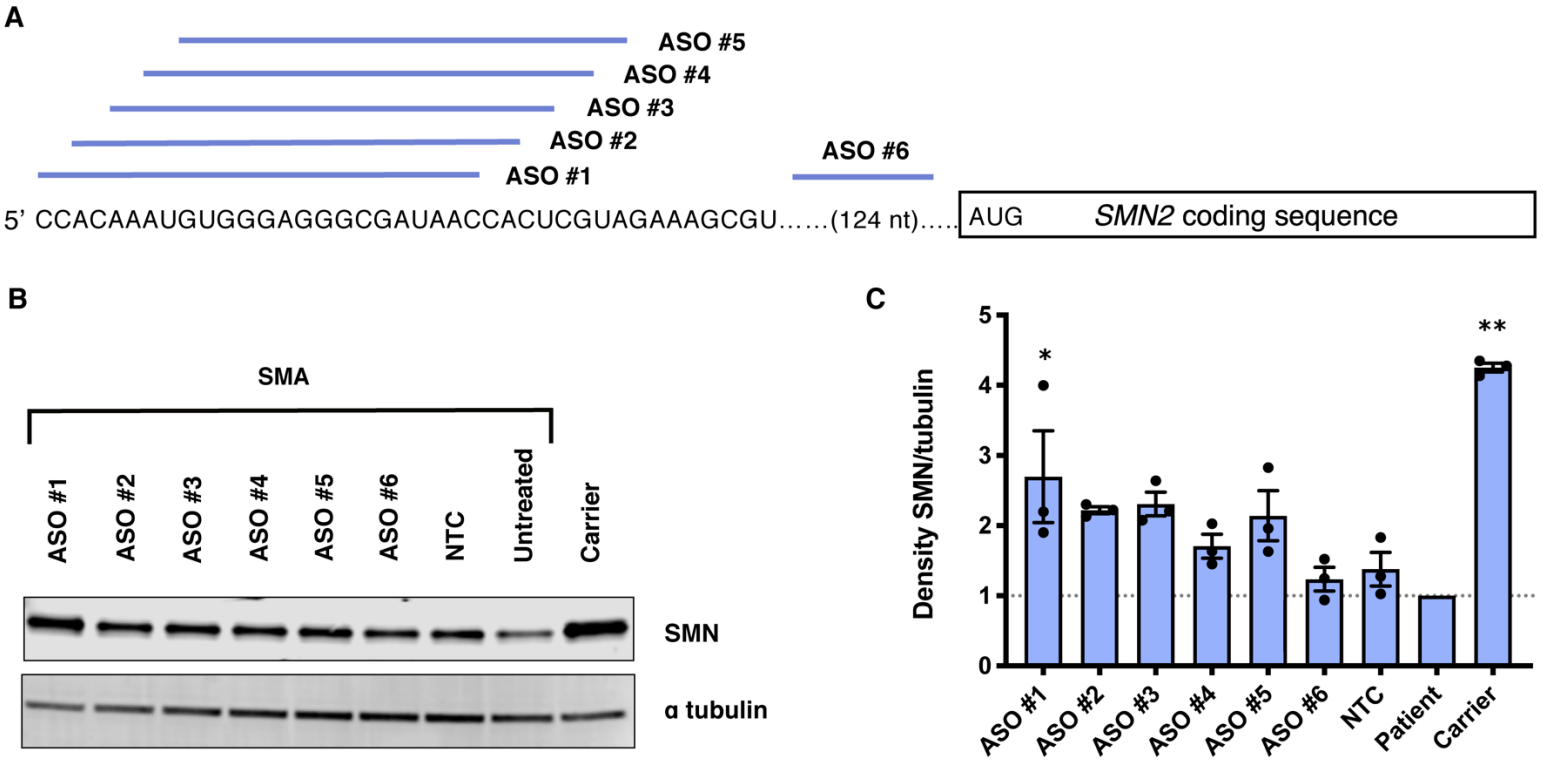

Figure 2.2 Targeting the 5' end of *SMN2* with 2'OMe ASOs increases levels of SMN in fibroblasts.

A) Schematic depicting the tiling of 2'-OMe ASOs in 2-nt increments along the beginning of the *SMN2* 5'UTR. B) Immunoblot (15 μg per lane) showing SMN protein levels in SMN-deficient fibroblasts (GM00232) treated with 600 nM 5'UTR ASOs or a non-targeting control (NTC) oligo, where indicated. C) SMN protein levels normalized to alpha tubulin and then calculated as a fold change relative to SMN levels in untreated SMA patient cells (represented by the dotted line). SMN levels from carrier cells are provided for reference. Error bars show SEM. Statistical significance determined by one-way ANOVA followed by Dunnett's test in comparison to NTC. n = 3; * $p = 0.02$; ** $p < 0.0001$.

2.3.2 *SMN2* uORF DOES NOT REDUCE SMN LEVELS

To better understand the mechanism of action of the 5'UTR ASO, I designed reporter constructs to study the effects of the uORF on SMN levels. To make the reporters more sensitive to endogenous gene regulation, they were designed to contain the well-characterized beta-globin gene (*HBB*) exon 2, intron 2, exon 3 splice junction. This feature is important since one of the means through which uORFs downregulate gene expression is promoting nonsense-mediated decay (Figure 2.1), a process that requires the presence of an exon junction complex.

In addition to a construct with enhanced green fluorescent protein (eGFP) under the control of the wild-type *SMN2* 5'UTR, constructs were made with 1) a mutation to remove the uORF start codon, 2) a mutation that strengthens the sequence context (Kozak sequence) surrounding the uORF start codon, and 3) a frame-shift mutation that extends the uORF coding sequence and places it in-frame with GFP (Figure 2.3A). The latter reporter was designed in order to be able to observe uORF translation initiation, since the uORF peptide is otherwise too small to detect by standard techniques.

Expressing these reporters in HEK293T cells showed that removing the upstream start codon (mutating ATG to ACG) does not increase eGFP levels (Figure 2.3B and 2.3C), suggesting that the uORF does not have a significant influence on gene expression. There is, however, decreased eGFP signal when a guanine is present in the +4 position ("uORF Optimized" reporter). We can infer from this that the non-optimized, native uORF is not functional. Although the +4 position is a known single nucleotide polymorphism site, the T allele frequency is 0.99996 (Ensembl variant rs1262481225). Finally, the larger protein encoded

by the “Frame Shift” reporter was only detectable at very low levels, indicating that ribosomes do not often engage the uORF (Supplementary Figure S3).

To rule out a lack of uORF effect being due to an artefact of the reporter system (e.g., use of a non-endogenous transcription start site), we[1] aligned publicly available ribosome profiling data to the *SMN2* locus (Figure 2.3D). Sequencing reads corresponding to *SMN1* and/or *SMN2* cannot be accurately mapped to standard reference genomes because multi-mapping reads are discarded. Thus, we used a custom reference genome in which only the *SMN2* sequence is present. In the ribosome profiling data, the absence of ribosome-protected fragments mapping to the *SMN2* uORF was in line with my reporter assay findings and supports the conclusion that the uORF in *SMN2* is not a meaningful regulator of *SMN2* expression in fibroblasts or in HEK293T cells.

[1] Kory Johnson (NINDS Bioinformatics Section) mapped the sequencing data to a custom reference genome shared by Corey Ruhno (The Ohio State University).

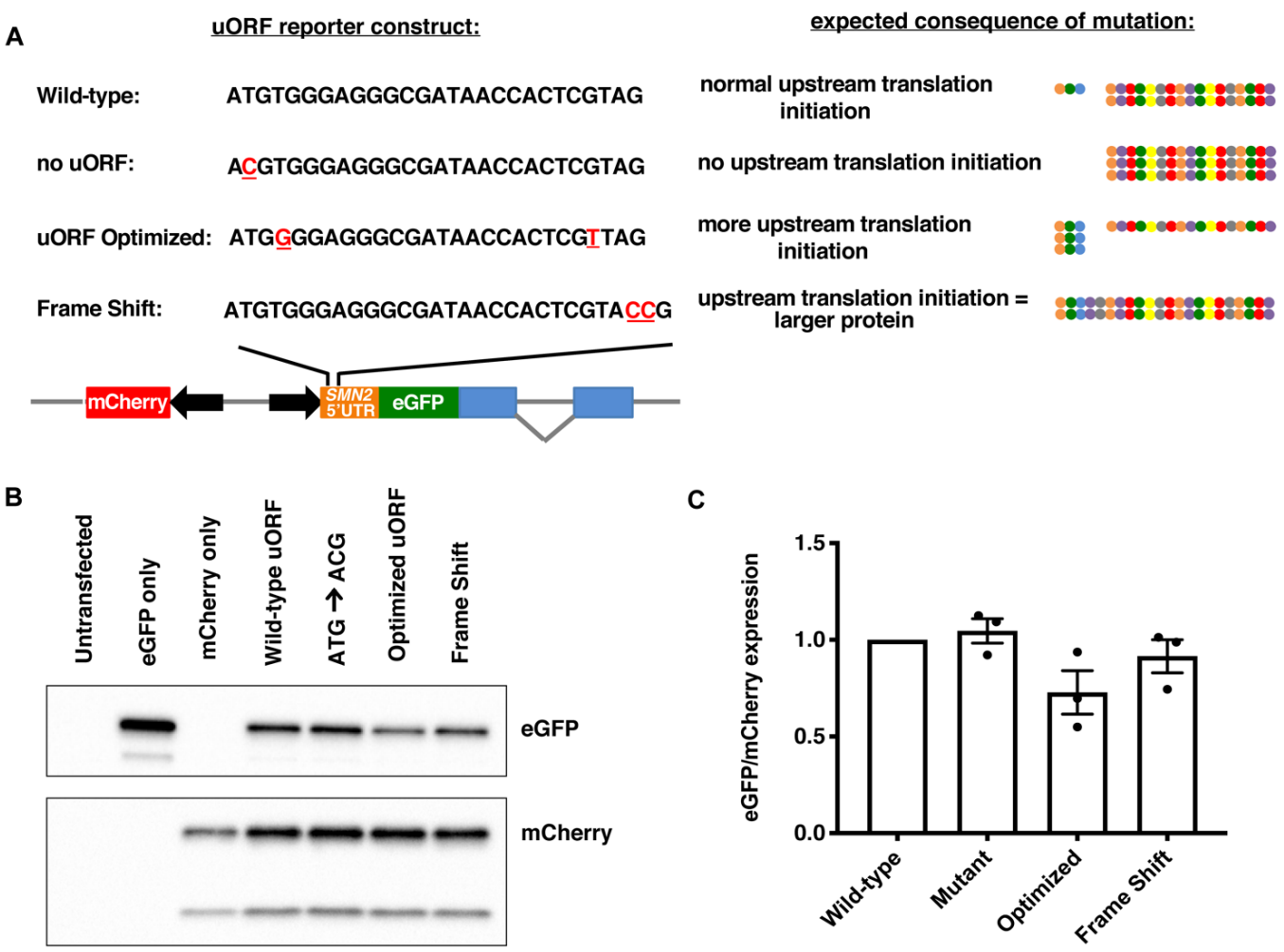
A
uORF reporter construct:
Wild-type: ATGTGGGAGGGCGATAACCACTCGTAG
no uORF: ACGTGGGAGGGCGATAACCACTCGTAG
uORF Optimized: ATGGGGAGGGCGATAACCACTCGTTAG
Frame Shift: ATGTGGGAGGGCGATAACCACTCGTACCG
mCherry
SMN2 5'UTR
eGFP
expected consequence of mutation:
normal upstream translation initiation
no upstream translation initiation
more upstream translation initiation
upstream translation initiation = larger protein
B
Untransfected
eGFP only
mCherry only
Wild-type uORF
ATG → ACG
Optimized uORF
Frame Shift
eGFP
mCherry
C
eGFP/mCherry expression
1.5
1.0
0.5
0.0
Wild-type
Mutant
Optimized
Frame Shift

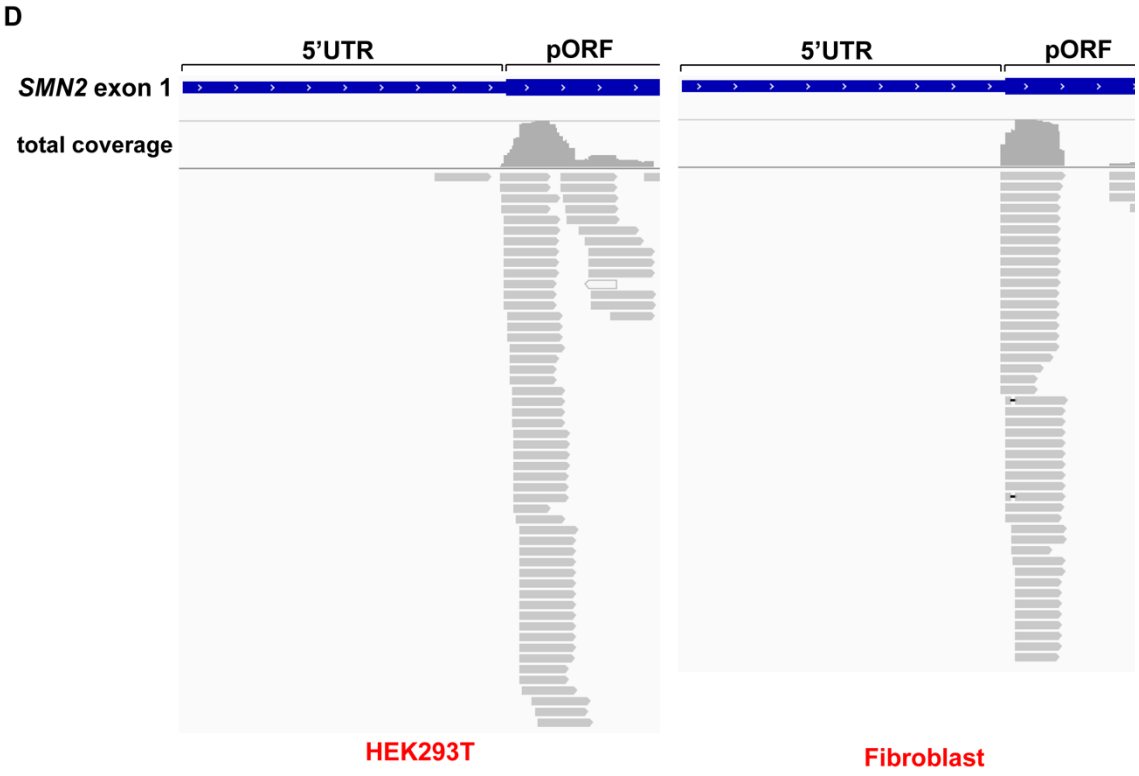

Figure 2.3 The *SMN2* uORF is not readily translated and does not reduce expression of the pORF. A) Schematic detailing reporter construct designs, with mutations underlined in red. Expected sizes and relative expression levels of protein products are indicated on the right. The uORF-encoded peptide is represented as the short string (3 circles), while the pORF-encoded peptide is represented as the longer string (17 circles). The protein encoded by the frame shift reporter (when translation initiates at the upstream start codon and continues through the 5'UTR and the pORF) is represented as the longest, continuous string. B) HEK293Ts were transfected with plasmids and expression levels determined by Western blot. 7.5 μg protein were resolved per lane. C) eGFP protein levels were normalized to mCherry levels, and then normalized to expression from cells transfected with the wild-type plasmid. Error bars represent SEM. D) Ribosome profiling data aligned to the *SMN2* locus and visualized using IGV. Gray lines represent individual sequencing reads, with arrows indicating read direction. Total coverage at a particular locus is indicated above reads.

2.3.3 THE 5'UTR ASO INCREASES STEADY-STATE LEVELS OF *SMN* mRNA

I performed RT-qPCR to determine whether *SMN* transcript levels also increase following 2'OMe ASO treatment. Compared to untreated cells or cells treated with a non-targeting control ASO, the 5'UTR ASO significantly increases total *SMN* mRNA levels in both SMA patient fibroblasts and carrier fibroblasts (Figure 2.4A and 2.4D). Total *SMN* mRNA levels were measured with primers spanning the exon 2a-2b junction and are thus irrespective of exon 7 inclusion.

Transcripts containing exon 7 are the most therapeutically relevant, as they encode the full-length SMN protein. This prompted me to check levels of the full-length and Δ7 *SMN* isoforms by RT-PCR and by RT-qPCR. Surprisingly, the 5'UTR ASO led to a shift toward full-length transcript (with exon 7 inclusion) in patient fibroblasts (Figures 2.4B and 2.4C). In carrier fibroblasts from an unaffected individual with higher baseline SMN levels, the ASO increases steady-state mRNA without affecting the ratio of full length to total transcripts (Figure 2.4D). Thus, I suspect that an increase in the level of total *SMN* mRNA is a direct effect of the 5'UTR ASO, but increased exon 7 inclusion is likely due to SMN feedback in states of SMN deficiency rather than a primary mechanism of action of the ASO.

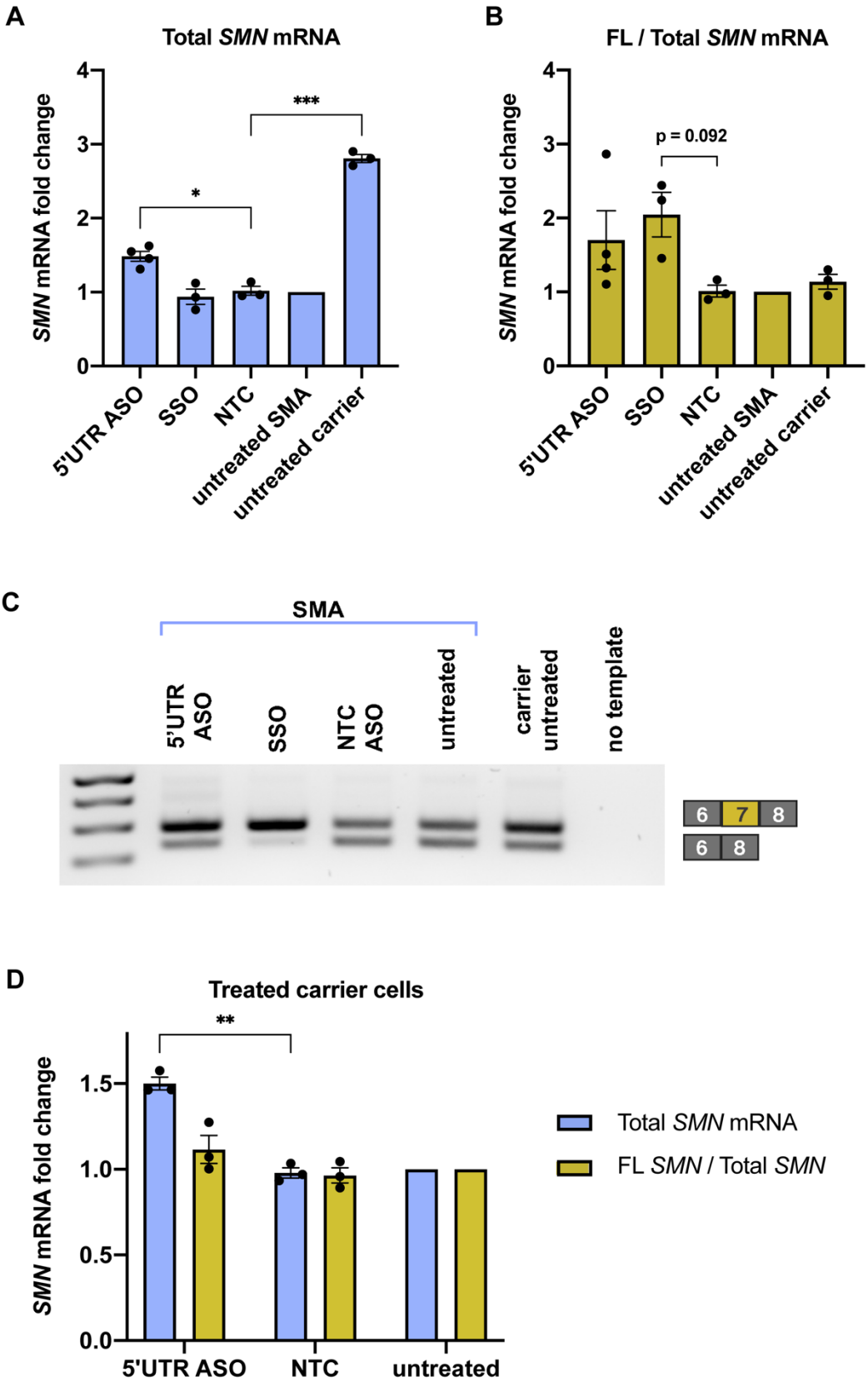
A
Total SMN mRNA
SMN mRNA fold change
4
3
2
1
0
*
***
5'UTR ASO
SSO
NTC
untreated SMA
untreated carrier
B
FL / Total SMN mRNA
SMN mRNA fold change
p = 0.092
5'UTR ASO
SSO
NTC
untreated SMA
untreated carrier
C
SMA
5'UTR ASO
SSO
NTC ASO
untreated
carrier untreated
no template
6 7 8
6 8
D
Treated carrier cells
SMN mRNA fold change
**
1.5
1.0
0.5
0.0
5'UTR ASO
NTC
untreated
Total SMN mRNA
FL SMN / Total SMN

Figure 2.4 A 2'OMe ASO targeting the 5' end of *SMN2* increases *SMN* mRNA levels. A) SMA fibroblasts were transfected with 600 nM 2'-OMe 5'UTR ASO, splice-switching oligonucleotide (SSO), or non-targeting control (NTC) ASO. RT-qPCR measured total *SMN* mRNA levels. Expression was normalized to *GAPDH* and calculated as a fold change relative to levels in untreated SMA cells. B) RT-qPCR analysis of the ratio of full-length (FL) *SMN* to total *SMN* transcript levels, measured with primers overlapping exon 7 or primers spanning the exon 2a-2b junction, respectively. C) RT-PCR to qualitatively visualize alternative splicing with 600 nM ASO treatment. The amplicon from the full-length isoform is 292 bp while the amplicon from the Δ7 isoform is 238 bp. D) As in panels A and B, levels of total *SMN* mRNA or the ratio of full-length (FL) to total *SMN* mRNA were measured via RT-qPCR. The data in this panel is from ASO treatment in fibroblasts from a carrier of SMA (1 copy *SMN1*, 5 copies *SMN2*). Expression was normalized to *GAPDH* and calculated as a fold change relative to levels in untreated SMA cells. Error bars show SEM. Statistical significance determined by one-way ANOVA followed by Dunnett's test in comparison to NTC. n = 3/4; * $p < 0.005$; $p < 0.001$; *** $p < 0.0001$.

2.3.4 5'UTR ASO DOES NOT AFFECT *SMN2* TRANSCRIPTION RATE

A higher steady state level of mRNA, as described in section 2.3.3, could either be due to an increased rate of transcription or to a decreased rate of RNA decay. To distinguish between the two possibilities, I pulsed cells with a uridine analog, 5-ethynyl uridine (EU), to measure newly transcribed *SMN2*. Biotinylating the EU allowed me to isolate and quantify only those RNAs transcribed during the one-hour pulse by using RT-qPCR. I confirmed assay specificity by blocking transcription with actinomycin D and observing an increase in C_t values (of four to eight cycles) for *GAPDH* and *SMN* (Supplementary Table S7). As a positive control, I used SMA carrier fibroblasts that have one copy of *SMN1* and five copies of *SMN2* and thus should transcribe more *SMN* than our patient fibroblasts, which have no copies of *SMN1* and only two copies of *SMN2*. With this RNA labeling method, I saw no difference in nascent *SMN2* transcript levels between fibroblasts treated with the 5'UTR 2'MOE ASO, fibroblasts treated with the non-targeting control 2'MOE ASO, or untreated fibroblasts (Figure 2.5). This indicates that the higher steady-state level of *SMN2* in cells treated with the 5'UTR 2'MOE ASO is not due to increased transcription but is due instead to slower RNA turnover.

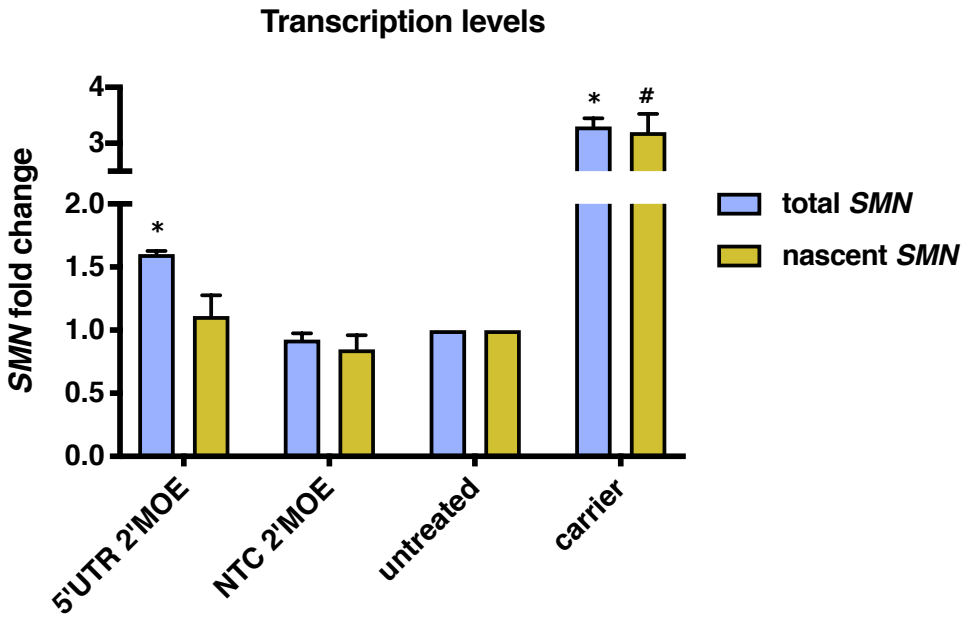

Figure 2.5 A 2'MOE ASO targeting the 5' end of *SMN2* increases the level of steady-state *SMN* mRNA without changing the transcription rate. SMA fibroblasts were transfected with 150 nM 2'MOE 5'UTR ASO or non-targeting control (NTC) ASO. RT-qPCR measured steady-state *SMN* mRNA levels or nascent (biotinylated) *SMN* RNA levels. Expression was normalized to *GAPDH* and compared to levels in untreated SMA cells. Statistical significance was determined by one-way ANOVA followed by Dunnett's test in comparison to the NTC sample in its group; n = 3; * $p \leq 0.007$; # $p < 0.0001$.

2.3.5 ASO-MEDIATED STABILIZATION OF *SMN* mRNA

It would follow that if the increased *SMN* mRNA levels are not the result of increased transcription, they must instead be the result of decreased turnover and therefore an increase in the half-life of *SMN* transcripts. Indeed, by treating cells with actinomycin D (which prevents transcription) and collecting RNA at different time points, I found that *SMN* transcripts are more stable in cells treated with the 5'UTR 2'OMe ASO (Figure 2.6).

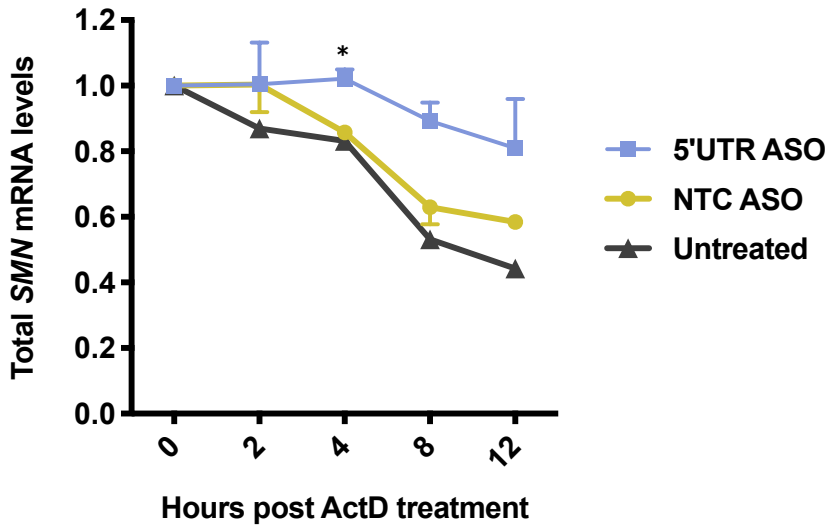

Figure 2.6 The 5'UTR 2'OMe ASO increases *SMN* mRNA levels by slowing their decay. 48 hours post-transfection with 600 nM 2'OMe ASOs, SMA fibroblasts were treated with actinomycin D (ActD) and collected in TRIzol at the specified time points. RT-qPCR measured total *SMN* mRNA. n = 2; * $p < 0.05$ by *t* test in comparison to NTC ASO at given time point.

2.3.6 DECAPPING FACTOR KNOCKDOWN DOES NOT CANCEL ASO EFFECT

The ability of an ASO to block the activty of the yeast decapping enzyme Dcp2p *in vitro* was previously demonstrated (Steiger et al. 2003). Decapping enzyme human homologs are thus candidate factors through which our 5‘UTR ASO is mediating its effect. To investigate this possibility, I selected the most well-characterized human decapping factors and exoribonucleases involved in 5‘ to 3‘ RNA decay. Using RNA-seq data available in our lab, I checked that these genes are expressed in fibroblasts (data not shown). I knocked down these decapping factors and exoribonucleases individually using 100 nM siRNA. The next day, I treated cells with either the 5‘UTR ASO or a scrambled ASO to see whether knockdown abrogated the effect of the ASO.

I found that the 5‘UTR 2‘MOE ASO increased SMN protein levels in the presence of each of the siRNAs (Figure 2.7). Compared to cells transfected with a negative control siRNA, there was no significant difference in the ability of the 5‘UTR ASO to increase SMN protein levels in any of the conditions. Further, knocking down XRN1, the exoribonuclease that degrades mRNAs after they have been decapped, did not increase SMN mRNA levels (Supplementary Figure S4).

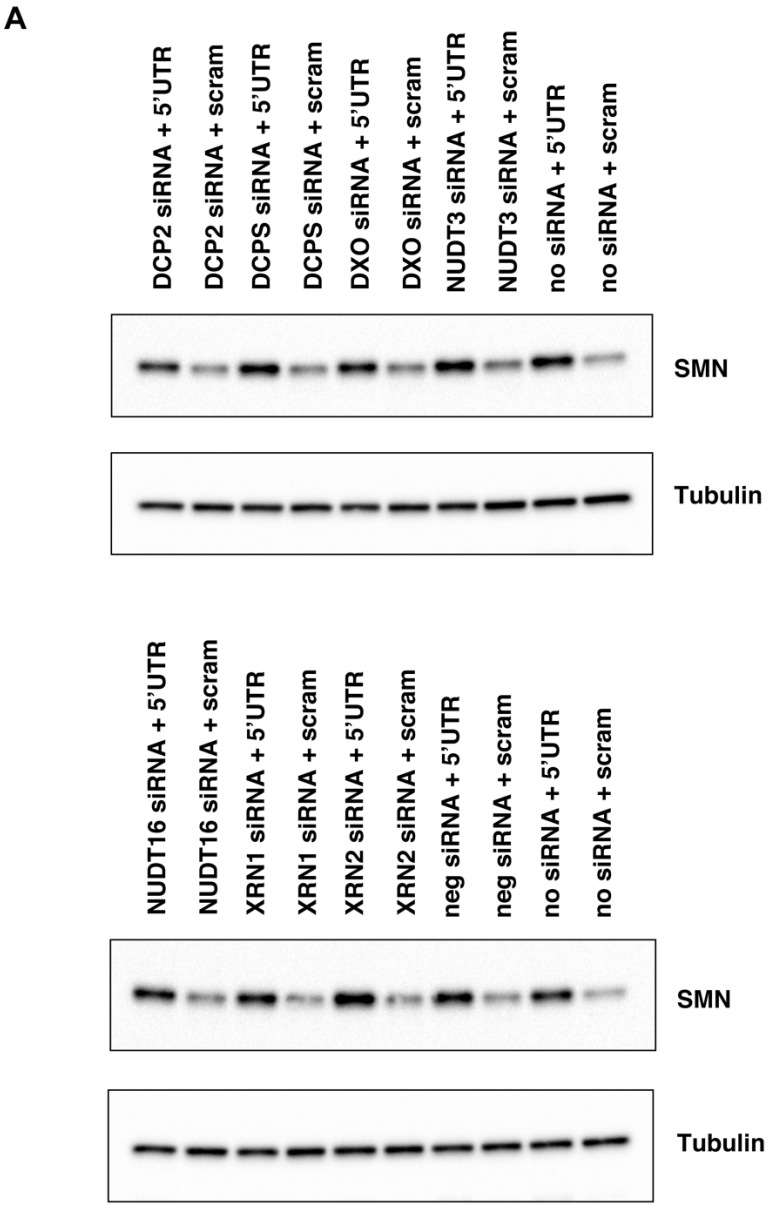
A
DCP2 siRNA + 5'UTR
DCP2 siRNA + scram
DCPS siRNA + 5'UTR
DCPS siRNA + scram
DXO siRNA + 5'UTR
DXO siRNA + scram
NUDT3 siRNA + 5'UTR
NUDT3 siRNA + scram
no siRNA + 5'UTR
no siRNA + scram
SMN
Tubulin
NUDT16 siRNA + 5'UTR
NUDT16 siRNA + scram
XRN1 siRNA + 5'UTR
XRN1 siRNA + scram
XRN2 siRNA + 5'UTR
XRN2 siRNA + scram
neg siRNA + 5'UTR
neg siRNA + scram
no siRNA + 5'UTR
no siRNA + scram
SMN
Tubulin

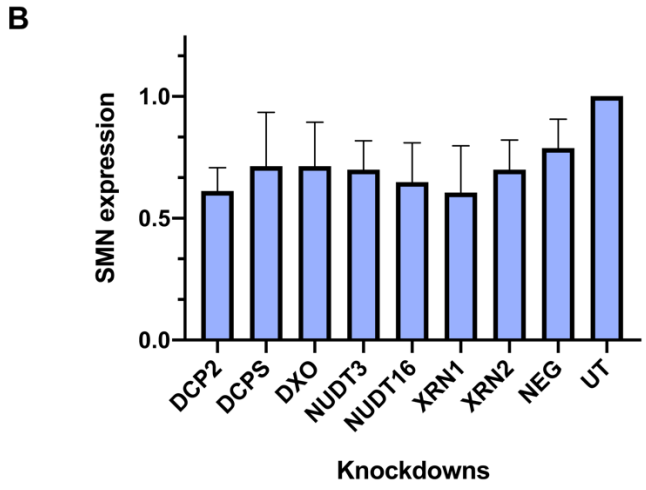
B
SMN expression
1.0
0.5
0.0
DCP2
DCPS
DXO
NUDT3
NUDT16
XRN1
XRN2
NEG
UT
Knockdowns

Figure 2.7 Knockdown of decapping factors and exoribonucleases does not abrogate 5'UTR 2'MOE ASO activity. Enzymes involved in RNA decay were knocked down with 100 nM siRNA in GM0232 (SMA) fibroblasts. The next day, the cells were transfected with 300 nM 5'UTR 2'MOE or scrambled 2'MOE. A) Immunoblots (15 μg per lane) showing SMN protein levels in SMN-deficient fibroblasts treated with siRNA and ASO combinations indicated. B) SMN protein levels were normalized to alpha tubulin and then calculated as a fold change relative to normalized SMN levels in cells treated with ASO but not siRNA. UT = no siRNA treatment. Error bars show SEM. There was no statistical significance between conditions, as determined by one-way ANOVA followed by Dunnett's test in comparison to NTC. n = 3/4.

2.3.7 ASO-MEDIATED INCREASE IN SMN-ASSOCIATED PROTEIN LEVELS

The SMN protein is part of a large protein complex where it associates with Gemin proteins. It has been shown that levels of a subset of these Gemins (Gemin2, Gemin6 and Gemin8) are decreased in the spinal cord of SMA mice, while levels of other SMN complex members (Gemin4 and unrip) are unaffected by SMN expression (Gabanella et al. 2007). I sought to determine whether Gemin levels also correlate to SMN levels in our cells. If so, this would be a good molecular indicator of functional correction with ASO treatment.

First, I confirmed that Gemin levels are lower in SMA than in carrier fibroblasts, and that the levels decrease when SMN is transiently knocked down in carrier fibroblasts (Supplementary Figure S5). Thus, the pattern reported *in vivo* in mouse spinal cord is also present *in vitro* in human fibroblasts. I further hypothesized that this correlation between SMN and the Gemins would hold true in the reverse direction; that is, when SMN levels increase following treatment with the 5'UTR 2'MOE ASO, levels of Gemin6 and Gemin8 will also increase. Indeed, by immunoblot I found a 3.7-fold increase in SMN to be accompanied by a 1.9- and 3.4- fold increase in Gemin6 and Gemin8, respectively (Figure 2.8A and 2.8B).

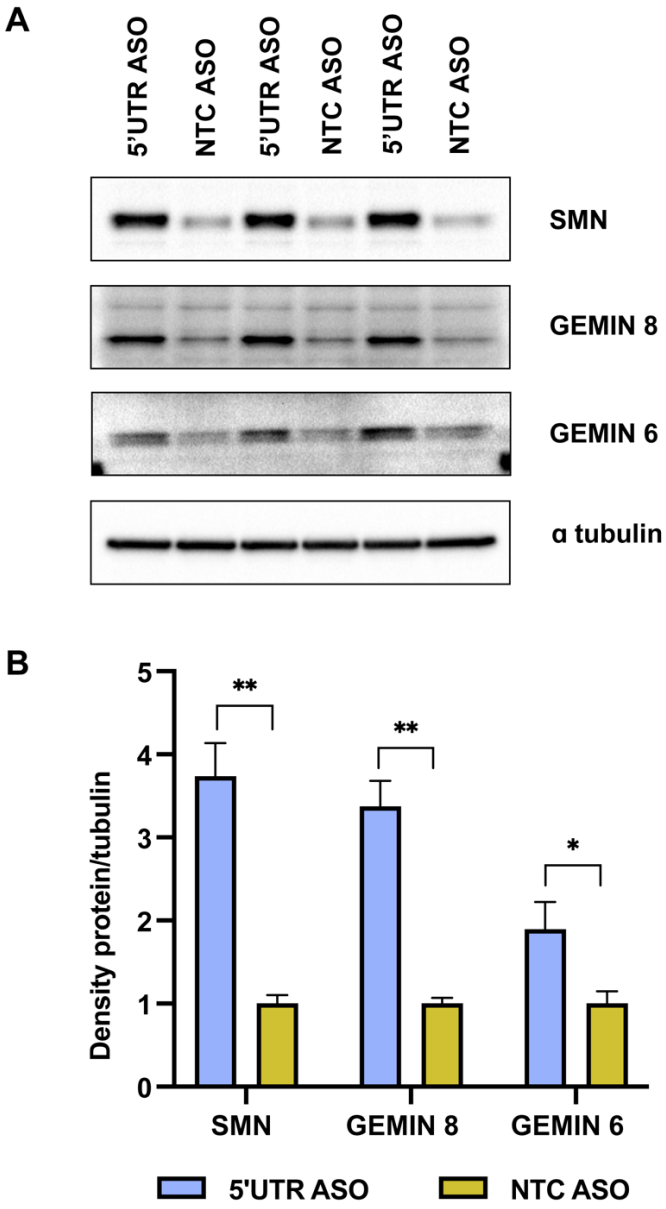

Figure 2.8 Levels of SMN complex members increase with 5'UTR 2'MOE ASO treatment. A) Immunoblot showing levels of SMN, Gemin6 and Gemin8 in SMA fibroblasts following transfection with 300 nM ASO. ASOs were fully modified with 2'MOE bases and PS linkages. 35 μg protein per sample were resolved due to difficulty in detecting Gemin6. B) Levels of the proteins of interest were normalized to alpha tubulin, and this ratio was then averaged for the two sample groups (5'UTR ASO and NTC ASO, in triplicate). The graph shows the level of each protein as a fold change relative to protein levels in cells transfected with the NTC ASO. Error bars show propagated error. Statistical significance was determined by *t*-test between the normalized signal intensity values for the two sample groups. n = 3; * $p < 0.02$; ** $p < 0.0002$.

2.3.8 COMBINATION OF 5'UTR ASO AND SSO FURTHER INCREASES SMN

As discussed in Chapter 1, novel strategies to complement splice modulation of *SMN2* may be especially useful for those individuals with SMA who have low *SMN2* copy numbers. The 5'UTR ASO and SSO were designed to target distinct RNA processes, leading us to investigate whether a combination of these two oligonucleotides overcomes the ceiling effect associated with the SSO. Although the 5'UTR ASO causes a shift in exon 7 inclusion in SMN-deficient cells (Figure 2.4), it does not do so as consistently or as robustly as the SSO. This suggests that there is room for improvement of SMN induction using a combinatorial strategy.

Therefore, I tested the 2'OMe splice-switching oligonucleotide and the 2'OMe 5'UTR ASO separately and jointly. I found that concurrent use of the two ASOs in SMA patient fibroblasts increases SMN protein levels significantly more than use of the SSO alone (Figure 2.9A and 2.9B). While the combination treatment still does not result in the same level of SMN seen in carrier fibroblasts, it is worth bearing in mind that this experiment was performed using 2'OMe ASOs. The optimized splice-switching oligonucleotide that became nusinersen is a 2'MOE. I, too, saw a robust effect using the 5'UTR ASO in the 2'MOE chemistry. It would be worth repeating this experiment using ASOs in the 2'MOE chemistry.

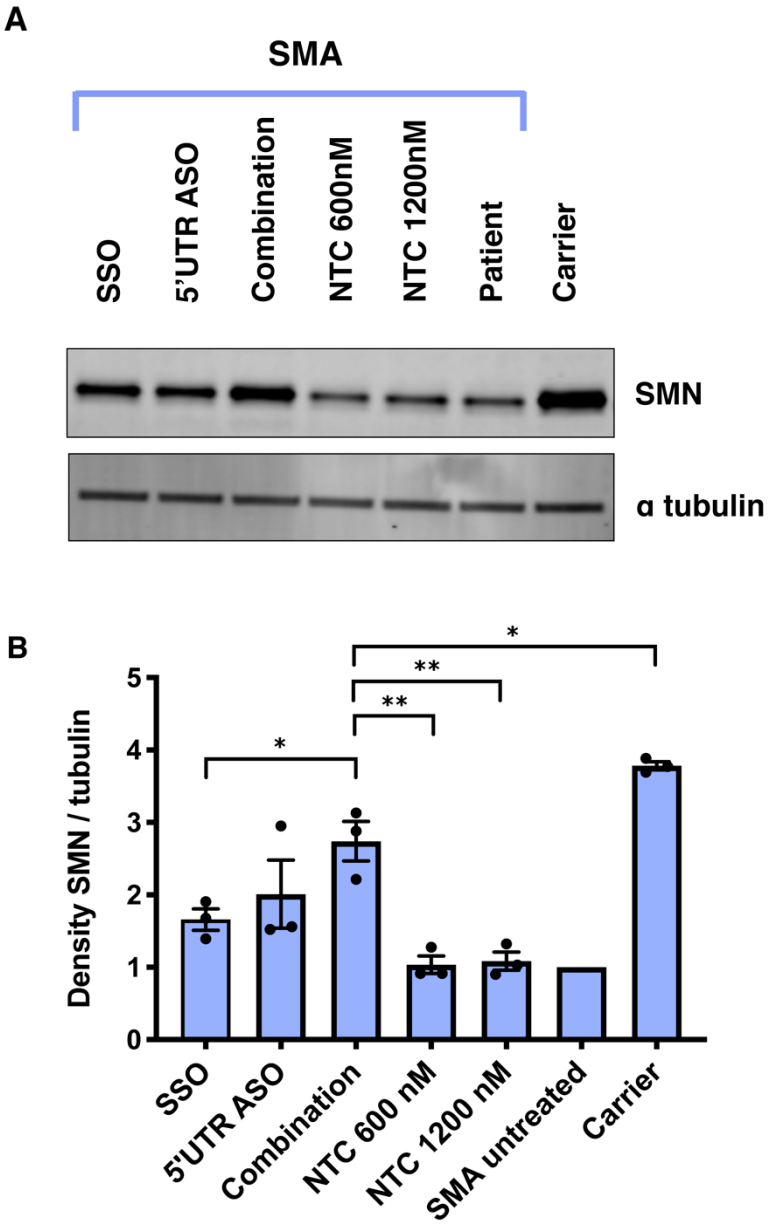

Figure 2.9 Using a 5'UTR 2'OMe ASO in combination with a SSO increases SMN protein levels more than using the SSO alone. A) SMA fibroblasts were transfected with the 2'OMe 5'UTR ASO (600 nM), the 2'OMe splice-switching oligonucleotide (SSO) (600 nM), a combination of the two (1200 nM total), or the 2'OMe non-targeting control (NTC) ASO. 15 μg protein were resolved per lane. B) SMN levels were normalized to alpha tubulin, and expression was compared to levels in untreated SMA cells. Error bars show SEM. Statistical significance determined by one-way ANOVA followed by Dunnett's test in comparison to combination. n = 3; * $p < 0.05$; ** $p < 0.001$.

2.4 DISCUSSION

Previously, histone deacetylase (HDAC) inhibitors were shown to increase *SMN2* levels (Chang et al. 2001; Sumner et al. 2003; Avila et al. 2007). HDAC inhibitors are not specific to the *SMN2* gene, however, and transcriptionally activate a broad array of genes. Some of these non-specific changes in gene expression may benefit the SMA phenotype, but others may not (Liu et al. 2014; Butchbach et al. 2016). Thus, a method for increasing SMN production in a more specific way that can be used to complement the splice-switching approach is therapeutically desirable. Here, I show that an ASO with a sequence complementary to the 5'UTR of *SMN2* increases *SMN* mRNA and protein levels in fibroblasts.

I show that with the increase in *SMN* mRNA levels there is a concurrent increase in the ratio of full-length to exon 7 excluded transcripts, albeit not significant. Other compounds that increase levels of SMN have been shown to increase exon 7 inclusion, including an HDAC inhibitor and an ASO that knocks down the antisense transcript, *SMN-AS1* (Riessland et al. 2006; D'Ydewalle et al. 2017). In the case of the HDAC inhibitor, M344, it was proposed that the observed shift in splicing is due to an increase in levels of the splicing factor Htra2-β1 (Riessland et al. 2006). In the case of the *SMN-AS1* gapmer, it was proposed that the observed shift in exon 7 inclusion is due to altered RNA polymerase II elongation rates (D'Ydewalle et al. 2017). Unlike these two compounds, the 5'UTR ASO works by a transcription-independent mechanism, and I propose that the shift in splicing is due to SMN autoregulation. One possibility is that the increase in SMN protein levels due to 5'UTR ASO treatment increases the pool of snRNPs, and this, in turn, increases the efficiency of some

splicing events. Since the inclusion of exon 7 is relatively inefficient, this particular splicing event may be preferentially increased in this manner. This hypothesis is supported by our observation that there is no change in exon 7 inclusion in carrier fibroblasts treated with the 5'UTR ASO, where SMN levels (and snRNP levels) are not low enough to cause any phenotype at baseline.

In addition to the SMN protein, I show that levels of at least two SMN-associated proteins (Gemin6 and Gemin8) increase with ASO treatment. This is likely because as SMN levels increase there are more SMN complexes to which Gemin6 and Gemin8 can bind and this confers stability. Details about the stoichiometry of proteins in the SMN complex are unknown. The 5'UTR ASO may thus be useful in future experiments intended to study how proteins such as Gemin6 and Gemin8 are incorporated into the SMN complex, as well as in studying other pathways in which the SMN protein is involved more generally.

Other future experiments to be done relate to elucidating the ASO's mechanism of action. My initial hypothesis was that by blocking translation of the uORF, the 5'UTR ASO promotes translation of the primary ORF. However, with multiple techniques we found that the *SMN2* uORF is not normally translated. This may be due to the short distance between the 5' cap and the uORF start codon (7 nucleotides) or to the weak sequence context surrounding the start codon (T at the +4 position).

While this work was in progress, two papers describing the antisense strand of *SMN* (called *SMN-AS1*) were published (D'Ydewalle et al. 2017; Woo et al. 2017). This long non-coding RNA is transcribed from *SMN* intron 1 but binds directly to the *SMN* transcription start site region. Here, it recruits PRC2 and reduces transcription of *SMN2*. Due to the proximity in binding locales, we

wondered whether the 5'UTR ASO repressed *SMN-AS1* activity. However, I found no difference in the transcription rate of *SMN2* with ASO treatment, indicating that the mechanism of action is likely independent of *SMN-AS1*.

Instead, the 5'UTR ASO stabilizes *SMN2* mRNA. While it has been established that the SMN protein is degraded by the E3 ubiquitin ligase mind bomb 1 and the proteasome, the process through which SMN transcripts are degraded is less clear (Kwon et al. 2013). A high-throughput screen identified a quinazoline compound that, by inhibiting the mRNA decapping enzyme DcpS, increases *SMN2* promoter activity in cell-based assays (Jarecki et al. 2005). Follow up studies found that this small molecule increases survival and motor function in SMA mice (Gogliotti et al. 2013; Van Meerbeke et al. 2013; Gopalsamy et al. 2017). While it is known that DcpS hydrolyzes cap structures from mRNA fragments that are generated by extensive 3′ to 5′ exonuclease decay, the specific mechanism through which the quinazoline compound increases *SMN2* expression is unknown.

The idea that the 5'UTR ASO operates via a mechanism related to decapping is compelling since the ASO is complementary to the *SMN2* sequence immediately adjacent to the 5' cap. However, I did not see a significant difference in the ASO's ability to upregulate SMN levels in cells in which decapping factors were knocked down. We cannot rule out this mechanism of action entirely since it is possible that with the knockdown of individual enzymes there was compensation by other RNA decay machinery. This may explain why *MYC* levels (our positive control) were not significantly increased in cells lacking XRN1. Alternatively, although *MYC* was previously reported to undergo XRN1-mediated decay, recent evidence suggests that steady-state levels of *MYC* are

not reduced with XRN1 knockdown due to a simultaneous reduction in its transcription rate (Singh et al. 2019). Our inability to see any effect in these experiments could also have been due to an insufficient knockdown of the target genes for which siRNA effectiveness could not be determined (*DCP2*, *DCPS*, *DXO*, *NUDT16*).

2.5 ONGOING AND FUTURE EXPERIMENTS

The published guidelines for ASO and double-stranded RNA experiments state that "potential alternative hypotheses that might explain results but do not involve 'on-target' engagement must be acknowledged" (Gagnon and Corey 2019). One source of off-target engagement is electrostatic interactions or sequence-specific interactions between ASOs and proteins. In a cell, this type of interaction may effectively sequester the protein and prevent it from performing its usual function.

To address the possibility that our ASO increases SMN levels not through its direct binding to the *SMN2* 5'UTR but rather through its interaction with a cellular protein, I performed a pull-down using biotinylated ASOs to identify the proteins to which they bind. I did pull-downs in lysates from SMA patient fibroblasts with a) the 5'UTR ASO, b) the scrambled ASO that does not significantly increase SMN levels, and c) the non-targeting control ASO with a sequence unrelated to the 5'UTR ASO. Following gel electrophoresis and a high-sensitivity total protein stain, I identified two bands that were present in the 5'UTR ASO pull-down samples but absent in pull-downs using the control ASOs (Supplementary Figure S6). These bands were gel excised and submitted for

mass spectrometry[2] for protein identification. A summary of data filtering methods and results for one of the bands of interest is provided in Supplementary Table S8.

A few of the proteins identified by mass spectrometry as 5'UTR ASO binders are of special interest (CTIF, PATL1, BCDIN3D, and ALYREF) because of their roles in capping or cap-binding. In fact, CTIF is a component of the CBP80/CBP20 cap-binding complex. The orthologs found in *D. melanogaster* and *C. elegans* (Cbp20 and ncbp-2, respectively) were previously found to be modifiers of SMN loss of function phenotypes in these invertebrates (Dimitriadi et al. 2010). The top protein candidates from the mass spectrometry datasets will receive follow-up investigation, including Western blotting to validate their differential abundances in targeting ASO versus control ASO pull-down samples. The top candidates will then be knocked down in cells to determine what effect, if any, this has on *SMN2* expression.

Additionally, we performed RNA-sequencing[3] of ASO-treated fibroblasts in order to determine a) what changes in gene expression occur when we treat cells with the 5'UTR ASO (i.e., what changes in gene expression do we see that may indicate a functional benefit of ASO treatment in SMN-deficient cells) and b) what the representation of reads looks like for the *SMN2* transcript itself (i.e., is the ASO changing the splicing, transcription start site, etc. of *SMN2*?). These data (which require validation) are shown in Supplementary Table S9 and S10. Expressed genes that were up- or down-regulated at least 1.5-fold and had a p-value less than 0.05 between the 2 treatment groups (5'UTR ASO versus non-

[2] Mass spectrometry was performed by Yan Li, Director of the NINDS Protein/Peptide Sequencing Facility.
[3] Library preparation and sequencing was done at the NHLBI DNA Sequencing and Genomics Core. Kory Johnson (NINDS Bioinformatics Section) processed the sequencing reads.

targeting control ASO) were used for pathway analysis. There is evidence in the literature to support the dysregulation of 2 of the top 5 pathways in SMA. In our dataset, a significant number of differentially expressed genes are involved in virus entry via endocytic pathways and glucocorticoid receptor signaling (Supplementary Table S10). A number of studies have shown impaired endocytosis in SMN-deficient cells, with one in particular showing that fibroblasts from a SMA type 1 patient are resistant to infection (Dimitriadi et al. 2016). Additionally, metabolic abnormalities have been reported in SMA, including differential expression of the glucocorticoid receptor and its downstream effector, *Klf15* (Walter et al. 2018). Taken together, these data suggest that 5'UTR ASO treatment may restore the activity of pathways that are disrupted in SMA. Further experiments could help to confirm whether these changes in gene expression are accompanied by functional changes.

Chapter 3

INVESTIGATING OUR THERAPEUTIC STRATEGY IN OTHER SMA MODEL SYSTEMS

3.1 ABSTRACT

The results discussed in Chapter 2 provide the evidence necessary to initiate a pre-clinical study of the 5'UTR ASO. We[4] used a mouse null for mouse *Smn* with insertion of the human *SMN2* transgene, which models severe SMA. We observed no increase in survival or SMN levels in SMA mice. Follow-up studies with cultured mouse fibroblasts showed that the 5'UTR ASO has a human-specific effect. Thus, we returned to a human cell model and tested the 5'UTR ASO conjugated to a cell-penetrating peptide in SMA motor neuron-like cells differentiated from induced pluripotent stem cells. We found that, compared to a non-targeting control ASO, the 5'UTR ASO increases SMN levels in this disease-relevant cell type.

3.2 INTRODUCTION

In addition to the compelling disease genetics, another factor that has contributed to the success and efficiency of therapeutics development for SMA is the availability of model systems for studying SMN function and for preclinical efficacy studies.

SMN homologs have been well characterized in *Schizosaccharomyces pombe*, *Caenorhabditis elegans*, *Drosophila melanogaster*, *Danio rerio*, *Xenopus laevis*, *Mus musculus*, and *Homo sapiens*. None of these organisms are viable when there is a complete absence of SMN, suggesting a core SMN function that is critical in eukaryotes. Aligning the amino acid sequences of SMN homologs across these species shows that the highest levels of conservation are toward

[4] Suzan Hammond (Wood Lab, Department of Paediatrics, University of Oxford) managed the SMA mouse colony, contributed to study design, and performed injections and tissue harvests.

the amino- (N-) and carboxy- (C-) terminals of the protein, which contain the Gemin2 binding domain and the YG-box (tyrosine/glycine-rich sequence), respectively (Osman et al. 2019) (Figure 1.2). Although the yeast homolog is conserved at the N- and C- terminals, it is the only homolog of those listed above that lacks the Tudor domain, which is necessary for the interaction of SMN with many of its protein partners and for spliceosome assembly (Schmid and DiDonato 2007; Osman et al. 2019). Exogenous expression of some, but not all, of these homologs can rescue phenotypes caused by SMN-deficiency in another species. For example, viral delivery of human, frog, and zebrafish (but not fly, worm, and yeast) SMN homologs significantly increase survival, weight, and motor function in SMA mice (Osman et al. 2019).

The mouse is the most commonly used SMA animal model. Mice have only one *Smn* gene, and its knockout is embryonic lethal (Schrank et al. 1997; Hsieh-Li et al. 2000). Introducing mutations that only partially deplete *Smn* levels, as in the $Smn^{2B/-}$ model, is one approach to modeling the disease (Hammond et al. 2010). Alternatively, inserting the human *SMN2* gene on a null *Smn* background is a second option for disease modeling that prevents embryonic lethality (Hsieh-Li et al. 2000; Monani et al. 2000). There are, therefore, a number of SMA mouse models, each containing different mutations in the endogenous *Smn* gene and each with the insertion of different *SMN2* copy numbers (Bebee et al. 2012). Similar to what is observed in humans, higher copy numbers of the *SMN2* transgene reduce disease severity in mice (Monani et al. 2000; Le et al. 2005). Thus, some of these mouse lines have a severe phenotype and some have a milder phenotype (depending on *Smn* and *SMN2*

gene dosage), with survival ranging from as few as five days to a normal lifespan (Schmid and DiDonato 2007; Bebee et al. 2012).

I set out to determine whether the 5'UTR ASO discussed in Chapter 2 increases *SMN2* expression *in vivo* and whether this ameliorates the disease phenotype in mice. The animal model used here was generated by the Li lab and further characterized by the DiDonato group (Hsieh-Li et al. 2000; Gogliotti et al. 2010). In these mice, referred to hereafter as the Hsieh-Li mice, *Smn* loss of function was achieved by targeted replacement of *Smn* exon 7. An advantage of this model is that mice can be bred in such a way that 50% of offspring are affected, compared to other models in which only 25% of offspring are affected. This reduces the number of mice needed, the amount of time required, and the amount of therapeutic agent necessary for experimentation. Furthermore, we used the Hsieh-Li mice, as opposed to the $Smn^{2B/-}$ mice which were also available in our lab, because the 5'UTR ASO identified in Chapter 2 is complementary to the human *SMN2* gene sequence, which is not present in the $Smn^{2B/-}$ mice (Bowerman et al. 2009).

Overall, I found that the efficacy of our 5'UTR 2'MOE in human fibroblasts does not translate into mice. There was no increase in SMN levels in mouse tissues/cells following ASO treatment, and, as a result, there was no phenotypic correction. Mouse fibroblast studies show that the effect of the 5'UTR 2'MOE on *SMN2* expression is species-specific. Returning to a human disease model, we show that a 5'UTR ASO increases SMN levels in SMA motor neurons derived from induced pluripotent stem cells (iPSCs).

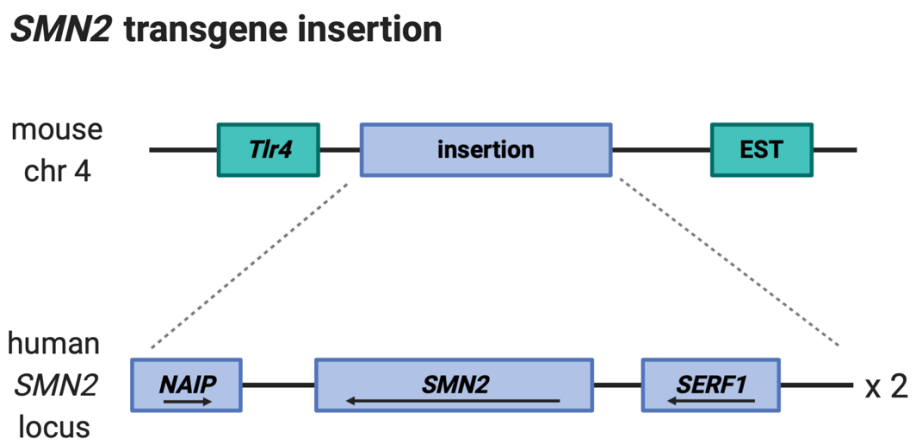

Figure 3.1 Integration of the *SMN2* human transgene into mouse.

115 kb of human DNA sequence spanning from 55 kb upstream of *SMN2* through to exon 10 of centromeric *NAIP* were integrated downstream of *Toll like receptor 4* (*Tlr4*) on murine chromosome 4 (Hsieh-Li et al. 2000; Gogliotti et al. 2010). EST = novel, uncharacterized expressed sequence tag.

3.3 MOUSE STUDY AIMS AND STUDY DESIGN

To examine the *in vivo* effects of the 5'UTR-targeting 2'MOE on the SMA phenotype, we initiated a study in the Hsieh-Li SMA mouse model. Our study had 4 aims, with Aims 3 and 4 contingent on the results of Aims 1 and 2:

Aim 1: To determine the maximum tolerated dose of the 5'UTR-targeting 2'MOE, and to assess its efficacy in SMA phenotypic correction at this dose as compared to injection of a non-targeting control (NTC) 2'MOE.

Aim 2: To assess the effect of the 5'UTR-targeting 2'MOE on *SMN2* expression levels.

Aim 3: To determine how the 5'UTR-targeting 2'MOE compares to the intronic splicing silencer N1 (ISS-N1)-targeting 2'MOE, and to establish the lowest effective dose of ISS-N1 2'MOE for use in Aim 4.

Aim 4: To evaluate the efficacy of combinatorial treatment on the SMA phenotype and on *SMN2* expression.

Beginning with Aim 1, we designed a dose escalation study and treated 1 to 5 mice at each dose in order to determine a) the maximum tolerated dose and b) the treatment effect size. These findings would permit us to select the appropriate dose for a study with a larger number of mice (including the NTC 2'MOE treatment group) and a power analysis in the study design.

Efficacy in our dose escalation study was defined as increased survival, increased body weight, or delayed age of tail or ear necrosis onset in mice treated with the 5'UTR 2'MOE compared to saline-treated pups. Our dosing regimen entailed subcutaneously injecting mice on day of birth (PND0). Previous reports have demonstrated ASO activity in the CNS when the ASO is delivered

peripherally in young mice (PND0-PND3). For example, early subcutaneous injection of a 2'MOE that promotes *SMN2* exon 7 inclusion (later to become nusinersen) resulted in increased exon 7 inclusion in brain, spinal cord, liver, kidney, and muscle, indicating broad ASO distribution following peripheral administration (Hua et al. 2011). It is possible that a different ASO sequence will result in a different pattern of cellular uptake.

The doses of 2'MOE selected for our dose escalation study were chosen to be in line with the Hua et al. experimental design. We planned to administer the 2'MOE at 60, 120, 180, and 240 μg per g of body weight (μg/g). We elected to perform single administrations (on PND0 exclusively) in order to reduce variability.

For Aim 2, we planned to treat mice with the highest tolerated and lowest effective doses identified in Aim 1 using the same mode of administration. Tissues were harvested ten days after 2'MOE administration (PND10), and from these tissues levels of mRNA and protein produced by the human *SMN2* transgene were measured.

Based on the results of the experiments designed to address Aims 1 and 2 (discussed in the sections that follow), we decided not to proceed with Aims 3 and 4 of the *in vivo* study.

3.4 RESULTS

3.4.1 5'UTR ASO DOES NOT IMPROVE SURVIVAL IN SEVERE SMA MICE

Untreated Hsieh-Li SMA mice with two copies of the *SMN2* transgene live less than two weeks (Hsieh-Li et al. 2000; Hammond et al. 2016). We did not see an extension in lifespan in mice treated with the 5'UTR ASO in the 2'MOE chemistry at doses ranging from 120 to 240 μg/g. The longest-lived mice reached the humane endpoint by 10 days of age. The humane endpoint was reached when the mouse did not gain weight for 2 successive days.

Table 3.1 Survival data for treated mice.

Mice were treated with the indicated amount of 5'UTR 2'MOE by a single, subcutaneous injection on PND0. Saline-treated mice were given two injections between PND0 and PND2. *n* = number of mice per treatment group. Median and mean survival values are given in days, as are age range values. Mean survival includes plus or minus standard deviation.

Dose	*n*	Median survival	Mean survival	Age range
120 mg/kg 5'UTR MOE	3	10	8 ± 3.5	4 – 10
180 mg/kg 5'UTR MOE	1	2	2	2
240 mg/kg 5'UTR MOE	5	8	8 ± 1.6	6 – 10
2x Saline	4	6.5	6.5 ± 0.6	6 – 7

3.4.2 *SMN2* EXPRESSION IN TISSUES OF TREATED MICE

An ASO may engage with its target but not change gene expression to a degree high enough for phenotypic correction. Alternatively, the timing of ASO activity may impact its ability to rescue disease manifestations. This is especially true in the severe SMA mouse model, in which a rapid and high level of SMN induction is required to rescue the SMA phenotype.

Therefore, although we observed no improvement in survival of mice treated with the 5'UTR 2'MOE, we looked to see whether ASO treatment had an effect on *SMN2* expression. Using RT-qPCR, we measured levels of *SMN2* mRNA in PND10-PND12 tissue from heterozygous mice (with the endogenous, unperturbed mouse *Smn* gene and the human *SMN2* transgene). These mice were given a single, subcutaneous injection of 240 μg/g 5'UTR 2'MOE or saline on PND0. There was no difference in total *SMN2* mRNA levels in brain or skeletal muscle in mice treated with the 5'UTR 2'MOE compared to saline-treated mice (Figure 3.2A). Of note, the 5'UTR ASO increased SMN mRNA levels in heterozygous human fibroblasts (Figure 2.4D).

Having previously demonstrated in human fibroblasts that the mechanism of action of the 5'UTR 2'MOE involves stabilization of *SMN2* mRNA, I would expect any ASO activity to be reflected at the mRNA level. Nonetheless, we also extracted protein from these tissues and examined SMN levels by Western blot. In line with the RT-qPCR data, there was no difference in the level of SMN protein in skeletal muscle of treated and saline-control mice (Figure 3.2C). There was, however, a slight increase (~25%) in the level of SMN protein in brain samples (Figure 3.2B). Such a modest increase should be interpreted with caution since a) Western blotting is only semi-quantitative, b) no increase in SMN

protein was detectable in skeletal muscle, and c) no increase was detectable in *SMN2* mRNA levels in brain or skeletal muscle.

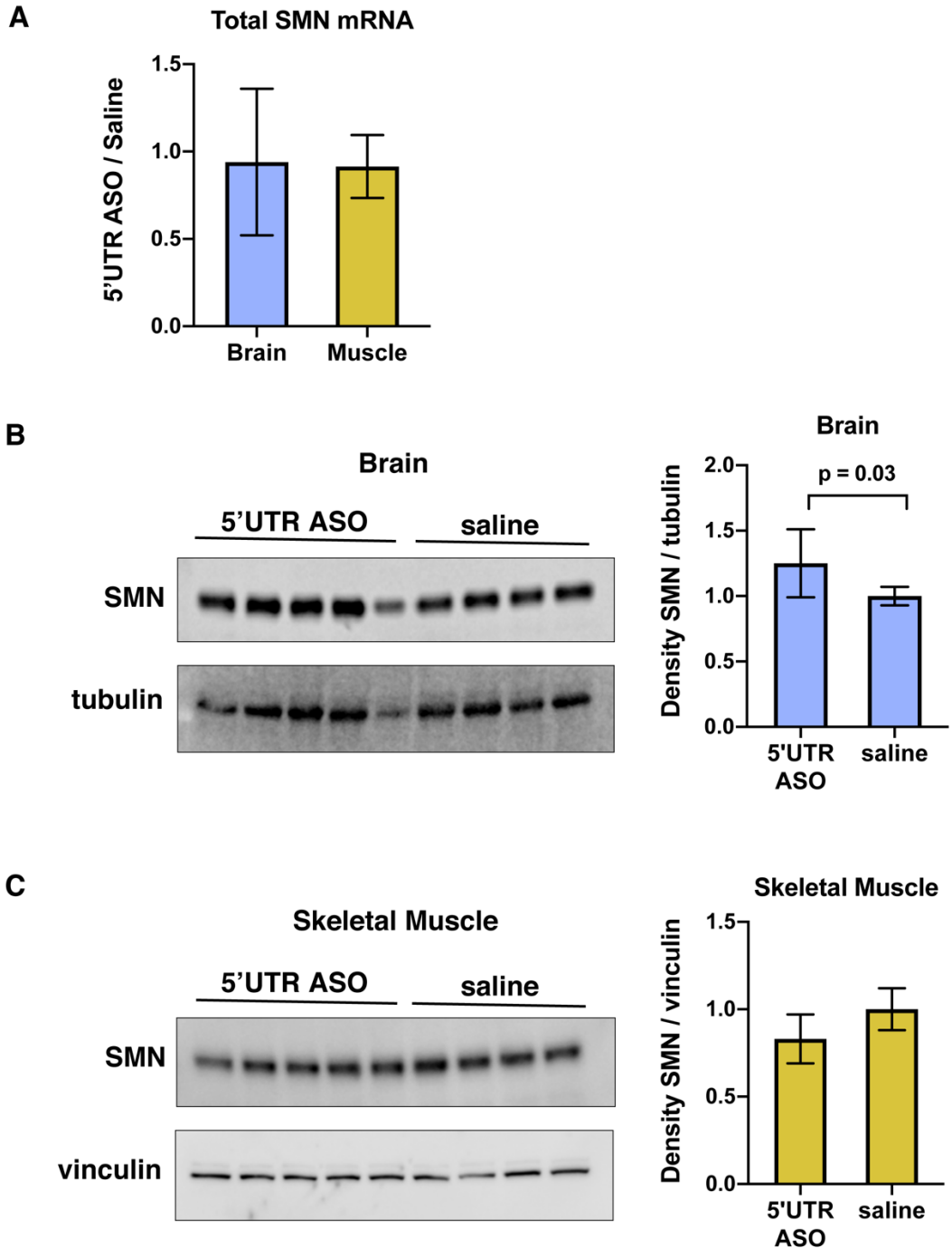

Figure 3.2 The effect of the 5'UTR ASO on *SMN2* expression seen in human fibroblasts is not reproducible in mouse tissue. A) Levels of *SMN2* mRNA from the human transgene were measured via RT-qPCR in tissues harvested from heterozygous mice treated with 240 μg/g ASO. Expression was normalized to *PolJ* and calculated as a fold change relative to levels in saline-treated mice. B) Protein was extracted from brain samples from panel A and lysates were probed for SMN levels by immunoblot. SMN levels were normalized to tubulin, and expression was compared to levels in saline-treated mice. C) Protein was extracted from skeletal muscle samples from panel A and lysates were probed for SMN levels by immunoblot. SMN levels were normalized to vinculin, and expression was compared to levels in saline-treated mice. Error bars represent SEM. 5'UTR ASO n = 5; saline n = 4.

3.4.3 ASO DOES NOT ALTER SMN LEVELS IN CULTURED MOUSE CELLS

A number of factors may explain why the 5'UTR 2'MOE increases expression of *SMN2* in cultured human fibroblasts but not in mice. The first explanation is that the ASO is effective in an *in vitro* system but not in an *in vivo* system. Among other reasons, the lack of efficacy *in vivo* could be due to delivery, biodistribution, and pharmacokinetics. A second possible explanation is that the mechanism by which the ASO functions in human cells is not active in mouse cells. These hypotheses can be addressed by treating mouse cells grown in culture with the 5'UTR 2'MOE.

We isolated mouse embryonic fibroblasts (MEFs) from the Hsieh-Li mice. After expanding the fibroblasts, I treated them with the 5'UTR 2'MOE or the non-targeting control (NTC) 2'MOE. As a positive control, I treated the MEFs from one embryo with a splice-switching oligonucleotide (SSO) which targets the ISSN1 sequence in the *SMN2* human transgene and increases exon 7 inclusion. While the SSO increased SMN protein levels, the 5'UTR 2'MOE did not have a significant effect on SMN protein levels in fibroblasts isolated from SMA embryos (Figure 3.3A and 3.3B). I simultaneously tested the 5'UTR 2'MOE on MEFs isolated from heterozygous embryos since our data examining *SMN2* expression in mouse tissue was obtained using heterozygous mice (Figure 3.3A). As in SMA MEFs, ASO treatment had no effect on SMN levels in heterozygous MEFs. These results indicate that the 5'UTR 2'MOE works in a species-specific manner.

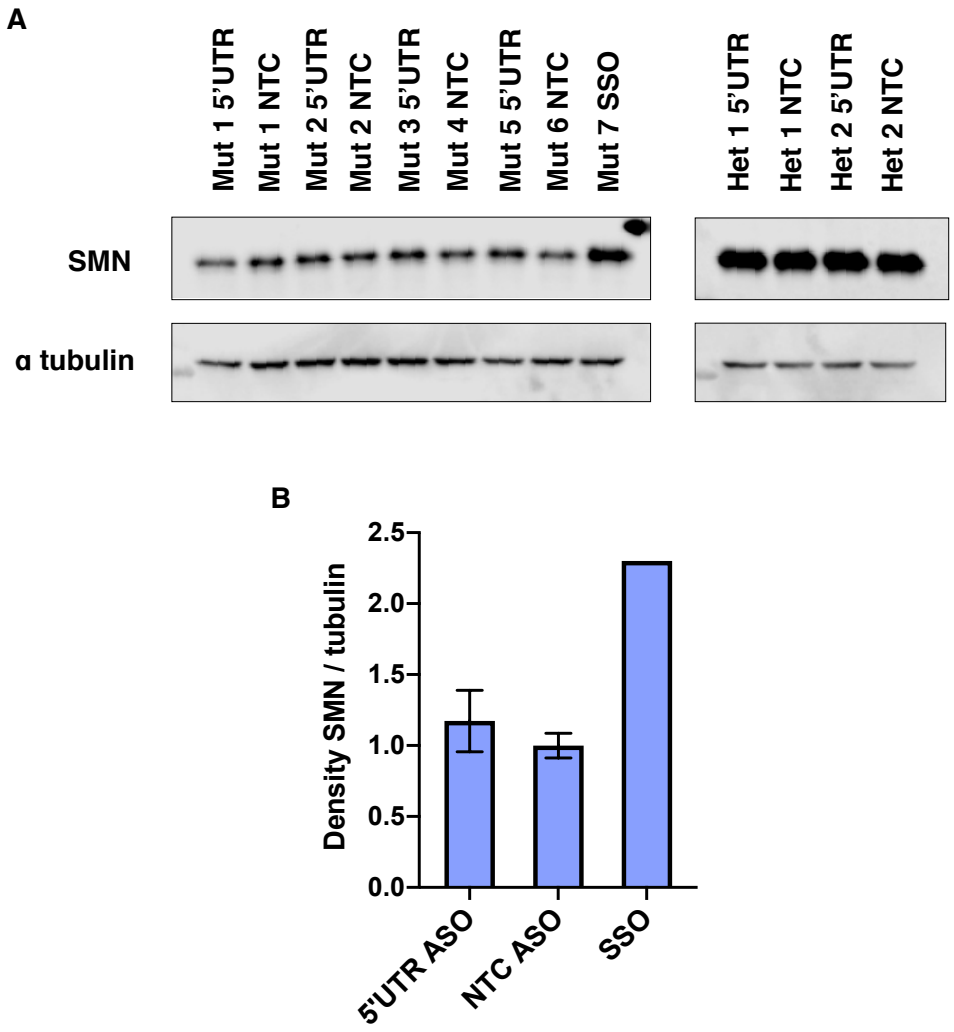

Figure 3.3 The 5'UTR ASO does not increase SMN levels in cultured mouse cells. A) Immunoblot (20 μg per lane) showing SMN protein levels from mouse embryonic fibroblasts treated with 150 nM 2'MOE ASOs. The SSO was used as a transfection positive control and was in the 2'OMe chemistry. Mut = mutant (SMA genotype); Het = heterozygous (control genotype). The number in the sample name indicates the embryo from which cells were isolated and grown. B) Densitometry from immunoblot of mutant cells in panel A. SMN protein levels were normalized to alpha tubulin and then calculated as a fold change relative to SMN levels in cells treated with the NTC ASO. Error bars show propagated error.

3.4.4 INCREASING SMN IN A DISEASE-RELEVANT, HUMAN CELL TYPE

After obtaining negative results in the mouse model, we returned to a human system for further analysis. Ultimately, the cell type of highest interest for SMN restoration in SMA is the motor neuron since the primary disease pathology is death of alpha motor neurons. ASO characterization was, to this point, completed in fibroblasts. Transcription start sites, uORF recognition by ribosomes, and regulatory RNP levels vary from one tissue type to another, so we asked whether the 5'UTR ASO leads to SMN induction in this disease-relevant cell type.

We[5] tested a 5'UTR ASO in motor neuron-like cells chemically differentiated from SMA patient-derived iPSCs (Supplementary Table 7.11). Due to the fragility of the motor neuron-like cells and their resulting intolerance of lipid-based transfection reagents, we tested a PMO conjugated to a cell-penetrating peptide (pPMO) which avoids the need for any vehicle or transfection reagents for delivery. We found that low dose (500 nM) treatment with a Pip9b2-conjugated 5'UTR pPMO increases SMN protein levels in motor neuron-like cells modeling type I SMA, type II SMA, and type III SMA (Figures 3.4B and 3.4C). This is compared to cells treated with a control Pip9b2 pPMO (sequence: 5'-CAG_7). This control pPMO which was developed for myotonic dystrophy (DM1) targets the CUG expansion in *DMPK* and we do not expect it to change *SMN2* expression (Klein et al. 2019).

[5] Sukrat Arya (Talbot Lab, Nuffield Department of Clinical Neurosciences, University of Oxford) treated his motor neuron-like cells with our pPMO and completed the Western blotting.

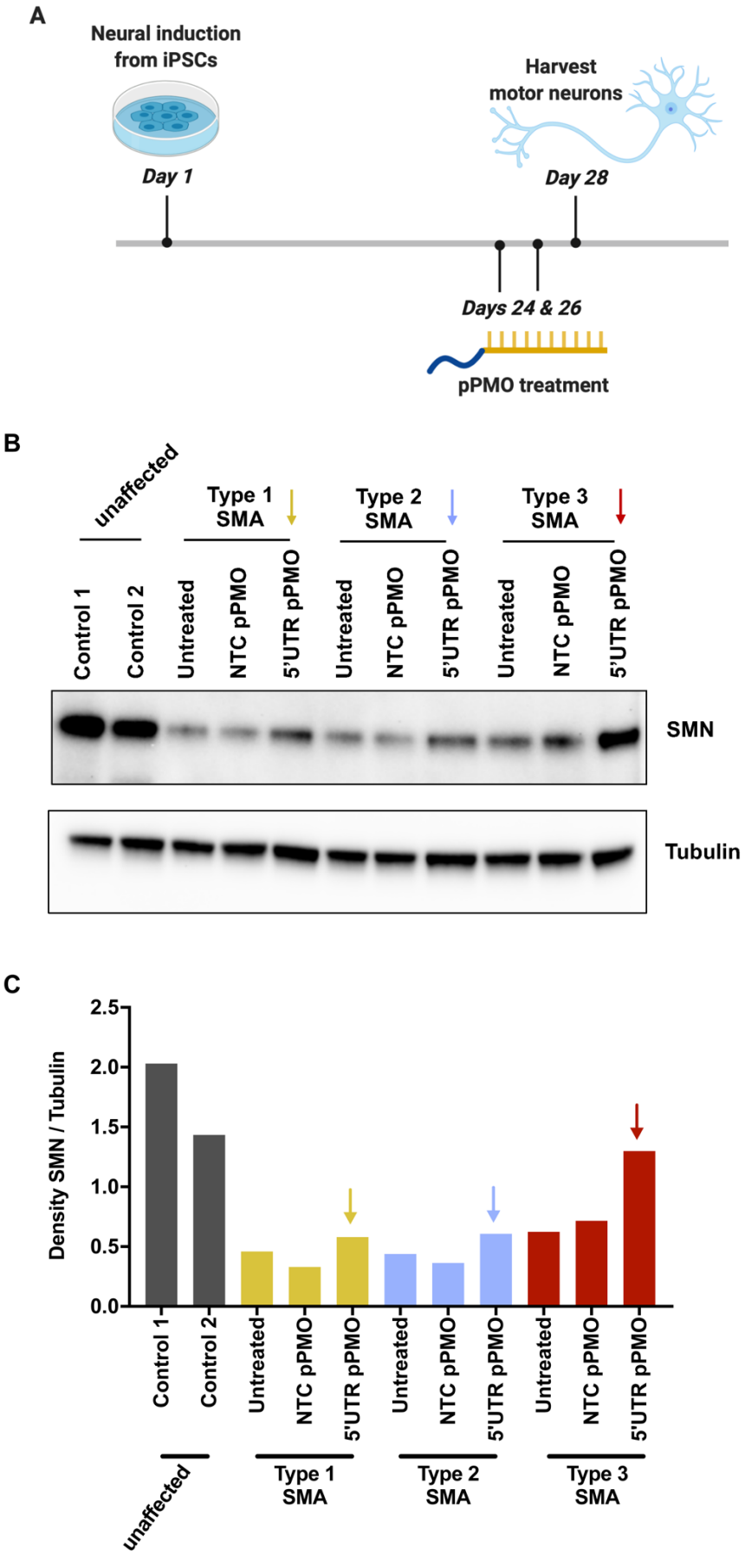
A
Neural induction
from iPSCs
Day 1
Harvest
motor neurons
Day 28
Days 24 & 26
pPMO treatment
B
unaffected
Type 1
SMA
Type 2
SMA
Type 3
SMA
Control 1
Control 2
Untreated
NTC pPMO
5'UTR pPMO
Untreated
NTC pPMO
5'UTR pPMO
Untreated
NTC pPMO
5'UTR pPMO
SMN
Tubulin
C
Density SMN / Tubulin
2.5
2.0
1.5
1.0
0.5
0.0
Control 1
Control 2
Untreated
NTC pPMO
5'UTR pPMO
Untreated
NTC pPMO
5'UTR pPMO
Untreated
NTC pPMO
5'UTR pPMO
unaffected
Type 1
SMA
Type 2
SMA
Type 3
SMA

Figure 3.4 The 5'UTR pPMO increases SMN protein levels in iPSC-derived motor neurons. A) Schematic illustrating timing of treatment and protein extraction in the motor neuron differentiation process. In total, cells were exposed to pPMO for 4 days. B) Immunoblot (4-12% Bis-Tris gel) of motor neuron-like cells (MNs) chemically differentiated from iPSCs derived from control, type I SMA, type II SMA, or type III SMA individuals. MNs were treated with 0.5 μM 5'UTR pPMO or 1 μM NTC pPMO. B) Densitometry from immunoblot in panel B. SMN protein levels were normalized to alpha tubulin. n = 1 per cell line.

3.5 DISCUSSION

The availability of animal models that accurately reflect disease is imperative to therapeutics development. Indeed, lack of good model systems has impeded ASO development for other diseases (Lek et al. 2015; Ansseau et al. 2017). The SMA research community is fortunate to have many model systems in which to study regulation of *SMN2* expression and basic diseases mechanisms. These models have been especially valuable for studying neuromuscular junction and motor neuron pathologies in SMA, since these cannot be readily studied in human tissue samples (except in the case of autopsy). The development of iPSC-derived motor neurons has begun to bridge this gap.

We tested our 5'UTR ASO in motor neuron-like cells differentiated from SMA iPSCs. In these cells, we saw increased SMN protein levels following ASO treatment. Repeating this experiment in order to obtain replicate values for each cell line is important and will enable us to perform statistical analyses. Moving forward, this model system will allow us not only to study the effects of our ASO on the regulation of *SMN2* expression, but also to determine whether there is treatment-associated correction of phenotypic markers, such as a reduction in cleaved caspase-3.

SMA animal models have been critical for preclinical testing of many drug candidates. In our study, we did not see the dramatic effect that early, rapid induction of SMN can have on the SMA phenotype. It is possible that the effect size of the 5'UTR ASO on the SMA phenotype is too small to see with the number of mice we used. However, increasing our *n* is not warranted since phenotypic correction is not expected without SMN restoration and we did not

observe increased *SMN2* mRNA levels in SMA tissues or increased SMN protein levels in mouse embryonic fibroblasts.

The mouse model used in our therapeutics study contains a 115 kilobase DNA insertion containing the human *SMN2* gene (Hsieh-Li et al. 2000). The insertion encompasses the gene upstream of *SMN2* (centromeric *SERF1*) in its entirety and a portion of the gene downstream of *SMN2* (centromeric *NAIP*). Thus, the human *SMN2* untranslated regions, promoter elements, and regulatory features contained in the intergenic region are present in these mice. This means, therefore, that the observed species specificity is not likely related to the absence of critical human *SMN2* sequence in the mouse but is due instead to how *SMN2* expression is controlled by mouse *trans*-factors. However, we did not sequence the human insert in these mice, so we did not rule out the presence of an unrecognized sequence variant which prevents 5'UTR ASO efficacy.

There are two known *SMN2* transcription start sites. One of these generates a transcript with a 5'UTR that is 163 nucleotides long. The other transcription start site generates a transcript with a 5'UTR that is 246 nucleotides long. This further upstream transcription start site is used in human fetal tissues (Germain-Desprez et al. 2001). I have not confirmed from which site transcription initiation occurs in the Hsieh-Li mouse model. I and others (personal communication with the Sumner lab) have been unsuccessful in performing a 5' rapid amplification of cDNA ends (RACE) for the *SMN2* transcript, perhaps due to a secondary structure at the 5' end of the RNA that inhibits adapter ligation or reverse transcription. If the start site in the mouse is different from that in human fibroblasts, this could explain the lack of ASO efficacy in mouse cells. Compared to the shorter 5'UTR, the longer 5'UTR may form significantly different secondary

structures and harbor sequence motifs that recruit different sets of proteins, perhaps eliminating the opportunity for ASO-mediated *SMN2* upregulation. Additionally, if ASO proximity to the 5' cap is critical for ASO function, the 83-nucleotide gap between the first base of the longer 5'UTR and the ASO binding site may eliminate its activity.

Another potential explanation for the species-specific effect is that the steric blocking capacity or molecular sponge activity of the 5'UTR 2'MOE is unnecessary in the mouse because the protein or non-coding RNA with which it interacts is not present. The precise mechanism of action of the 5'UTR 2'MOE remains unclear. When the mechanism is established through further experiments in human cells (e.g., when the *trans*-acting factor that the ASO is blocking, sequestering, etc. is identified), I can look in the mouse tissue to see whether that factor is expressed. If absent or only lowly expressed in mouse tissue, this would not only explain the lack of efficacy in mice but would also serve as a validation of the proposed mechanism.

In any case, the untranslatability of our particular approach into the Hsieh-Li SMA mouse model is an obstacle to preclinical development. It is possible that a different SMA mouse model (i.e., the delta 7 model) would yield a different result. Future studies performed in a humanized mouse model may be insightful. Such models have been generated, especially for use in immunology research (Murphy et al. 2014). Alternatively, a porcine SMA model has recently been published (Duque et al. 2015). This particular pig could not be used for our study as it models the disease via viral delivery of shRNA against endogenous pig SMN and thus does not have the human sequence our ASO targets. Preliminary work was done toward the creation of a porcine model with the human transgene

inserted, which may be an option for future preclinical studies (Lorson et al. 2011).

Chapter 4

General Discussion and Concluding Remarks

4.1 ADVANTAGES AND LIMITATIONS OF SMA THERAPEUTICS

The success of nucleic acid therapeutics for SMA is altering the disease course in clinically meaningful ways, but challenges remain. Clinical trials over recent years have shown that post-symptomatic treatment with SMN-targeted therapeutics does not completely correct the neuromuscular phenotype. The degree of phenotypic correction is better with initiation of treatment early in the disease course. Even so, there are 'non-responders' who do not benefit from currently available therapeutics.

In contrast, when SMA infants are treated presymptomatically (and before 6 weeks of age) with nusinersen or AVXS-101, some follow the developmental trajectory of unaffected children. However, while 100% of infants treated with nusinersen presymptomatically achieved independent sitting, 4 out of 25 did not meet this milestone within the timeframe considered healthy by the World Health Organization (WHO) (De Vivo et al. 2019). 73% of infants achieved the ability to walk independently within the WHO-specified timeframe. Of presymptomatically treated infants with 2 copies of *SMN2*, 47% presented with SMA symptoms by 24 months of age. These clinical manifestations were milder than expected, however, based both on natural history data and the disease course of their affected siblings. Two major takeaways from this study are 1) the importance of newborn screening for SMA in order to initiate early treatment and 2) the observation that even presymptomatic treatment does not always prevent disease onset.

One explanation for the incomplete amelioration of phenotype includes the possibility that motor neuron degeneration had begun before drug administration, even though it was not detectable clinically. An outstanding question in the field

is precisely when does SMA pathogenesis begin (and thus, when is therapeutic intervention required?). In addition, it is possible that the ASO did not distribute throughout the nervous system sufficiently. This point reflects another outstanding question in the field, which is where are increased levels of SMN required (and thus, where must therapeutic compounds be adequately delivered?). Finally, it may be that the level of SMN induction was insufficient to prevent motor neuron loss. This last point, in particular, highlights the need for combinatorial therapeutic strategies, such as the 5'UTR ASO.

4.2 COMBINATION THERAPIES

Combinatorial therapeutics for SMA are a popular area of investigation. Several approaches are being pursued using different combinations of SMN-dependent and SMN-independent strategies. A recent study examined the effect of co-administration of the HDAC inhibitor LBH589 with a nusinersen-like SSO (Pagliarini et al. 2019). Treating SMA fibroblasts with a low dose of the nusinersen-like SSO and a suboptimal dose of LBH589 significantly improves the efficacy of the SSO. In fact, the increase in SMN seen with low doses of LBH589 and SSO is comparable to the increase in SMN seen with a 5-fold higher dose of SSO alone. The possibility of increased efficacy with lower doses may allow for improved patient outcomes with reduced side effects. Furthermore, this may enable the use of compounds that, though efficacious, have a narrow therapeutic window.

SMA genetic modifiers identified through population studies have revealed therapeutic candidates that can be pursued in combinatorial strategies involving SMN-dependent plus SMN-independent approaches. A gapmer was developed

for one such genetic modifier, neurocalcin delta (*NCALD*), since it was previously observed that low *NCALD* expression has protective effects on the SMA phenotype (Riessland et al. 2017). Mice injected with a low dose of SSO followed by a gapmer that knocks down NCALD have improved electrophysiological findings and improved motor function compared to those mice that only receive a low dose of SSO (Torres-Benito et al. 2019).

An SMN-restoring drug can also be paired with a therapeutic that is not SMA-specific. Myostatin inhibition, for example, is a viable therapeutic strategy for many diseases in which muscle atrophy occurs (including Duchenne muscular dystrophy). Antibody-based and viral-based approaches to blocking the myostatin pathway with concurrent SSO treatment improve muscle mass and strength in SMA mice (Long et al. 2019; Zhou et al. 2020).

Combination therapies are beginning to be tested in humans. For example, with regulatory approval of both nusinersen and AVXS-101, this pairing has been used in conjunction in infants with SMA type 1 (Lee et al. 2019). Additionally, as SMN inducing compounds become commercially available and part of the standard of care for SMA, it will become practically (and ethically) unfeasible to run clinical trials in drug naïve populations. A clinical trial for the myostatin monoclonal antibody-based inhibitor SRK-015 is underway, in which participants are permitted to receive nusinersen (Long et al. 2019) (NCT03921528, ClinicalTrials.gov).

The 5'UTR ASO described here represents a novel target for SMN induction with a primary mechanism of action that is independent from that of splice-switching compounds. I showed that, when used in combination with a SSO, our ASO increases SMN levels above those achieved with the SSO alone.

Thus, this ASO, or a compound that similarly acts to stabilize the *SMN2* mRNA, should be considered as a combinatorial approach for treating SMA.

4.3 REGULATION OF *SMN2* EXPRESSION

SMN protein levels change during development, with a significant reduction of SMN occurring in spinal cord and muscle between the fetal and postnatal stages (Ramos et al. 2019). Additionally, *SMN2* mRNA levels decrease between prenatal and early postnatal development. SMN levels also vary across cell types (Ramos et al. 2019, Human Protein Atlas). Untranslated regions are candidate sites to identify such elements that tune SMN expression across tissue types and during development. Elucidation of the mechanism of action of the 5'UTR ASO will not only enable a better understanding of the therapeutic agent (and potentially facilitate its optimization), but it should also inform our understanding of the regulation of *SMN2* expression.

Genetic experiments to test whether the 5'UTR ASO is working by direct base-pairing to the 5' UTR of *SMN2* will be important. This could be tested in a reporter construct (similar to Figure 2.3A) by changing nucleotides in the target and/or ASO sequence that would be expected to either disrupt or restore base-pairing in this region. These experiments may be helpful in determining the mechanism of action of the ASO.

4.4 SPLICE-SWITCHING FOR N-OF-1 THERAPY

The experience with SMA can inform therapeutics development for a broad range of patients with neurological disorders. The accelerated disease-gene identification enabled by sequencing technologies has been met with an

increase in the targeting of these genes with sequence-based approaches. In a pioneering N-of-1 study, Kim et al. went from mutation identification to clinical application of an ASO for a 6-year-old patient in under one year's time (Kim et al. 2019). A clinical diagnosis of Batten's disease was genetically confirmed by whole-genome sequencing, which revealed a retrotransposon insertion leading to activation of a cryptic splice site in *CLN7*. A panel of ASOs designed to correct the missplicing event were screened in patient fibroblasts. Following toxicology studies in rodents, one of the ASOs, later termed milasen, was administered to the patient after approval of an Expanded-Access Investigational New Drug Application by the US Food and Drug Administration (FDA). Clinical data indicated decreased frequency and duration of seizures in the patient after ASO treatment.

The speed with which milasen reached the clinic can be partially attributed to the development and 2016 FDA approval of nusinersen for SMA. Milasen and nusinersen are similar in size, have the same chemical modifications (fully modified with phosphorothioate linkages and 2'MOE bases), and both are targeted toward the CNS (Finkel et al. 2017; Kim et al. 2019). This allowed Yim et al. to design the clinical trial protocol and calculate appropriate doses of milasen on the basis of the FDA-approved regimen for nusinersen. This example highlights how increasing experience in bringing ASOs to the clinic may facilitate the process for other diseases. Perhaps ASOs for Fukuyama muscular dystrophy, similarly caused by retrotransposon insertion, will follow suit (Taniguchi-Ikeda et al. 2011).

The N-of-1 milasen success story forecasts ethical challenges pertaining to societal responsibility that will no doubt become commonplace. With the

accessibility of sequencing technologies resulting in the identification of very rare mutations and with feasible options for their therapeutic correction, what will it take to deliver personalized medicine to populations of smaller and smaller size?

4.5 5'UTR TARGETING BEYOND *SMN2*

Determining the mechanism of action of the 5'UTR ASO may reveal that this approach can be applied to increase the expression of other genes in a targeted manner. For example, up-regulating utrophin may be used for the treatment of Duchenne muscular dystrophy (Shieh 2018). With more than 6500 hereditary diseases with known genetic cause (https://omim.org/), we hope that, through shared experience, the field can accelerate the rate at which treatments are developed.

Chapter 5

MATERIALS AND METHODS

5.1 ANTISENSE OLIGONUCLEOTIDE SYNTHESIS

Three types of ASOs were used in this study: (1) those fully modified with 2'-O-methyl (2'OMe) bases and phosphorothioate linkages; (2) those fully modified with 2′-O-(2-methoxyethyl) (2'MOE) bases and phosphorothioate linkages; (3) phosphorodiamidate morpholino oligomers (PMOs). All 2'OMe and 2'MOE ASOs were purchased from Integrated DNA Technologies (IDT). PMOs were purchased from Gene Tools, LLC and subsequently conjugated to Pip9b2 as described previously. ASO sequences are provided in Supplementary Table S1.

5.2 CELL CULTURE

SMA patient (Coriell GM00232 and GM03813) and carrier (Coriell GM03814) fibroblasts were cultured in Dulbecco's Modified Eagle Medium (DMEM) supplemented with 15% fetal bovine serum (FBS) and maintained in a 37°C incubator with 5% CO_2. Fibroblast transfections were performed using RNAiMAX transfection reagent (Invitrogen). For each well of a 6-well plate, ASOs or siRNA were complexed with 7.5 µL RNAiMAX in 300 µL Opti-MEM and added to cells at 70% confluency. The next day, media was changed to remove transfection reagents, and cells were harvested two days post-transfection (unless stated otherwise in the figure legends). The siRNAs used in these transfections were DCP2 (Dharmacon, 167227), DCPS (Dharmacon, 28960), DXO (Dharmacon, 1797), NUDT3 s22028 (Thermo Fisher Scientific), NUDT16 (Dharmacon, 131870), SMN1/SMN2 (Thermo Fisher Scientific, s446415), XRN2 (Thermo Fisher Scientific, s22412), Negative Control No. 1 (Thermo Fisher

Scientific, 4390843), siGENOME Non-Targeting siRNA #2 (Dharmacon, D-001210-02-05).

HEK293T cells (ATCC) were cultured in DMEM supplemented with 10% FBS and maintained in a 37°C incubator with 5% CO_2. Plasmids were transfected using Lipofectamine 3000 (Invitrogen). Each well of a 6-well plate was transfected with 1 µg DNA complexed with 3.75 uL Lipofectamine 3000 reagent and 4 uL P3000 reagent in 250 uL Opti-MEM. Media was changed 24 hours later, and cells were harvested two days after transfection.

Induced pluripotent stem cells (iPSCs) were derived from fibroblasts in the James Martin Stem Cell Facility, University of Oxford, using the method indicated in Supplementary Table S11. iPSCs were differentiated into motor neuron-like cells as described previously (Dafinca et al. 2016; Ababneh et al. 2019). Briefly, the iPSCs were grown on Matrigel. They were then induced using equal volumes of DMEM/F12 and Neurobasal medias supplemented with N2, B27, ascorbic acid (0.5 µM), 2-mercaptoethanol, compound C (3 µM) and Chir99021 (3 µM). After 4 days in culture, media was further supplemented with retinoic acid (1 µM) and smoothened agoinst (500 nM). The following day, the media was changed to media without compound C and Chir99021. The cells were then cultured for 4–5 additional days before being split 1:3. After splitting, the media was supplemented with growth factors BDNF (10 ng/mL), GDNF (10 ng/mL), N-[N-(3,5-Difluorophenacetyl)-L-ala- nyl]-S-phenylglycine t-butyl ester (DAPT) (10 mM), and laminin (0.5 mg/mL) for 7 days. DAPT and laminin were then removed from the media, and the neurons remained in culture until day 28. Neurons were treated with ASOs (with no transfection reagents) on day 24 and again on day 26, before collection on day 28.

5.3 CLONING

To test the effect of the upstream start codon on gene expression, reporter constructs were created using the pBI-CMV4 bidirectional promoter vector (Takara Bio). The plasmid backbone was double digested with BglII and EcoRI and gel extracted using the NucleoSpin Gel and PCR Clean-Up kit (Takara Bio). Then, DsRed2 was replaced with PCR-amplified mCherry using the In-Fusion HD Cloning Plus kit (Takara Bio). Mini-prepped mCherry plasmid was double digested with BamHI and NotI for insertion of the reporter protein coding sequence. As template for the reporter, we used a gBlocks Gene Fragment (IDT) containing the 5'UTR of *SMN2* followed by the coding sequence of enhanced green fluorescent protein (eGFP) followed by exon 2 through exon 3 of *HBB*. The gBlocks Gene Fragment was PCR amplified using CloneAmp HiFi PCR Premix (Takara Bio) and 500 nM each primer, where the forward primer contained the desired uORF mutation(s). Primer sequences are provided in Supplementary Table S3. One of the reporters ("frame shift") required a second gBlocks Gene Fragment in order to obtain a plasmid with the desired mutation (Supplementary Table S2). These PCR products and digested plasmids were gel extracted and cloned using the In-Fusion HD Cloning Plus kit (Takara Bio), as above.

For all cloning work, One Shot TOP10 Chemically Competent *E. coli* (Invitrogen) were transformed with In-Fusion reaction products. Plasmids were extracted from bacterial cultures using the QIAprep Spin Miniprep Kit (QIAGEN) and tested by restriction enzyme digest. Selected clones were expanded and plasmids extracted using the HiSpeed Plasmid Maxi Kit (QIAGEN). The sequences of inserted DNA fragments were verified in all plasmids by Sanger

sequencing (GENEWIZ). Details of primers used for sequencing are provided in Supplementary Table S4.

5.4 IMMUNOBLOTTING

Lysates were prepared in RIPA buffer (50mM Tris-HCl pH 8.0, 150mM NaCl, 5mM EDTA, 1% NP-40 (IGEPAL), 1% sodium deoxycholate, 0.1% SDS) supplemented with Halt Protease and Phosphatase Inhibitor Cocktail (Thermo Fisher Scientific) or cOmplete Protease Inhibitor Cocktail (Roche). After lysing on ice, samples were centrifuged (15 min, 14,000 x g, 4°C) to remove pelleted material. Protein concentrations were determined by Bradford assay using Protein Assay Dye Reagent Concentrate (Bio-Rad). Samples were then prepared in RIPA and 4x sample loading buffer (H_2O, Tris-HCl, 40% glycerol, 0.08 g/mL sodium dodecyl sulfate (SDS), 5% (vol/vol) 2-mercaptoethanol, Bromophenol blue). Proteins were resolved on Novex 4-20% Tris-Glycine WedgeWell gels (Invitrogen) and transferred to 0.45 μm PVDF membrane. The µg amount of protein loaded per lane is indicated in the relevant figure legend. Membranes were blocked with 5% (wt/vol) milk in Tris-buffered saline and 0.1% Tween (TBST) before incubation with primary antibodies at the indicated dilutions: mouse anti-SMN (BD Biosciences 610647, 1:1000 dilution), anti-Gemin6 (Abcam ab88290, 1:500 dilution), and anti-Gemin8 (Abcam ab46778, 1:1000 dilution), rabbit anti-alpha tubulin (Abcam ab4074, 1:5000 dilution; or Cell Signaling 2144, 1:2000), rabbit anti-HSP90 (Cell Signaling 4874, 1:5000 dilution), rabbit anti-GFP (Abcam ab290, 1:10000 dilution), mouse anti-mCherry (Abcam ab125096, 1:2000 dilution). Membranes were then incubated with either IRDye or HRP secondary antibodies and detected on a LI-COR Odyssey or a Bio-Rad

ChemiDoc XRS+ imaging system, respectively. Primary antibodies and secondary antibodies incubated overnight at 4°C or one hour at room temperature with shaking and were followed by three washes with TBST. Densitometric analysis of protein signal was done using ImageJ software.

5.5 RNA STABILITY ASSAY

For mRNA stability assays, fibroblasts were transfected with 600 nM 2'OMe ASOs as described above. Two days post-transfection, fibroblasts were treated with media containing 5 µg/mL actinomycin D (Sigma Aldrich). The cells were then collected in 0.5 mL TRIzol at the indicated time points after treatment with actinomycin D. After adding 100 µL chloroform, the samples were vortexed and centrifuged (15 min, 12,000 x g, 4°C). The supernatant was transferred to a new tube, to which 1.5 volumes of 100% ethanol were added. The samples were then pipetted into columns and RNA purification continued according to the miRNeasy Mini Kit manual (QIAGEN). Total RNA was converted into cDNA using the High Capacity cDNA Reverse Transcription Kit (Applied Biosystems). qRT-PCRs were performed in triplicate using the QuantStudio 6 Flex Real-Time PCR System (Applied Biosystems). 10 µL qRT-PCR reactions contained Power Sybr Green (Applied Biosystems) with 200 nM of each target primer and cDNA diluted in nuclease-free water (to a concentration for which primers have 90-110% efficiency). Primer sequences are provided in Supplementary Table S5.

5.6 TRANSCRIPTION ASSAY

Transcription was measured using the Click-iT Nascent RNA Capture Kit (Invitrogen). In summary, 3 days after ASO transfection, SMA fibroblasts were

pulsed with 0.5 mM 5-ethynyl uridine (EU) for one hour and then collected in 0.5 mL TRIzol. 100 µL chloroform were added to each sample, which was then vortexed and centrifuged (15 min, 12,000 x g, 4°C). The supernatant was transferred to a new tube and 1.5 volumes of 100% ethanol were added. The samples were then pipetted into columns and RNA purification continued according to the RNeasy Mini Kit manual (QIAGEN).

750 ng purified RNA was used in each Click reaction. Subsequently, 400 ng biotinylated RNA were mixed with 25 µL magnetic bead suspension for each binding reaction. After washing away un-bound RNA, on-bead cDNA synthesis was performed using the SuperScript VILO cDNA synthesis kit (Thermo Fisher Scientific) in a 50 µL final reaction volume. 500 ng total RNA (pre-biotinylation) was also converted to cDNA in a 15 µL reaction using the SuperScript VILO cDNA synthesis kit, which represents steady-state mRNA.

RT-qPCRs were performed as 20 µL reactions in triplicate. Reactions contained Power Sybr Green (Applied Biosystems), 200 nM of each target primer, 1 µL cDNA, and nuclease-free water. cDNA of total RNA was diluted 1:4 in nuclease-free water, while cDNA of biotinylated RNA was undiluted. RT-qPCR plates were run on the StepOnePlus Real-Time PCR System (Applied Biosystems).

5.7 SPLICE ISOFORM ANALYSIS

SMN2 exon 7 splicing was qualitatively assessed by performing gel electrophoresis of RT-PCR products. First, RNA was extracted and cDNA was converted according to the protocol described above for the RNA stability assay. The cDNA from ASO-treated samples was used as template for PCR. The

reaction was performed with PCR Master (Roche) and with primers situated in exon 5 and exon 8 of *SMN2*. Primer sequences are provided in Supplementary Table S6. Amplicons were resolved on 2% agarose gels. To ensure that the full-length amplicon did not sequester the Δ7 amplicon, a test run was performed in which samples were diluted, denatured by heating to 95°C for 5 min, and then immediately placed on ice until being loaded on a gel. The results were consistent between heated and unheated samples, so the extra denaturing and steps were omitted.

Exon 7 splicing was quantitatively assessed for the same samples using the RT-qPCR protocol described for the RNA stability assay.

5.8 PULL-DOWN AND MASS SPECTROMETRY

Dynabeads MyOne Streptavidin C1 (Thermo Fisher Scientific) were resuspended by gently vortexing. The desired volume of beads (1 mg beads (100 µL) per pull-down) were transferred to a new tube and washed three times with Binding Buffer (1x phosphate-buffered saline with 0.2% Tween-20). For each pull-down, 1.5 nmol ASO with a 5' Biotin-TEG attachment (IDT) were added to 1 mg washed beads, for a total volume of 100 µL. Binding of the biotinylated ASOs to the magnetic beads was allowed to proceed for 30 min at room temperature with shaking. After 30 min, ASO-coated beads were washed three times with binding buffer. 2, 15 cm plates of SMA fibroblasts per condition were trypsinized and washed in PBS, and pelleted. The cell pellets were re-suspended in ice cold Pierce IP Lysis Buffer (Thermo Fisher Scientific) + 1x Halt Protease and Phosphatase Inhibitor Cocktail. The samples were incubated on ice for ~45 min, mixing periodically. The lysates were centrifuged at 13,000 x g

for 10 min at 4ºC to remove cell debris. The ASO-coated beads were resuspended in 100 µL homogenous lysate and incubated at 30°C with shaking. After 1 hr, the beads were washed ten times using Binding Buffer with 100 mM NaCl. After removing the last wash, a 50 µL volume of elution buffer (20 mM Hepes, 100 mM NaCl) with 3 nmol non-biotinylated ASO were added to the beads and placed back on the 30°C agitator block for an additional 5 min. The supernatant containing proteins that bound to the competitor ASO was transferred to a new tube, to which 4x sample loading buffer was added. 20% of each sample was run on a 4-20%, 15-well Tris-Glycine gel. The gel was then stained with SYPRO Ruby Protein Gel Stain (Thermo Fisher Scientific) according to the Basic Protocol and imaged on a Bio-Rad ChemiDoc XRS+ imaging system.

Pull-downs for each condition (biotinylated 5'UTR ASO, biotinylated NTC ASO, biotinylated Scrambled ASO) were performed in duplicate and in two independent trials (total n=4). In each trial, a negative control was also included in which beads were coated with the biotinylated Scrambled ASO but no competitor ASO was added. Bands of interest were selected for protein identification by mass spectrometry, which was performed by the NINDS Protein/Peptide Sequencing Facility.

The gel bands were cut and washed overnight, reduced by 10 mM tris(2-carboxyethyl)phosphine for 1 hr, alkylated by 10 mM N-ethylmaleimide for 15 min, and digested with trypsin for 18 hr. Then, the extracted peptides were desalted using an Oasis HLB 96-well plate (Waters) and eluted with 100 µL methanol. The peptides were dried using a SpeedVac and resuspend in 0.1% TFA. They were then analyzed on a Fusion Lumos mass spectrometer (Thermo

Fisher Scientific) connected to an Ultimate Ultra3000 chromatography system (Thermo Fisher Scientific) incorporating an auto-sampler. The resuspended peptides were loaded onto an ES802 column (25 mm length, 75 µm internal diameter) and separated by an increasing acetonitrile (ACN) gradient, using a 70 min reverse phase gradient increasing mobile phase B (98% ACN, 0.1% formic acid) from 3% to 36% at a flow rate of 300 nL/min. Liquid chromatography tandem-mass spectrometry (LC/MS/MS) data were acquired in data-dependent acquisition (DDA) mode. Database search and label-free quantitation was performed using the Proteome Discoverer 2.4 software.

5.9 RNA-SEQUENCING

GM00232 fibroblasts were treated with 300 nM 2'MOE ASO (5'UTR or NTC, in triplicate). RNA was extracted 3 days post-transfection using TRIzol and the RNeasy Plus Mini Kit (QIAGEN), as described above. The following steps were performed at the NHLBI DNA Sequencing and Genomics Core. RNA quality was checked on the Agilent 2100 Bioanalyzer (model G2938B). Sequencing libraries were constructed from 100 ng – 1,000 ng of total RNA using Illumina's TruSeq Stranded Total RNA kit with Ribo-Zero following the manufacturer's instructions. The quality of sequencing libraries was checked on the MiSeq System (Illumina) and library concentrations were determined using a Qubit instrument (Life Technologies). The libraries were loaded onto the Illumina NOVASEQ 6000 for 2 x 50 bp paired-end read sequencing. FASTQ files were generated using the bcl2fastq software for further analysis.

5.10 BIOINFORMATICS

Ribosome profiling sequencing data from GEO sample accessions GSM1047584, GSM1047585, and GSM3566399 were downloaded in the fastq format using the fastq-dump command supported in the NCBI SRA Toolkit (https://ncbi.github.io/sra-tools/). The FastQC tool (https://www.bioinformatics.babraham.ac.uk/projects/fastqc/) was used to inspect the quality of the sequence data. To clip adaptor sequences that may be present and to remove low quality sequences, the Trimmomatic tool (http://www.usadellab.org/cms/?page=trimmomatic) was used with the following command line specifications: "ILLUMINACLIP:TruSeq3-SE-2.fa:2:30:10 HEADCROP:11 TRAILING:20 SLIDINGWINDOW:4:20 MINLEN:15". Reads were mapped to a custom reference genome. The custom reference genome was constructed by deleting all *SMN* gene annotations from human reference genome hg19 and then, to the modified hg19, adding the 215P15 clone sequence as a separate contig, as described previously (Ruhno et al. 2019). For reference mapping against the customized version of the human genome, the RNA-Seq tool supported in the CLCbio Genomics Workbench (v11) was used under default parameters. Mapped reads were visualized using Integrative Genomics Viewer (IGV) version 2.4.8 (http://software.broadinstitute.org/software/igv/).

A similar pipeline was used to process RNA-Seq data generated from ASO-treated SMA fibroblasts. Quality inspection of the data was completed with the FastQC tool (https://www.bioinformatics.babraham.ac.uk/projects/fastqc/).

The Trimmomatic tool (http://www.usadellab.org/cms/?page=trimmomatic) was again used for adaptor clipping and low quality sequence trimming, but with parameters appropriate for paired-end reads (ILLUMINACLIP:/home/johnsonko/myTools/Trimmomatic/adapters/TruSeq3-PE-2.fa:2:30:10 SLIDINGWINDOW:4:20 MINLEN:15). For reference mapping against the custom reference genome, the RNA-Seq tool supported in the CLCbio Genomics Workbench (v11) was again used under default parameters. Expression for mapped reads was summarized in Transcripts Per Kilobase Million (TPM) units and the resulting mapping files were sorted and indexed using SAMtools (http://samtools.sourceforge.net/).

5.11 MICE

Mouse work was performed in the Biomedical Sciences Unit at the University of Oxford as authorized by the UK Home Office. All mice used in the experiments were the offspring of strain FVB.Cg-*Smn1*^{tm1}*Hung*Tg(SMN2)2Hung/J (Jackson Laboratory 005058) crossed with strain FVB.129P2(B6)-*Smn1*^{tm1Hung}/J (Jackson Laboratory 031678). The mice were bred and maintained as described on the Jackson Laboratory website and as described previously (Gogliotti et al. 2010).

Subcutaneous injections of 2'MOE diluted in 0.9% saline were administered between the shoulders on post-natal day 0 (PND0).

5.12 MOUSE EMBRYONIC FIBROBLAST ISOLATION AND CULTURE

Mouse embryonic fibroblasts (MEFs) were isolated as described previously (Jianming 2005). In brief, on embryonic day 14.5 (E14.5) the uterus was dissected from a pregnant female mouse and washed in sterile PBS. For each embryo therein, the liver, heart, and brain were discarded, and the remaining tissue was washed as above (a piece of discarded tissue was kept for genotyping). Using forceps, the tissue was broken into small pieces in 3 mL ice-cold 0.25% trypsin-EDTA and incubated overnight at 4°C to allow the trypsin to permeate the tissue. The next morning, most of the trypsin solution was aspirated (without disturbing the tissue at the bottom of the tube). The tubes, which contained approximately 2 volumes trypsin solution to 1 volume tissue, were incubated in a 37°C water bath. After 30 min, MEF culture medium (DMEM, 10% FBS, 0.1 mM 2-mercaptoethanol, 50 U penicillin, and 50 µg/ml streptomycin) was added to each tube, and the contents were pipetted vigorously in order to break up the digested tissues. The tubes were then left sitting upright for 1 min. The supernatants (containing cells in suspension) were transferred to new tubes. Additional MEF culture medium was added to the clumps left behind, which were once again vigorously pipetted and allowed to sediment. The supernatants were combined with the previously collected cell suspensions. The cells from each embryo were then plated in separate wells on a 6-well plate. The next day, wells were washed with PBS in order to remove nonadherent cells.

After two additional days of culturing in MEF culture medium, the cells were plated for ASO transfection. For the MEF lines with sufficient cell counts, duplicate wells were plated (one for transfection with the 5'UTR ASO and one for transfection with the non-targeting control ASO). Single wells were plated for the

MEF lines with fewer cells. The MEFs were transfected with 150 nM ASO using RNAi MAX as described above. Three days later, the MEFs were collected in RIPA buffer and subsequently assayed by immunoblotting.

5.13 DATA PRESENTATION

Data was analyzed in Microsoft Excel and graphs were made using GraphPad Prism 8. Some schematics were created using BioRender.com. Figures were assembled in Microsoft PowerPoint and Adobe Illustrator.

Chapter 6

REFERENCES

Ababneh N, Scaber J, Flynn R, Douglas A, Turner MR, Sims D, Dafinca R, Cowley SA, Talbot K. 2019. Correction of amyotrophic lateral sclerosis related phenotypes in induced pluripotent stem cell-derived motor neurons carrying a hexanucleotide expansion mutation in C9orf72 by CRISPR/Cas9 genome editing using homology-directed repair. bioRxiv. doi:10.1101/2019.12.17.864520.

Adams D, Gonzalez-Duarte A, O'Riordan WD, Yang CC, Ueda M, Kristen A V., Tournev I, Schmidt HH, Coelho T, Berk JL, et al. 2018. Patisiran, an RNAi therapeutic, for hereditary transthyretin amyloidosis. N Engl J Med. 379(1):11–21. doi:10.1056/NEJMoa1716153.

Akten B, Kye MJ, Hao LT, Wertz MH, Singh S, Nie D, Huang J, Merianda TT, Twiss JL, Beattie CE, et al. 2011. Interaction of survival of motor neuron (SMN) and HuD proteins with mRNA cpg15 rescues motor neuron axonal deficits. Proc Natl Acad Sci U S A. 108(25):10337–10342. doi:10.1073/pnas.1104928108.

Alterman JF, Godinho BMDC, Hassler MR, Ferguson CM, Echeverria D, Sapp E, Haraszti RA, Coles AH, Conroy F, Miller R, et al. 2019. A divalent siRNA chemical scaffold for potent and sustained modulation of gene expression throughout the central nervous system. Nat Biotechnol. 37(8):884–894. doi:10.1038/s41587-019-0205-0.

Ansseau E, Vanderplanck C, Wauters A, Harper SQ, Coppée F, Belayew A. 2017. Antisense oligonucleotides used to target the DUX4 mRNA as therapeutic approaches in faciosscapulohumeral muscular dystrophy (FSHD). Genes (Basel). 8(3). doi:10.3390/genes8030093.

Avila AM, Burnett BG, Taye AA, Gabanella F, Knight MA, Hartenstein P, Cizman Z, Di Prospero NA, Pellizzoni L, Fischbeck KH, et al. 2007. Trichostatin A increases SMN expression and survival in a mouse model of spinal muscular atrophy. J Clin Invest. 117(3):659–671. doi:10.1172/JCI29562.

Barbosa C, Peixeiro I, Romão L. 2013. Gene expression regulation by upstream open reading frames and human disease. PLoS Genet. 9(8):1–12. doi:10.1371/journal.pgen.1003529.

Bebee TW, Dominguez CE, Chandler DS. 2012. Mouse models of SMA: tools for disease characterization and therapeutic development. Hum Genet. 131(8):1277–1293. doi:10.1007/s00439-012-1171-5.

Bennett CF, Krainer AR, Cleveland DW. 2019. Antisense oligonucleotide therapies for neurodegenerative diseases. Annu Rev Neurosci. 42(1):385–406. doi:10.1146/annurev-neuro-070918-050501.

Boardman FK, Sadler C, Young PJ. 2018. Newborn genetic screening for spinal muscular atrophy in the UK: The views of the general population. Mol Genet Genomic Med. 6(1):99–108. doi:10.1002/mgg3.353.

Boemer F, Caberg JH, Dideberg V, Dardenne D, Bours V, Hiligsmann M, Dangouloff T, Servais L. 2019. Newborn screening for SMA in Southern Belgium. Neuromuscul Disord. 29(5):343–349. doi:10.1016/j.nmd.2019.02.003.

Bolduc V, Reghan Foley A, Solomon-Degefa H, Sarathy A, Donkervoort S, Hu Y, Chen GS, Sizov K, Nalls M, Zhou H, et al. 2019. A recurrent COL6A1 pseudoexon insertion causes muscular dystrophy and is effectively targeted by splice-correction therapies. JCI Insight. 4(6). doi:10.1172/jci.insight.124403.

Bolduc V, Zou Y, Ko D, Bönnemann CG. 2014. siRNA-mediated allele-specific silencing of a COL6A3 mutation in a cellular model of dominant ullrich muscular dystrophy. Mol Ther - Nucleic Acids. 3. doi:10.1038/mtna.2013.74.

Bowerman M, Anderson CL, Beauvais A, Boyl PP, Witke W, Kothary R. 2009. SMN, profilin IIa and plastin 3: A link between the deregulation of actin dynamics and SMA pathogenesis. Mol Cell Neurosci. 42(1):66–74. doi:10.1016/j.mcn.2009.05.009.

Bowerman M, Becker CG, Yáñez-Muñoz RJ, Ning K, Wood MJA, Gillingwater TH, Talbot K. 2017. Therapeutic strategies for spinal muscular atrophy: SMN and beyond. DMM Dis Model Mech. 10(8):943–954. doi:10.1242/dmm.030148.

Brzustowicz L, Lehner T, Castilla L, Penchaszadeh G, Wilhelmsen K, Daniels R, Davies K, Leppert M, Ziter F, Wood D, et al. 1990. Genetic mapping of chronic childhood-onset spinal muscular atrophy to chromosome 5q11.2-13.3. Nature. 344(April):540–541.

Buiting K, Williams C, Horsthemke B. 2016. Angelman syndrome-insights into a rare neurogenetic disorder. Nat Rev Neurol. 12(10):584–593. doi:10.1038/nrneurol.2016.133.

Burnett BG, Munoz E, Tandon A, Kwon DY, Sumner CJ, Fischbeck KH. 2009. Regulation of SMN protein stability. Mol Cell Biol. 29(5):1107–1115. doi:10.1128/mcb.01262-08.

Butchbach MER, Lumpkin CJ, Harris AW, Saieva L, Edwards JD, Workman E, Simard LR, Pellizzoni L, Burghes AHM. 2016. Protective effects of butyrate-based compounds on a mouse model for spinal muscular atrophy. Exp Neurol. 279:13–26. doi:10.1016/j.expneurol.2016.02.009. http://dx.doi.org/10.1016/j.expneurol.2016.02.009.

Cafiero C, Marangi G, Orteschi D, Ali M, Asaro A, Ponzi E, Moncada A, Ricciardi S, Murdolo M, Mancano G, et al. 2015. Novel de novo heterozygous loss-of-function variants in MED13L and further delineation of the MED13L haploinsufficiency syndrome. Eur J Hum Genet. 23(11):1499–1504. doi:10.1038/ejhg.2015.19.

Calucho M, Bernal S, Alías L, March F, Venceslá A, Rodríguez-Álvarez FJ, Aller E, Fernández RM, Borrego S, Millán JM, et al. 2018. Correlation between SMA type and SMN2 copy number revisited: An analysis of 625 unrelated Spanish patients and a compilation of 2834 reported cases. Neuromuscul Disord. 28(3):208–215. doi:10.1016/j.nmd.2018.01.003. https://doi.org/10.1016/j.nmd.2018.01.003.

Calvo SE, Pagliarini DJ, Mootha VK. 2009. Upstream open reading frames cause widespread reduction of protein expression and are polymorphic among humans. Proc Natl Acad Sci. 106(18):7507–7512. doi:10.1073/pnas.0810916106.

Campagne S, Boigner S, Rüdisser S, Moursy A, Gillioz L, Knörlein A, Hall J, Ratni H, Cléry A, Allain FHT. 2019. Structural basis of a small molecule targeting RNA for a specific splicing correction. Nat Chem Biol. 15(12):1191–1198. doi:10.1038/s41589-019-0384-5. http://dx.doi.org/10.1038/s41589-019-0384-5.

Cartegni L, Hastings ML, Calarco JA, De Stanchina E, Krainer AR. 2006. Determinants of exon 7 splicing in the spinal muscular atrophy genes, SMN1 and SMN2. Am J Hum Genet. 78(1):63–77. doi:10.1086/498853.

Chang J-G, Hsieh-Li H-M, Jong Y-J, Wang NM, Tsai C-H, Li H. 2001. Treatment of spinal muscular atrophy by sodium butyrate. Proc Natl Acad Sci. 98(17):9808–9813. doi:10.1073/pnas.171105098.

Chatterjee S, Pal JK. 2009. Role of 5'- and 3'-untranslated regions of mRNAs in human diseases. Biol Cell. 101(5):251–262. doi:10.1042/bc20080104.

Chien YH, Chiang SC, Weng WC, Lee NC, Lin CJ, Hsieh WS, Lee WT, Jong YJ, Ko TM, Hwu WL. 2017. Presymptomatic diagnosis of spinal muscular atrophy through newborn screening. J Pediatr. 190:124-129.e1. doi:10.1016/j.jpeds.2017.06.042. https://doi.org/10.1016/j.jpeds.2017.06.042.

Chiurazzi P, Pomponi MG, Willemsen R, Oostra BA, Neri G. 1998. In vitro reactivation of the FMR1 gene involved in fragile X syndrome. Hum Mol Genet. 7(1):109–113. doi:10.1093/hmg/7.1.109.

Coffee B, Zhang F, Warren ST, Reines D. 1999. Acetylated histones are associated with FMR1 in normal but not fragile X-syndrome cells. Nat Genet. 22(1):98–101. doi:10.1038/8807.

Crawford TO, Pardo CA. 1996. The neurobiology of childhood spinal muscular atrophy. Neurobiol Dis. 3(2):97–110. doi:10.1006/nbdi.1996.0010.

Crawford TO, Paushkin S V., Kobayashi DT, Forrest SJ, Joyce CL, Finkel RS, Kaufmann P, Swoboda KJ, Tiziano D, Lomastro R, et al. 2012. Evaluation of SMN protein, transcript, and copy number in the biomarkers for spinal muscular atrophy (BforSMA) clinical study. PLoS One. 7(4). doi:10.1371/journal.pone.0033572.

Czibere L, Burggraf S, Fleige T, Glück B, Keitel LM, Landt O, Durner J, Röschinger W, Hohenfellner K, Wirth B, et al. 2020. High-throughput genetic newborn screening for spinal muscular atrophy by rapid nucleic acid extraction from dried blood spots and 384-well qPCR. Eur J Hum Genet. 28(1):23–30. doi:10.1038/s41431-019-0476-4.

D'Ydewalle C, Ramos DM, Pyles NJ, Ng SY, Gorz M, Pilato CM, Ling K, Kong L, Ward AJ, Rubin LL, et al. 2017. The antisense transcript SMN-AS1 regulates SMN expression and is a novel therapeutic target for spinal muscular atrophy. Neuron. 93(1):66–79. doi:10.1016/j.neuron.2016.11.033. http://dx.doi.org/10.1016/j.neuron.2016.11.033.

Dafinca R, Scaber J, Ababneh N, Lalic T, Weir G, Christian H, Vowles J, Douglas AGL, Fletcher-Jones A, Browne C, et al. 2016. C9orf72 hexanucleotide expansions are associated with altered endoplasmic reticulum calcium homeostasis and stress granule formation in induced pluripotent stem cell-derived neurons from patients with amyotrophic lateral sclerosis and frontotemporal demen. Stem Cells. 34(8):2063–2078. doi:10.1002/stem.2388.

Dangouloff T, Burghes A, Tizzano EF, Servais L, Bertini E, Boemer F, Hiligsmann M, Mueller-Felber W, Tiziano D, Young P, et al. 2020. 244th ENMC international workshop: Newborn screening in spinal muscular atrophy May 10–12, 2019, Hoofdorp, The Netherlands. Neuromuscul Disord. 30(1):93–103. doi:10.1016/j.nmd.2019.11.002.

Darras BT, Chiriboga CA, Iannaccone ST, Swoboda KJ, Montes J, Mignon L, Xia S, Bennett CF, Bishop KM, Shefner JM, et al. 2019. Nusinersen in later-onset spinal muscular atrophy: Long-term results from the phase 1/2 studies. Neurology. 92(21):e2492–e2506. doi:10.1212/WNL.0000000000007527.

De Sanctis R, Coratti G, Pasternak A, Montes J, Pane M, Mazzone ES, Young SD, Salazar R, Quigley J, Pera MC, et al. 2016. Developmental milestones in type I spinal muscular atrophy. Neuromuscul Disord. 26(11):754–759. doi:10.1016/j.nmd.2016.10.002. http://dx.doi.org/10.1016/j.nmd.2016.10.002.

De Vivo DC, Bertini E, Swoboda KJ, Hwu WL, Crawford TO, Finkel RS, Kirschner J, Kuntz NL, Parsons JA, Ryan MM, et al. 2019. Nusinersen initiated in infants during the presymptomatic stage of spinal muscular atrophy: Interim efficacy and safety results from the Phase 2 NURTURE study. Neuromuscul Disord. 29(11):842–856. doi:10.1016/j.nmd.2019.09.007.

Dimitriadi M, Derdowski A, Kalloo G, Maginnis MS, O'Hern P, Bliska B, Sorkaç A, Nguyen KCQ, Cook SJ, Poulogiannis G, et al. 2016. Decreased function of survival motor neuron protein impairs endocytic pathways. Proc Natl Acad Sci. 113(30):E4377–E4386. doi:10.1073/pnas.1600015113.

Dimitriadi M, Sleigh JN, Walker A, Chang HC, Sen A, Kalloo G, Harris J, Barsby T, Walsh MB, Satterlee JS, et al. 2010. Conserved genes act as modifiers of invertebrate SMN loss of function defects. PLoS Genet. 6(10). doi:10.1371/journal.pgen.1001172.

Duan D. 2018. Systemic AAV micro-dystrophin gene therapy for duchenne muscular dystrophy. Mol Ther. 26(10):2337–2356. doi:10.1016/j.ymthe.2018.07.011.

Dubowitz V. 1964. Infantile muscular atrophy a prospective study with particular reference to a slowly progressive variety. Brain. 87(4):707–718. doi:10.1093/brain/87.4.707.
Duque SI, Arnold WD, Odermatt P, Li X, Porensky PN, Schmelzer L, Meyer K, Kolb SJ, Schümperli D, Kaspar BK, et al. 2015. A large animal model of spinal muscular atrophy and correction of phenotype. Ann Neurol. 77(3):399–414. doi:10.1002/ana.24332.

Duygu B, Juni R, Ottaviani L, Bitsch N, Wit JBM, de Windt LJ, da Costa Martins PA. 2019. Comparison of different chemically modified inhibitors of miR-199b in vivo. Biochem Pharmacol. 159:106–115. doi:10.1016/j.bcp.2018.11.013.

Echevarría L, Aupy P, Goyenvalle A. 2018. Exon-skipping advances for Duchenne muscular dystrophy. Hum Mol Genet. 27(R2):R163–R172. doi:10.1093/hmg/ddy171.

Eckstein F. 2014. Phosphorothioates, essential components of therapeutic oligonucleotides. Nucleic Acid Ther. 24(6):374–387. doi:10.1089/nat.2014.0506.

Ellsworth JL, Gingras J, Smith LJ, Rubin H, Seabrook TA, Patel K, Zapata N, Olivieri K, O'Callaghan M, Chlipala E, et al. 2019. Clade F AAVHSCs cross the blood brain barrier and transduce the central nervous system in addition to peripheral tissues following intravenous administration in nonhuman primates. PLoS One. 14(11):1–33. doi:10.1371/journal.pone.0225582.

Fallini C, Donlin-Asp PG, Rouanet JP, Bassell GJ, Rossoll W. 2016. Deficiency of the survival of motor neuron protein impairs mRNA localization and local translation in the growth cone of motor neurons. J Neurosci. 36(13):3811–3820. doi:10.1523/jneurosci.2396-15.2016.

Farooq F, Abadía-Molina F, MacKenzie D, Hadwen J, Shamim F, O'Reilly S, Holcik M, MacKenzie A. 2013. Celecoxib increases SMN and survival in a severe spinal muscular atrophy mouse model via p38 pathway activation. Hum Mol Genet. 22(17):3415–3424. doi:10.1093/hmg/ddt191.

Farooq F, Balabanian S, Liu X, Holcik M, MacKenzie A. 2009. p38 Mitogen-activated protein kinase stabilizes SMN mRNA through RNA binding protein HuR. Hum Mol Genet. 18(21):4035–4045. doi:10.1093/hmg/ddp352.

Feldkötter M, Schwarzer V, Wirth R, Wienker TF, Wirth B. 2002. Quantitative analyses of SMN1 and SMN2 based on real-time lightcycler PCR: Fast and highly reliable carrier testing and prediction of severity of spinal muscular atrophy. Am J Hum Genet. 70(2):358–368. doi:10.1086/338627.

Finkel RS, Chiriboga CA, Vajsar J, Day JW, Montes J, De Vivo DC, Yamashita M, Rigo F, Hung G, Schneider E, et al. 2016. Treatment of infantile-onset spinal muscular atrophy with nusinersen: a phase 2, open-label, dose-escalation study. Lancet. 388(10063):3017–3026. doi:10.1016/S0140-6736(16)31408-8. http://dx.doi.org/10.1016/S0140-6736(16)31408-8.

Finkel RS, Mercuri E, Darras BT, Connolly AM, Kuntz NL, Kirschner J, Chiriboga CA, Saito K, Servais L, Tizzano E, et al. 2017. Nusinersen versus sham control in infantile-onset spinal muscular atrophy. N Engl J Med. 377(18):1723–1732. doi:10.1056/NEJMoa1702752. http://www.ncbi.nlm.nih.gov/pubmed/29091570.

Finkel RS, Mercuri E, Meyer OH, Simonds AK, Schroth MK, Graham RJ, Kirschner J, Iannaccone ST, Crawford TO, Woods S, et al. 2018. Diagnosis and management of spinal muscular atrophy: Part 2: Pulmonary and acute care; medications, supplements and immunizations; other organ systems; and ethics. Neuromuscul Disord. 28(3):197–207. doi:10.1016/j.nmd.2017.11.004. https://doi.org/10.1016/j.nmd.2017.11.004.

Francis MJ, Morrison KE, Campbell L, Grewal PK, Christodoulou Z, Daniels RJ, Monaco AP, Frischauf AM, Mcpherson J, Wasmuth J, et al. 1993. A contig of non-chimaeric YACs containing the spinal muscular atrophy gene in 5q13. Hum Mol Genet. 2(8):1161–1167. doi:10.1093/hmg/2.8.1161.

Furtado D, Björnmalm M, Ayton S, Bush AI, Kempe K, Caruso F. 2018. Overcoming the blood–brain barrier: the role of nanomaterials in treating neurological diseases. Adv Mater. 30(46). doi:10.1002/adma.201801362.

Gabanella F, Butchbach MER, Saieva L, Carissimi C, Burghes AHM, Pellizzoni L. 2007. Ribonucleoprotein assembly defects correlate with spinal muscular atrophy severity and preferentially affect a subset of spliceosomal snRNPs. PLoS One. 2(9). doi:10.1371/journal.pone.0000921.

Gagnon KT, Corey DR. 2019. Guidelines for experiments using antisense oligonucleotides and double-stranded RNAs. Nucleic Acid Ther. 29(3):116–122. doi:10.1089/nat.2018.0772.

Gao Z, Cooper TA. 2013. Antisense oligonucleotides: rising stars in eliminating RNA toxicity in myotonic dystrophy. Hum Gene Ther. 24(5):499–507. doi:10.1089/hum.2012.212.

Germain-Desprez D, Brun T, Rochette C, Semionov A, Rouget R, Simard LR. 2001. The SMN genes are subject to transcriptional regulation during cellular differentiation. Gene. 279(2):109–117. doi:10.1016/S0378-1119(01)00758-2.

Gilliam TC, Brzustowicz LM, Castilla LH, Lehner T, Penchaszadeh GK, Daniels RJ, Byth BC, Knowles J, Hislop JE, Shapira Y, et al. 1990. Genetic homogeneity between acute and chronic forms of spinal muscular atrophy. Nature. 345(6278):823–825. doi:10.1038/345823a0.

Gogliotti RG, Cardona H, Jasbir S, Bail S, Emery C, Kuntz N, Jorgensen M, Durens Madel M, Xia B, Barlow C, et al. 2013. The DcpS inhibitor RG3039 improves survival, function and motor unit pathologies in two SMA mouse models. Hum Mol Genet. 22(20):4084–4101. doi:10.1093/hmg/ddt258.

Gogliotti RG, Hammond SM, Lutz C, DiDonato CJ. 2010. Molecular and phenotypic reassessment of an infrequently used mouse model for spinal muscular atrophy. Biochem Biophys Res Commun. 391(1):517–522. doi:10.1016/j.bbrc.2009.11.090.

Gopalsamy A, Narayanan A, Liu S, Parikh MD, Kyne RE, Fadeyi O, Tones MA, Cherry JJ, Nabhan JF, LaRosa G, et al. 2017. Design of potent mRNA decapping scavenger enzyme (DcpS) inhibitors with improved physicochemical properties to investigate the mechanism of therapeutic benefit in spinal muscular atrophy (SMA). J Med Chem. 60(7):3094–3108. doi:10.1021/acs.jmedchem.7b00124.

Grisch-Chan HM, Schwank G, Harding CO, Thöny B. 2019. State-of-the-art 2019 on gene therapy for phenylketonuria. Hum Gene Ther. 30(10):1274–1283. doi:10.1089/hum.2019.111.

Haenfler JM, Skariah G, Rodriguez CM, Monteiro da Rocha A, Parent JM, Smith GD, Todd PK. 2018. Targeted reactivation of FMR1 transcription in fragile X syndrome embryonic stem cells. Front Mol Neurosci. 11:1–26. doi:10.3389/fnmol.2018.00282. https://www.frontiersin.org/article/10.3389/fnmol.2018.00282/full.

Hagedorn PH, Yakimov V, Ottosen S, Kammler S, Nielsen NF, Høg AM, Hedtjärn M, Meldgaard M, Møller MR, Ørum H, et al. 2013. Hepatotoxic potential of therapeutic oligonucleotides can be predicted from their sequence and modification pattern. Nucleic Acid Ther. 23(5):302–310. doi:10.1089/nat.2013.0436.

Hammond SM, Gogliotti RG, Rao V, Beauvais A, Kothary R, DiDonato CJ. 2010. Mouse survival motor neuron alleles that mimic SMN2 splicing and are inducible rescue embryonic lethality early in development but not late. PLoS One. 5(12). doi:10.1371/journal.pone.0015887.

Hammond SM, Hazell G, Shabanpoor F, Saleh AF, Bowerman M, Sleigh JN, Meijboom KE, Zhou H, Muntoni F, Talbot K, et al. 2016. Systemic peptide-mediated oligonucleotide therapy improves long-term survival in spinal muscular atrophy. Proc Natl Acad Sci. 113(39):10962–10967. doi:10.1073/pnas.1605731113. http://www.pnas.org/lookup/doi/10.1073/pnas.1605731113.

Harada Y, Sutomo R, Sadewa AH, Akutsu T, Takeshima Y, Wada H, Matsuo M, Nishio H. 2002. Correlation between SMN2 copy number and clinical phenotype of spinal muscular atrophy: Three SMN2 copies fail to rescue some patients from the disease severity. J Neurol. 249(9):1211–1219. doi:10.1007/s00415-002-0811-4.

Heier CR, Gogliotti RG, DiDonato CJ. 2007. SMN transcript stability: Could modulation of messenger RNA degradation provide a novel therapy for spinal muscular atrophy? J Child Neurol. 22(8):1013–1018. doi:10.1177/0883073807305669.

Hosseinibarkooie S, Peters M, Torres-Benito L, Rastetter RH, Hupperich K, Hoffmann A, Mendoza-Ferreira N, Kaczmarek A, Janzen E, Milbradt J, et al. 2016. The power of human protective modifiers: PLS3 and CORO1C unravel impaired endocytosis in spinal muscular atrophy and rescue SMA phenotype. Am J Hum Genet. 99(3):647–665. doi:10.1016/j.ajhg.2016.07.014. [accessed 2019 Mar 17]. https://linkinghub.elsevier.com/retrieve/pii/S0002929716302889.

Hsieh-Li HM, Chang J, Jong Y, Wu M, Wang NM, Tsai CH, Li H. 2000. A mouse model for spinal muscular atrophy. Nat Genet. 24(1):66–70. doi:10.1038/71709. http://www.nature.com/doifinder/10.1038/71709.

Hua Y, Sahashi K, Rigo F, Hung G, Horev G, Bennett CF, Krainer AR. 2011. Peripheral SMN restoration is essential for long-term rescue of a severe spinal muscular atrophy mouse model. Nature. 478(7367):123–126. doi:10.1038/nature10485.

Hua Y, Vickers TA, Okunola HL, Bennett CF, Krainer AR. 2008. Antisense masking of an hnRNP A1/A2 intronic splicing silencer corrects SMN2 splicing in transgenic mice. Am J Hum Genet. 82(4):834–848. doi:10.1016/j.ajhg.2008.01.014.

Ito K, Patel PN, Gorham JM, McDonough B, DePalma SR, Adler EE, Lam L, MacRae CA, Mohiuddin SM, Fatkin D, et al. 2017. Identification of pathogenic gene mutations in LMNA and MYBPC3 that alter RNA splicing. Proc Natl Acad Sci U S A. 114(29):7689–7694. doi:10.1073/pnas.1707741114.

Jangi M, Fleet C, Cullen P, Gupta S V., Mekhoubad S, Chiao E, Allaire N, Bennett CF, Rigo F, Krainer AR, et al. 2017. SMN deficiency in severe models of spinal muscular atrophy causes widespread intron retention and DNA damage. Proc Natl Acad Sci U S A. 114(12):E2347–E2356. doi:10.1073/pnas.1613181114.

Jarecki J, Chen X, Bernardino A, Coovert DD, Whitney M, Burghes A, Stack J, Pollok BA. 2005. Diverse small-molecule modulators of SMN expression found by high-throughput compound screening: early leads towards a therapeutic for spinal muscular atrophy. Hum Mol Genet. 14(14):2003–2018. doi:10.1093/hmg/ddi205.

Jianming. 2005. Preparation, culture, and immortalization of mouse embryonic fibroblasts. In: Stem Cell Reviews. Vol. Chapter 28. http://www.ncbi.nlm.nih.gov/pubmed/18265366.

Kariyawasam DST, Russell JS, Wiley V, Alexander IE, Farrar MA. 2020. The implementation of newborn screening for spinal muscular atrophy: the Australian experience. Genet Med. 22(3):557–565. doi:10.1038/s41436-019-0673-0.

Kim J, Hu C, El Achkar CM, Black LE, Douville J, Larson A, Pendergast MK, Goldkind SF, Lee EA, Kuniholm A, et al. 2019. Patient-customized oligonucleotide therapy for a rare genetic disease. N Engl J Med. 381(17):1644–1652. doi:10.1056/NEJMoa1813279.

Klein AF, Varela MA, Arandel L, Holland A, Naouar N, Arzumanov A, Seoane D, Revillod L, Bassez G, Ferry A, et al. 2019. Peptide-conjugated oligonucleotides evoke long-lasting myotonic dystrophy correction in patient-derived cells and mice. J Clin Invest. 129(11):4739–4744. doi:10.1172/JCI128205.

Kleyn PW, Wang CH, Lien LL, Vitale E, Pan J, Ross BM, Grunn A, Palmer DA, Warburton D, Brzustowicz LM, et al. 1993. Construction of a yeast artificial chromosome contig spanning the spinal muscular atrophy disease gene region. Proc Natl Acad Sci U S A. 90(14):6801–6805. doi:10.1073/pnas.90.14.6801.

Kolb SJ, Battle DJ, Dreyfuss G. 2007. Molecular functions of the SMN complex. J Child Neurol. 22(8):990–994. doi:10.1177/0883073807305666.

Kraszewski JN, Kay DM, Stevens CF, Koval C, Haser B, Ortiz V, Albertorio A, Cohen LL, Jain R, Andrew SP, et al. 2018. Pilot study of population-based newborn screening for spinal muscular atrophy in New York state. Genet Med. 20(6):608–613. doi:10.1038/gim.2017.152.

Kwon DY, Dimitriadi M, Terzic B, Cable C, Hart AC, Chitnis A, Fischbeck KH, Burnett BG. 2013. The E3 ubiquitin ligase mind bomb 1 ubiquitinates and promotes the degradation of survival of motor neuron protein. Mol Biol Cell. 24(12):1863–1871. doi:10.1091/mbc.E13-01-0042.

Le TT, Pham LT, Butchbach MER, Zhang HL, Monani UR, Coovert DD, Gavrilina TO, Xing L, Bassell GJ, Burghes AHM. 2005. SMNΔ7, the major product of the centromeric survival motor neuron (SMN2) gene, extends survival in mice with spinal muscular atrophy and associates with full-length SMN. Hum Mol Genet. 14(6):845–857. doi:10.1093/hmg/ddi078.

Lee BH, Collins E, Lewis L, Guntrum D, Eichinger K, Voter K, Abdel-Hamid HZ, Ciafaloni E. 2019. Combination therapy with nusinersen and AVXS-101 in SMA type 1. Neurology. 93(14):640–641. doi:10.1212/WNL.0000000000008207.

Lefebvre S, Bürglen L, Reboullet S, Clermont O, Burlet P, Viollet L, Benichou B, Cruaud C, Millasseau P, Zeviani M, et al. 1995. Identification and characterization of a spinal muscular atrophy-determining gene. Cell. 80:155–165. doi:10.1016/0888-7543(95)80053-O.

Lek A, Rahimov F, Jones PL, Kunkel LM. 2015. Emerging preclinical animal models for FSHD. Trends Mol Med. 21(5):295–306. doi:10.1016/j.molmed.2015.02.011. http://dx.doi.org/10.1016/j.molmed.2015.02.011.

Li B, Niu Y, Ji W, Dong Y. 2020. Strategies for the CRISPR-based therapeutics. Trends Pharmacol Sci. 41(1):55–65. doi:10.1016/j.tips.2019.11.006.

Liang X, Sun H, Shen W, Wang S, Yao J, Migawa MT, Bui H-H, Damle SS, Riney S, Graham MJ, et al. 2017. Antisense oligonucleotides targeting translation inhibitory elements in 5' UTRs can selectively increase protein levels. Nucleic Acids Res. 45(16):9528–9546. doi:10.1093/nar/gkx632.

Liang XH, Shen W, Sun H, Migawa MT, Vickers TA, Crooke ST. 2016. Translation efficiency of mRNAs is increased by antisense oligonucleotides targeting upstream open reading frames. Nat Biotechnol. 34(8):875–880. doi:10.1038/nbt.3589.

Lima WF, Prakash TP, Murray HM, Kinberger GA, Li W, Chappell AE, Li CS, Murray SF, Gaus H, Seth PP, et al. 2012. Single-stranded siRNAs activate RNAi in animals. Cell. 150(5):883–894. doi:10.1016/j.cell.2012.08.014.

Liu H, Yazdani A, Murray LM, Beauvais A, Kothary R. 2014. The Smn-independent beneficial effects of trichostatin a on an intermediate mouse model of spinal muscular atrophy. PLoS One. 9(7):3–11. doi:10.1371/journal.pone.0101225.

Liu XS, Wu H, Krzisch M, Wu X, Graef J, Muffat J, Hnisz D, Li CH, Yuan B, Xu C, et al. 2018. Rescue of fragile X syndrome neurons by DNA methylation editing of the FMR1 gene. Cell. 172(5):979–992. doi:10.1016/j.cell.2018.01.012. https://doi.org/10.1016/j.cell.2018.01.012.

Long KK, O'Shea KM, Khairallah RJ, Howell K, Paushkin S, Chen KS, Cote SM, Webster MT, Stains JP, Treece E, et al. 2019. Specific inhibition of myostatin activation is beneficial in mouse models of SMA therapy. Hum Mol Genet. 28(7):1076–1089. doi:10.1093/hmg/ddy382.

Lorson CL, Hahnen E, Androphy EJ, Wirth B. 1999. A single nucleotide in the SMN gene regulates splicing and is responsible for spinal muscular atrophy. Proc Natl Acad Sci U S A. 96(11):6307–11. http://www.ncbi.nlm.nih.gov/pubmed/10339583%0Ahttp://www.pubmedcentral.nih.gov/articlerender.fcgi?artid=PMC26877.

Lorson CL, Strasswimmer J, Yao J-M, Baleja JD, Hahnen E, Wirth B, Le T, Burghes AHM, Androphy EJ. 1998. SMN oligomerization defect correlates with spinal muscular atrophy severity. Int Pediatr. 13(2):90–93.

Lorson MA, Spate LD, Samuel MS, Murphy CN, Lorson CL, Prather RS, Wells KD. 2011. Disruption of the survival motor neuron (SMN) gene in pigs using ssDNA. Transgenic Res. 20(6):1293–1304. doi:10.1007/s11248-011-9496-8.

Lotti F, Imlach WL, Saieva L, Beck ES, Hao LT, Li DK, Jiao W, Mentis GZ, Beattie CE, McCabe BD, et al. 2012. An SMN-dependent U12 splicing event essential for motor circuit function. Cell. 151(2):440–454. doi:10.1016/j.cell.2012.09.012. http://dx.doi.org/10.1016/j.cell.2012.09.012.

Mailman MD, Heinz JW, Papp AC, Snyder PJ, Sedra MS, Wirth B, Burghes AHM, Prior TW. 2002. Molecular analysis of spinal muscular atrophy and modification of the phenotype by SMN2. Genet Med. 4(1):20–26. doi:10.1097/00125817-200201000-00004.

Markowitz JA, Singh P, Darras BT. 2012. Spinal muscular atrophy: A clinical and research update. Pediatr Neurol. 46(1):1–12. doi:10.1016/j.pediatrneurol.2011.09.001. http://dx.doi.org/10.1016/j.pediatrneurol.2011.09.001.

Mazur C, Powers B, Zasadny K, Sullivan JM, Dimant H, Kamme F, Hesterman J, Matson J, Oestergaard M, Seaman M, et al. 2019. Brain pharmacology of intrathecal antisense oligonucleotides revealed through multimodal imaging. JCI Insight. 4(20). doi:10.1172/jci.insight.129240.

Melki J, Abdelhak S, Sheth P, Bachelot MF, Burlet P, Marcadet A, Aicardi J, Barois A, Carriere JP, Fardeau M, et al. 1990. Gene for chronic proximal spinal muscular atrophies maps to chromosome 5q. Nature. 344(6268):767–768. doi:10.1038/344767a0.

Melki J, Lefebvre S, Burglen L, Burlet P, Clermont O, Millasseau P, Reboullet S, Bénichou B, Zeviani M, Le Paslier D, et al. 1994. De novo and inherited deletions of the 5q13 region in spinal muscular atrophies. Science (80-). 264(5164):1474–1477. doi:10.1126/science.7910982.

Mendell JR, Al-Zaidy S, Shell R, Arnold WD, Rodino-Klapac LR, Prior TW, Lowes L, Alfano L, Berry K, Church K, et al. 2017. Single-dose gene-replacement therapy for spinal muscular atrophy. N Engl J Med. 377(18):1713–1722. doi:10.1056/NEJMoa1706198.

Meng L, Ward AJ, Chun S, Bennett CF, Beaudet AL, Rigo F. 2015. Towards a therapy for Angelman syndrome by targeting a long non-coding RNA. Nature. 518(7539):409–412. doi:10.1038/nature13975.

Mercuri E, Finkel RS, Muntoni F, Wirth B, Montes J, Main M, Mazzone E, Vitale M, Snyder B, Quijano-Roy S, et al. 2018. Diagnosis and management of spinal muscular atrophy: Part 1: Recommendations for diagnosis, rehabilitation, orthopedic and nutritional care. Neuromuscul Disord. 28(2):103–115. doi:10.1016/j.nmd.2017.11.005.

Meyer K, Ferraiuolo L, Schmelzer L, Braun L, McGovern V, Likhite S, Michels O, Govoni A, Fitzgerald J, Morales P, et al. 2015. Improving single injection CSF delivery of AAV9-mediated gene therapy for SMA: A dose-response study in mice and nonhuman primates. Mol Ther. 23(3):477–487. doi:10.1038/mt.2014.210. http://dx.doi.org/10.1038/mt.2014.210.

Mignone F, Gissi C, Liuni S, Pesole G. 2002. Untranslated regions of mRNAs. Genome Biol. 3(3):reviews0004.1-0004.10. http://www.ncbi.nlm.nih.gov/pubmed/11897027%0Ahttp://www.pubmedcentral.nih.gov/articlerender.fcgi?artid=PMC139023.

Monani UR, Lorson CL, Parsons DW, Prior TW, Androphy EJ, Burghes AHM, McPherson JD. 1999. A single nucleotide difference that alters splicing patterns distinguishes the SMA gene SMN1 from the copy gene SMN2. Hum Mol Genet. 8(7):1177–1183. doi:10.1093/hmg/8.7.1177.

Monani UR, Sendtner M, Coovert DD, Parsons DW, Andreassi C, Le TT, Jablonka S, Schrank B, Rossoll W, Prior TW, et al. 2000. The human centromeric survival motor neuron gene (SMN2) rescues embryonic lethality in Smn(-/-) mice and results in a mouse with spinal muscular atrophy. Hum Mol Genet. 9(3):333–339. http://www.ncbi.nlm.nih.gov/pubmed/10655541.

Munsat TL, Davies KE. 1992. International SMA consortium meeting. Neuromuscul Disord. 2(5–6):423–428. doi:10.1016/S0960-8966(06)80015-5.

Murphy AJ, Macdonald LE, Stevens S, Karow M, Dore AT, Pobursky K, Huang TT, Poueymirou WT, Esau L, Meola M, et al. 2014. Mice with megabase humanization of their immunoglobulin genes generate antibodies as efficiently as normal mice. Proc Natl Acad Sci. 111(14):5153–5158. doi:10.1073/PNAS.1324022111.

Osman EY, Bolding MR, Villalón E, Kaifer KA, Lorson ZC, Tisdale S, Hao Y, Conant GC, Pires JC, Pellizzoni L, et al. 2019. Functional characterization of SMN evolution in mouse models of SMA. Sci Rep. 9(1):9472. doi:10.1038/s41598-019-45822-8. http://www.nature.com/articles/s41598-019-45822-8.

Pagliarini V, Guerra M, Di Rosa V, Compagnucci C, Sette C. 2019. Combined treatment with the histone deacetylase inhibitor LBH589 and a splice-switch antisense oligonucleotide enhances SMN2 splicing and SMN expression in spinal muscular atrophy cells. J Neurochem. doi:10.1111/jnc.14935.

Pan J, Zhang C, Teng Y, Zeng S, Chen S, Liang D, Li Z, Wu L. 2020. Detection of spinal muscular atrophy using a duplexed real-time PCR approach with locked nucleic acid-modified primers. Ann Lab Med. 41(1):101–107. doi:10.3343/alm.2021.41.1.101.

Park CY, Halevy T, Lee DR, Sung JJ, Lee JS, Yanuka O, Benvenisty N, Kim DW. 2015. Reversion of FMR1 methylation and silencing by editing the triplet repeats in fragile X iPSC-derived neurons. Cell Rep. 13(2):234–241. doi:10.1016/j.celrep.2015.08.084. http://dx.doi.org/10.1016/j.celrep.2015.08.084.

Parsons DW, McAndrew PE, Iannaccone ST, Mendell JR, Burghes AHM, Prior TW. 1998. Intragenic telSMN mutations: Frequency, distribution, evidence of a founder effect, and modification of the spinal muscular atrophy phenotype by cenSMN copy number. Am J Hum Genet. 63(6):1712–1723. doi:10.1086/302160.

Pellizzoni L, Yong J, Dreyfuss G. 2002. Essential role for the SMN complex in the specificity of snRNP assembly. Science (80-). 298(5599):1775–1779. doi:10.1126/science.1074962.

Prior TW, Krainer AR, Hua Y, Swoboda KJ, Snyder PC, Bridgeman SJ, Burghes AHM, Kissel JT. 2009. A positive modifier of spinal muscular atrophy in the SMN2 gene. Am J Hum Genet. 85(3):408–413. doi:10.1016/j.ajhg.2009.08.002.

Prior TW, Swoboda KJ, Scott HD, Hejmanowski AQ. 2004. Homozygous SMN1 deletions in unaffected family members and modification of the phenotype by SMN2. Am J Med Genet. 130A(3):307–310. doi:10.1002/ajmg.a.30251.

Rage F, Boulisfane N, Rihan K, Neel H, Gostan T, Bertrand E, Bordonné R, Soret A. 2013. Genome-wide identification of mRNAs associated with the protein SMN whose depletion decreases their axonal localization. RNA. 19(12):1755–1766. doi:10.1261/rna.040204.113.

Ramírez-Cheyne JA, Duque GA, Ayala-Zapata S, Saldarriaga-Gil W, Hagerman P, Hagerman R, Payán-Gómez C. 2019. Fragile X syndrome and connective tissue dysregulation. Clin Genet. 95(2):262–267. doi:10.1111/cge.13469.

Ramos DM, d'Ydewalle C, Gabbeta V, Dakka A, Klein SK, Norris DA, Matson J, Taylor SJ, Zaworski PG, Prior TW, et al. 2019. Age-dependent SMN expression in disease-relevant tissue and implications for SMA treatment. J Clin Invest. 129(11):4817–4831. doi:10.1172/JCI124120.

Ramsbottom SA, Molinari E, Srivastava S, Silberman F, Henry C, Alkanderi S, Devlin LA, White K, Steel DH, Saunier S, et al. 2018. Targeted exon skipping of a CEP290 mutation rescues Joubert syndrome phenotypes in vitro and in a murine model. Proc Natl Acad Sci U S A. 115(49):12489–12494. doi:10.1073/pnas.1809432115.

Ratni H, Ebeling M, Baird J, Bendels S, Bylund J, Chen KS, Denk N, Feng Z, Green L, Guerard M, et al. 2018. Discovery of risdiplam, a selective survival of motor neuron-2 (SMN2) gene splicing modifier for the treatment of spinal muscular atrophy (SMA). J Med Chem. 61(15):6501–6517. doi:10.1021/acs.jmedchem.8b00741.

Richards DY, Winn SR, Dudley S, Nygaard S, Mighell TL, Grompe M, Harding CO. 2020. AAV-mediated CRISPR/Cas9 gene editing in murine phenylketonuria. Mol Ther - Methods Clin Dev. 17(June):234–245. doi:10.1016/j.omtm.2019.12.004. https://doi.org/10.1016/j.omtm.2019.12.004.

Riessland M, Brichta L, Hahnen E, Wirth B. 2006. The benzamide M344, a novel histone deacetylase inhibitor, significantly increases SMN2 RNA/protein levels in spinal muscular atrophy cells. Hum Genet. 120(1):101–110. doi:10.1007/s00439-006-0186-1.

Riessland M, Kaczmarek A, Schneider S, Swoboda KJ, Löhr H, Bradler C, Grysko V, Dimitriadi M, Hosseinibarkooie S, Torres-Benito L, et al. 2017. Neurocalcin delta suppression protects against spinal muscular atrophy in humans and across species by restoring impaired endocytosis. Am J Hum Genet. 100(2):297–315. doi:10.1016/j.ajhg.2017.01.005.

Rossoll W, Jablonka S, Andreassi C, Kröning AK, Karle K, Monani UR, Sendtner M. 2003. Smn, the spinal muscular atrophy-determining gene product, modulates axon growth and localization of β-actin mRNA in growth cones of motoneurons. J Cell Biol. 163(4):801–812. doi:10.1083/jcb.200304128.

Rouleau SG, Beaudoin JD, Bisaillon M, Perreault JP. 2015. Small antisense oligonucleotides against G-quadruplexes: Specific mRNA translational switches. Nucleic Acids Res. 43(1):595–606. doi:10.1093/nar/gku1311.

Ruhno C, McGovern VL, Avenarius MR, Snyder PJ, Prior TW, Nery FC, Muhtaseb A, Roggenbuck JS, Kissel JT, Sansone VA, et al. 2019. Complete sequencing of the SMN2 gene in SMA patients detects SMN gene deletion junctions and variants in SMN2 that modify the SMA phenotype. Hum Genet. 138(3):241–256. doi:10.1007/s00439-019-01983-0. http://dx.doi.org/10.1007/s00439-019-01983-0.

Russell S, Bennett J, Wellman JA, Chung DC, Yu ZF, Tillman A, Wittes J, Pappas J, Elci O, McCague S, et al. 2017. Efficacy and safety of voretigene neparvovec (AAV2-hRPE65v2) in patients with RPE65-mediated inherited retinal dystrophy: a randomised, controlled, open-label, phase 3 trial. Lancet. 390(10097):849–860. doi:10.1016/S0140-6736(17)31868-8.

Russman BS, Iannacone ST, Buncher CR, Samaha FJ, White M, Perkins B, Zimmerman L, Smith C, Burhans K, Barker L. 1992. Spinal muscular atrophy: new thoughts on the pathogenesis and classification schema. J Child Neurol. 7(4):347–353. doi:10.1177/088307389200700403.

Salcedo-Arellano MJ, Dufour B, McLennan Y, Martinez-Cerdeno V, Hagerman R. 2020. Fragile X syndrome and associated disorders: clinical aspects and pathology. Neurobiol Dis. 136. doi:10.1016/j.nbd.2020.104740.

Satou Y, Imai KS, Satoh N. 2001. Action of morpholinos in Ciona embryos. Genesis. 30(3):103–106. doi:10.1002/gene.1040.

Schmid A, DiDonato CJ. 2007. Animal models of spinal muscular atrophy. J Child Neurol. 22(8):1004–1012. doi:10.1177/0883073807305667.

Schoch KM, Miller TM. 2017. Antisense oligonucleotides: translation from mouse models to human neurodegenerative diseases. Neuron. 94(6):1056–1070. doi:10.1016/j.neuron.2017.04.010. http://dx.doi.org/10.1016/j.neuron.2017.04.010.

Schrank B, Götz R, Gunnersen JM, Ure JM, Toyka K V., Smith AG, Sendtner M. 1997. Inactivation of the survival motor neuron gene, a candidate gene for human spinal muscular atrophy, leads to massive cell death in early mouse embryos. Proc Natl Acad Sci U S A. 94(18):9920–9925. doi:10.1073/pnas.94.18.9920.

Setten RL, Rossi JJ, Han S. 2019. The current state and future directions of RNAi- based therapeutics. Nat Rev Drug Discov. 18(June):421–446.

Shen W, De Hoyos CL, Migawa MT, Vickers TA, Sun H, Low A, Bell TA, Rahdar M, Mukhopadhyay S, Hart CE, et al. 2019. Chemical modification of PS-ASO therapeutics reduces cellular protein-binding and improves the therapeutic index. Nat Biotechnol. 37(6):640–650. doi:10.1038/s41587-019-0106-2.

Shen X, Corey DR. 2018. Chemistry, mechanism and clinical status of antisense oligonucleotides and duplex RNAs. Nucleic Acids Res. 46(4):1584–1600. doi:10.1093/nar/gkx1239.

Sheng L, Rigo F, Bennett CF, Krainer AR, Hua Y. 2020. Comparison of the efficacy of MOE and PMO modifications of systemic antisense oligonucleotides in a severe SMA mouse model. Nucleic Acids Res. 48(6):2853–2865. doi:10.1093/nar/gkaa126.

Shieh PB. 2018. Emerging strategies in the treatment of Duchenne muscular dystrophy. Neurotherapeutics. 15(4):840–848. doi:10.1007/s13311-018-00687-z.

Singh P, James RS, Mee CJ, Morozov IY. 2019. mRNA levels are buffered upon knockdown of RNA decay and translation factors via adjustment of transcription rates in human HepG2 cells. RNA Biol. 16(9):1147–1155. doi:10.1080/15476286.2019.1621121.

Singh RN, Howell MD, Ottesen EW, Singh NN. 2017. Diverse role of survival motor neuron protein. Biochim Biophys Acta - Gene Regul Mech. 1860(3):299–315. doi:10.1016/j.bbagrm.2016.12.008. http://dx.doi.org/10.1016/j.bbagrm.2016.12.008.

Sleigh JN, Barreiro-Iglesias A, Oliver PL, Biba A, Becker T, Davies KE, Becker CG, Talbot K. 2014. Chondrolectin affects cell survival and neuronal outgrowth in in vitro and in vivo models of spinal muscular atrophy. Hum Mol Genet. 23(4):855–869. doi:10.1093/hmg/ddt477.

Stabley DL, Harris AW, Holbrook J, Chubbs NJ, Lozo KW, Crawford TO, Swoboda KJ, Funanage VL, Wang W, Mackenzie W, et al. 2015. SMN1 and SMN2 copy numbers in cell lines derived from patients with spinal muscular atrophy as measured by array digital PCR. Mol Genet Genomic Med. 3(4):248–257. doi:10.1002/mgg3.141.

Steiger M, Carr-Schmid A, Schwartz DC, Kiledjian M, Parker R. 2003. Analysis of recombinant yeast decapping enzyme. RNA. 9(2):231–238. doi:10.1261/rna.2151403.

Straarup EM, Fisker N, Hedtjärn M, Lindholm MW, Rosenbohm C, Aarup V, Hansen HF, Ørum H, Hansen JBR, Koch T. 2010. Short locked nucleic acid antisense oligonucleotides potently reduce apolipoprotein B mRNA and serum cholesterol in mice and non-human primates. Nucleic Acids Res. 38(20):7100–7111. doi:10.1093/nar/gkq457.

Sugarman EA, Nagan N, Zhu H, Akmaev VR, Zhou Z, Rohlfs EM, Flynn K, Hendrickson BC, Scholl T, Sirko-Osadsa DA, et al. 2012. Pan-ethnic carrier screening and prenatal diagnosis for spinal muscular atrophy: Clinical laboratory analysis of >72 400 specimens. Eur J Hum Genet. 20(1):27–32. doi:10.1038/ejhg.2011.134.

Sumner CJ, Huynh TN, Markowitz JA, Perhac JS, Hill B, Coovert DD, Schussler K, Chen X, Jarecki J, Burghes AHM, et al. 2003. Valproic acid increases SMN levels in spinal muscular atrophy patient cells. Ann Neurol. 54(5):647–654. doi:10.1002/ana.10743.

Taniguchi-Ikeda M, Kobayashi K, Kanagawa M, Yu CC, Mori K, Oda T, Kuga A, Kurahashi H, Akman HO, Dimauro S, et al. 2011. Pathogenic exon-trapping by SVA retrotransposon and rescue in Fukuyama muscular dystrophy. Nature. 478(7367):127–131. doi:10.1038/nature10456.

Taylor JL, Lee FK, Yazdanpanah GK, Staropoli JF, Liu M, Carulli JP, Sun C, Dobrowolski SF, Hannon WH, Vogt RF. 2015. Newborn blood spot screening test using multiplexed real-time PCR to simultaneously screen for spinal muscular atrophy and severe combined immunodeficiency. Clin Chem. 61(2):412–419. doi:10.1373/clinchem.2014.231019.

Taylor MF, Paulauskis JD, Weller DD, Kobzik L. 1996. In vitro efficacy of morpholino-modified antisense oligomers directed against tumor necrosis factor-α mRNA. J Biol Chem. 271(29):17445–17452. doi:10.1074/jbc.271.29.17445.

Thomas NH, Dubowitz V. 1994. The natural history of type I (severe) spinal muscular atrophy. Neuromuscul Disord. 4(5–6):497–502. doi:10.1016/0960-8966(94)90090-6.

Torres-Benito L, Schneider S, Rombo R, Ling KK, Grysko V, Upadhyay A, Kononenko NL, Rigo F, Bennett CF, Wirth B. 2019. NCALD antisense oligonucleotide therapy in addition to nusinersen further ameliorates spinal muscular atrophy in mice. Am J Hum Genet. 105(1):221–230. doi:10.1016/j.ajhg.2019.05.008. https://doi.org/10.1016/j.ajhg.2019.05.008.

Tushev G, Glock C, Heumüller M, Biever A, Jovanovic M, Schuman EM. 2018. Alternative 3’ UTRs modify the localization, regulatory potential, stability, and plasticity of mRNAs in neuronal compartments. Neuron. 98(3):495–511. doi:10.1016/j.neuron.2018.03.030.
Uchida S, Perche F, Pichon C, Cabral H. 2020. Nanomedicine-based approaches for mRNA delivery. Mol Pharm. doi:10.1021/acs.molpharmaceut.0c00618.

Uchida S, Perche F, Pichon C, Cabral H. 2020. Nanomedicine-based approaches for mRNA delivery. Mol Pharm. doi:10.1021/acs.molpharmaceut.0c00618.

Van Der Steege G, Grootscholten PM, Cobben JM, Zappata S, Scheffer H, Den Dunnen JT, Van Ommen GJB, Brahe C, Buys CHCM. 1996. Apparent gene conversions involving the SMN gene in the region of the spinal muscular atrophy locus on chromosome 5. Am J Hum Genet. 59(4):834–838.

Van Meerbeke JP, Gibbs RM, Plasterer HL, Miao W, Feng Z, Lin MY, Rucki AA, Wee CD, Xia B, Sharma S, et al. 2013. The DcpS inhibitor RG3039 improves motor functionin SMA mice. Hum Mol Genet. 22(20):4074–4083. doi:10.1093/hmg/ddt257.

Vill K, Kölbel H, Schwartz O, Blaschek A, Olgemöller B, Harms E, Burggraf S, Röschinger W, Durner J, Gläser D, et al. 2019. One year of newborn screening for SMA – Results of a German pilot project. J Neuromuscul Dis. 6(4):503–515. doi:10.3233/JND-190428.

Villiger L, Grisch-Chan HM, Lindsay H, Ringnalda F, Pogliano CB, Allegri G, Fingerhut R, Häberle J, Matos J, Robinson MD, et al. 2018. Treatment of a metabolic liver disease by in vivo genome base editing in adult mice. Nat Med. 24(10):1519–1525. doi:10.1038/s41591-018-0209-1.

Walter LM, Deguise MO, Meijboom KE, Betts CA, Ahlskog N, van Westering TLE, Hazell G, McFall E, Kordala A, Hammond SM, et al. 2018. Interventions targeting glucocorticoid-Krüppel-like factor 15-branched-chain amino acid signaling improve disease phenotypes in spinal muscular atrophy mice. EBioMedicine. 31:226–242. doi:10.1016/j.ebiom.2018.04.024.

Wan L, Battle DJ, Yong J, Gubitz AK, Kolb SJ, Wang J, Dreyfuss G. 2005. The survival of motor neurons protein determines the capacity for snRNP assembly: biochemical deficiency in spinal muscular atrophy. Mol Cell Biol. 25(13):5543–5551. doi:10.1128/mcb.25.13.5543-5551.2005.

Wang CH, Finkel RS, Bertini ES, Schroth M, Simonds A, Wong B, Aloysius A, Morrison L, Main M, Crawford TO, et al. 2007. Consensus statement for standard of care in spinal muscular atrophy. J Child Neurol. 22(8):1027–1049. doi:10.1177/0883073807305788.

Wang D, Tai PWL, Gao G. 2019. Adeno-associated virus vector as a platform for gene therapy delivery. Nat Rev Drug Discov. 18(5):358–378. doi:10.1038/s41573-019-0012-9.
Werdnig G. 1891. Two early infantile hereditary cases of progressive muscular atrophy simulating dystrophy, but on a neural basis. Arch Psychiat Nervenkrank. 22:437–480. doi:10.1007/BF02756452.

Wirth B, Brichta L, Schrank B, Lochmüller H, Blick S, Baasner A, Heller R. 2006. Mildly affected patients with spinal muscular atrophy are partially protected by an increased SMN2 copy number. Hum Genet. 119(4):422–428. doi:10.1007/s00439-006-0156-7.

Wittrup A, Lieberman J. 2015. Knocking down disease: A progress report on siRNA therapeutics. Nat Rev Genet. 16(9):543–552. doi:10.1038/nrg3978.

Wolfe JM, Fadzen CM, Choo ZN, Holden RL, Yao M, Hanson GJ, Pentelute BL. 2018. Machine learning to predict cell-penetrating peptides for antisense delivery. ACS Cent Sci. 4(4):512–520. doi:10.1021/acscentsci.8b00098.

Woo CJ, Maier VK, Davey R, Brennan J, Li G, Brothers J, Schwartz B, Gordo S, Kasper A, Okamoto TR, et al. 2017. Gene activation of SMN by selective disruption of lncRNA-mediated recruitment of PRC2 for the treatment of spinal muscular atrophy. Proc Natl Acad Sci U S A. 114(8):E1509–E1518. doi:10.1073/pnas.1616521114.

Wood MF, Hughes SC, Hache LP, Naylor EW, Abdel-Hamid HZ, Barmada MM, Dobrowolski SF, Stickler DE, Clemens PR. 2014. Parental attitudes toward newborn screening for Duchenne/Becker muscular dystrophy and spinal muscular atrophy. Muscle and Nerve. 49(6):822–828. doi:10.1002/mus.24100.

Wu X, Wang SH, Sun J, Krainer AR, Hua Y, Prior TW. 2017. A-44G transition in SMN2 intron 6 protects patients with spinal muscular atrophy. Hum Mol Genet. 26(14):2768–2780. doi:10.1093/HMG/DDX166.

Xie N, Gong H, Suhl JA, Chopra P, Wang T, Warren ST. 2016. Reactivation of FMR1 by CRISPR/Cas9-mediated deletion of the expanded CGG-repeat of the fragile X chromosome. PLoS One. 11(10). doi:10.1371/journal.pone.0165499.

Xu Y, Xiao B, Liu Y, Qu XX, Dai MY, Ying XM, Jiang WT, Zhang JM, Liu XQ, Chen YW, et al. 2020. Identification of novel SMN1 subtle mutations using an allelic-specific RT-PCR. Neuromuscul Disord. doi:10.1016/j.nmd.2019.11.010.

Yang J, Zhang X, Chen X, Wang L, Yang G. 2017. Exosome mediated delivery of miR-124 promotes neurogenesis after ischemia. Mol Ther - Nucleic Acids. 7(June):278–287. doi:10.1016/j.omtn.2017.04.010. http://dx.doi.org/10.1016/j.omtn.2017.04.010.

Zhang HL, Pan F, Hong D, Shenoy SM, Singer RH, Bassell GJ. 2003. Active transport of the survival motor neuron protein and the role of exon-7 in cytoplasmic localization. J Neurosci. 23(16):6627–6637.

Zhang J, Wang Y, Ma D, Sun Y, Li Y, Yang P, Luo C, Jiang T, Hu P, Xu Z. 2020. Carrier screening and prenatal diagnosis for spinal muscular atrophy in 13,069 Chinese pregnant women. J Mol Diagnostics. 22(6):817–822. doi:10.1016/j.jmoldx.2020.03.001. https://doi.org/10.1016/j.jmoldx.2020.03.001.

Zhang Z, Lotti F, Dittmar K, Younis I, Wan L, Kasim M, Dreyfuss G. 2008. SMN deficiency causes tissue-specific perturbations in the repertoire of snRNAs and widespread defects in splicing. Cell. 133(4):585–600. doi:10.1016/j.cell.2008.03.031.

Zhou H, Meng J, Malerba A, Catapano F, Sintusek P, Jarmin S, Feng L, Lu-Nguyen N, Sun L, Mariot V, et al. 2020. Myostatin inhibition in combination with antisense oligonucleotide therapy improves outcomes in spinal muscular atrophy. J Cachexia Sarcopenia Muscle. doi:10.1002/jcsm.12542.

Zhou M, Hu Z, Qiu L, Zhou T, Feng M, Hu Q, Zeng B, Li Z, Sun Q, Wu Y, et al. 2018. Seamless genetic conversion of SMN2 to SMN1 via CRISPR/Cpf1 and single-stranded oligodeoxynucleotides in spinal muscular atrophy patient-specific induced pluripotent stem cells. Hum Gene Ther. 29(11):1252–1263. doi:10.1089/hum.2017.255.

Zuo E, Huo X, Yao X, Hu X, Sun Y, Yin J, He B, Wang X, Shi L, Ping J, et al. 2017. CRISPR/Cas9-mediated targeted chromosome elimination. Genome Biol. 18(224). doi:10.1186/s13059-017-1354-4.

SUPPLEMENTARY MATERIAL

Table S1 Properties of ASOs used in experiments.

The first 7 ASOs listed were fully modified with 2'-O-methyl (2'OMe) bases and phosphorothioate (PS) linkages. The non-targeting control (NTC) ASO uses the "Standard Control" sequence which was described by Gene Tools, LLC as having no RNA target and minimal biological activity. The last 3 ASOs were fully modified with 2'-O-methoxyethyl (2'MOE) bases and phosphorothioate (PS) linkages.

Sequence name	ASO sequence (5' -> 3')	Chem	Molecular weight (Da)	% GC	T_m (°C)
ASO #1	GUUAUCGCCCUCCCACAUUUGUGG	OMe	8,249	54.2	51.3
ASO #2	UGGUUAUCGCCCUCCCACAUUUGU	OMe	8,210	50.0	51.2
ASO #3	AGUGGUUAUCGCCCUCCCACAUUU	OMe	8,233	50.0	51.7
ASO #4	CGAGUGGUUAUCGCCCUCCCACAU	OMe	8,271	58.3	56.5
ASO #5	UACGAGUGGUUAUCGCCCUCCCAC	OMe	8,271	58.3	58.6
ASO #6	UUCUGGGAGCGGAACAGUACGGUG	OMe	8,494	58.3	62.0
NTC	CCUCUUACCUCAGUUACAAUUUAUA	OMe	8,522	32.0	40.9
5'UTR ASO	GUUAUCGCCCUCCCACAUUUGUGG	MOE	9,530	54.2	
NTC	CCUCUUACCUCAGUUACAAUUUAUA	MOE	9,862	32.0	
Scrambled	GUGGUCGCAUUUCCUCGUUACCAC	MOE	9,530	54.2	

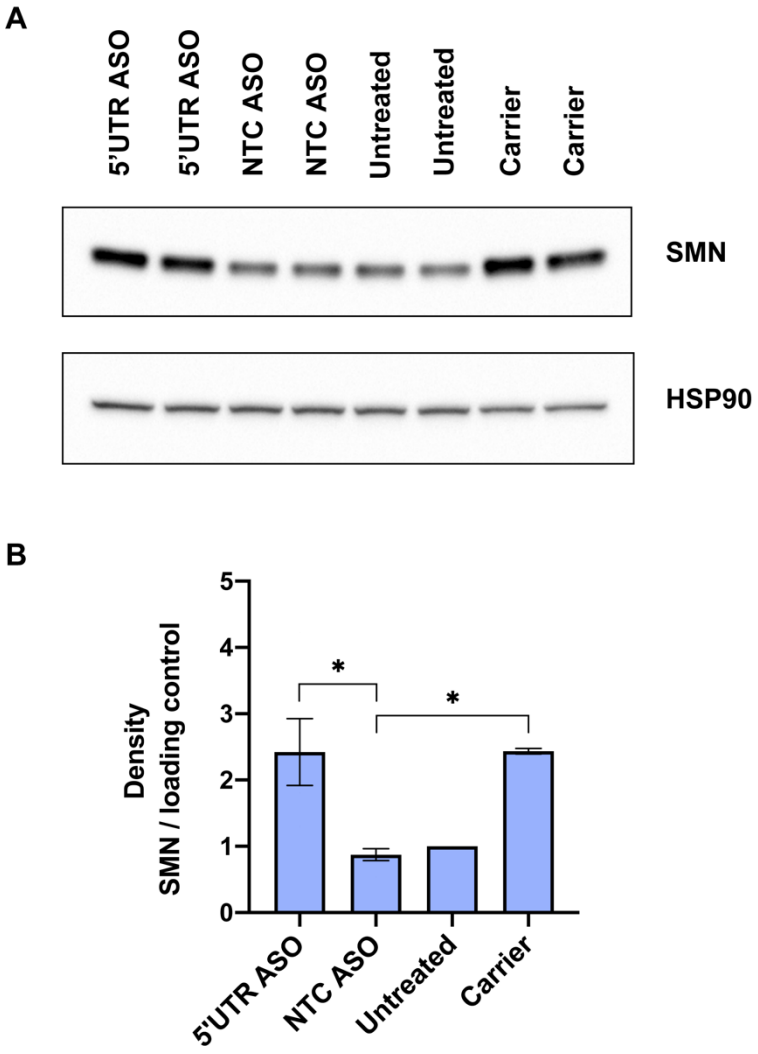

Figure S1 The 5'UTR ASO is effective in a second SMA fibroblast cell line.

A) Immunoblot (15 μg per lane) showing SMN protein levels in GM03813 fibroblasts treated with 600 nM 5'UTR ASO #1 or a non-targeting control (NTC) ASO. B) SMN protein levels normalized to a loading control (alpha tubulin or HSP90) and then calculated as a fold change relative to SMN levels in untreated SMA patient cells. Error bars show SEM. Statistical significance determined by one-way ANOVA followed by Dunnett's test in comparison to NTC ASO. n = 5, except n = 4 for carrier; * $p < 0.02$.

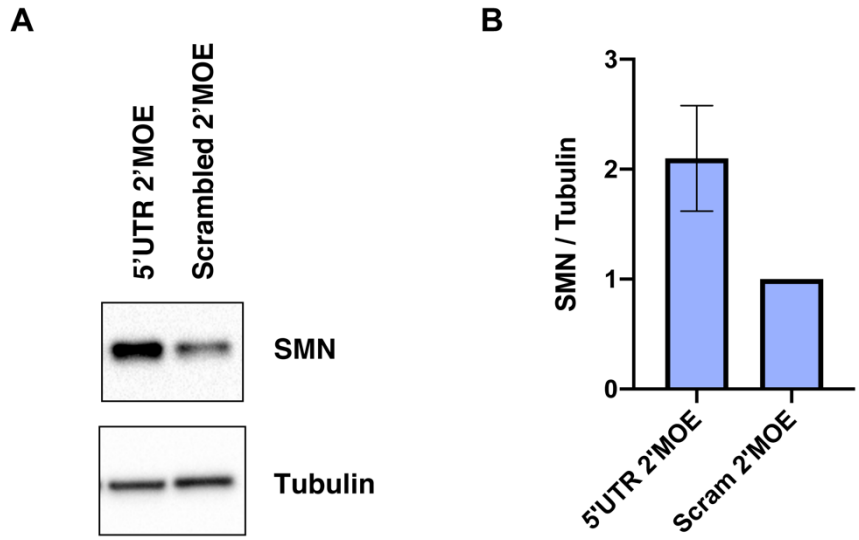

Figure S2 A 5'UTR 2'MOE increases SMN protein levels. A) Immunoblot (15 μg per lane) showing SMN protein levels in GM00232 fibroblasts treated with 300 nM 5'UTR ASO or a scrambled control ASO (Scram). B) SMN protein levels normalized to alpha tubulin and then calculated as a fold change relative to SMN levels in scrambled treated cells. Error bar shows SEM. n = 4.

Table S2 Double-stranded DNA fragments used in plasmid construction.

All sequences purchased as gBlocks Gene Fragments or Ultramer DNA Oligos from IDT. Lower case letters indicate intronic sequence.

DNA name	Sequence (5' -> 3')
gBlocks: *SMN2* 5'UTR + eGFP + *HBB*	CCACAAATGTGGGAGGGCGATAACCACTCGTAGAAAGCGTGAGAAG TTACTACAAGCGGTCCTCCCGGCCACCGTACTGTTCCGCTCCCAGA AGCCCCGGGCGGCGGAAGTCGTCACTCTTAAGAAGGGACGGGGCC CCACGCTGCGCACCCGCGGGTTTGCTATGGTGAGCAAGGGCGAGG AGCTGTTCACCGGGGTGGTGCCCATCCTGGTCGAGCTGGACGGCG ACGTAAACGGCCACAAGTTCAGCGTGTCCGGCGAGGGCGAGGGCG ATGCCACCTACGGCAAGCTGACCCTGAAGTTCATCTGCACCACCGG CAAGCTGCCCGTGCCCTGGCCCACCCTCGTGACCACCCTGACCTAC GGCGTGCAGTGCTTCAGCCGCTACCCCGACCACATGAAGCAGCAC GACTTCTTCAAGTCCGCCATGCCCGAAGGCTACGTCCAGGAGCGCA CCATCTTCTTCAAGGACGACGGCAACTACAAGACCCGCGCCGAGGT GAAGTTCGAGGGCGACACCCTGGTGAACCGCATCGAGCTGAAGGG CATCGACTTCAAGGAGGACGGCAACATCCTGGGGCACAAGCTGGA GTACAACTACAACAGCCACAACGTCTATATCATGGCCGACAAGCAGA AGAACGGCATCAAGGTGAACTTCAAGATCCGCCACAACATCGAGGA CGGCAGCGTGCAGCTCGCCGACCACTACCAGCAGAACACCCCCAT CGGCGACGGCCCCGTGCTGCTGCCCGACAACCACTACCTGAGCAC CCAGTCCGCCCTGAGCAAAGACCCCAACGAGAAGCGCGATCACATG GTCCTGCTGGAGTTCGTGACCGCCGCCGGGATCACTCTCGGCATG GACGAGCTGTACAAGCTGCTGGTGGTCTACCCTTGGACCCAGAGGT TCTTTGAGTCCTTTGGGGATCTGTCCACTCCTGATGCTGTTATGGGC AACCCTAAGGTGAAGGCTCATGGCAAGAAAGTGCTCGGTGCCTTTA GTGATGGCCTGGCTCACCTGGACAACCTCAAGGGCACCTTTGCCAC ACTGAGTGAGCTGCACTGTGACAAGCTGCACGTGGATCCTGAGAAC TTCAGGgtgagtctatgggacgcttgatgttttctttcccccttctttctatggttaagttcatgtcataggg aaggggataagtaacagggtacagtttagaatgggaaacagacgaatgattgcatcagtgtggaa gtctcaggatcgttttagtttcttttatttgctgttcataacaattgttttcttttgtttaattcttgctttctttttttttcttc tccgcaatttttactattatacttaatgccttaacattgtgtataacaaaaggaaatatctctgagatacatt aagtaacttaaaaaaaaactttacacagtctgcctagtacattactatttggaatatatgtgtgcttatttg catattcataatctccctactttatttttctttttatttttaattgatacataatcattatacatatttatgggttaaagt gtaatgttttaatatgtgtacacatattgaccaaatcagggtaattttgcatttgtaatttttaaaaaatgctttc ttcttttaatatacttttttgtttatcttatttctaatactttccctaatctctttctttcagggcaataatgatacaat gtatcatgcctctttgcaccattctaaagaataacagtgataatttctgggttaaggcaatagcaatatct ctgcatataaatatttctgcatataaattgtaactgatgtaagaggtttcatattgctaatagcagctacaa tccagctaccattctgcttttatttatggttgggataaggctggattattctgagtccaagctaggccctttt gctaatcatgttcatacctcttatcttcctcccacagCTCCTGGGCAACGTGCTGGTCTG TGTGCTGGCCCATCACTTTGGCAAAGAATTCACCCCACCAGTGCAG GCTGCCTATCAGAAAGTGGTGGCTGGTGTGGCTAATGCCCTGGCCC ACAAGTATCACTAAGCTCGCTTTCTTGCTGTCCAATTTCTATTAAAGG TTCCTTTGTTCCCTAAGTCCAACTACTAAACTGGGGGATATTATGAA GGGCCTTGAGCATCTGGATTCTGCC
5'UTR Frame Shift mutation	GTCAGATCCGCTAGGGATCCCCACAAATGTGGGAGGGCGATAACCA CTCGTACCGAAAGCGTGAGAAGTTACTACAAGCGGTCCTCCCGGCC ACCGTACTGTTCCGCTCCCAGAAGCCCCGGGCGGCGGAAGTCGTC ACTCTTAAGAAGGGACGGGGCCCCACGCTGCGCACCCGCGGGTTT GCTATGGTGAGCAAGGGCGAGGAGCTGTTCACCGGGGTGGTGCCC ATCCTGGTCGAGCTGGACGGCGACGTAAACGGCCACAAGTTCAGC GTGTCCGGCGAGGGCGAGGGCGATGCCACCTACGGCAAGCTGACC CTGAAGTTCATCTGCACCACCGGCAAGCTGCCCGTGCCCTGGCCCA CCCTCGTGACCACCCTGACCTACGGCGTGCAGTGCTTCAGCCGCTA CCCCGACCACATGAAGCAGCACGACTTCTTCAAGTCC
No mCherry	GACTGCAGCCTCAGGAGATCTGAATTCTCCAGGCGATCTGACGG

Table S3 Primers for PCRs for cloning.

PCR	Primer name	Primer sequence (5' -> 3')	T_a (ºC)
mCherry backbone	BglII-mCherry	ACTGCAGCCTCAGGAGATCTTTACTCGT CCATGCCGCCGG	70
	mCherry-EcoRI	CAGATCGCCTGGAGAATTCATGGTGAG CAAGGGCGAGGAG	
Wild-type	BamHI WT	CAGATCCGCTAGGGATCCCCACAAATG TGGGAGGGCG	62
	β Globin Rev	AAGCTTATCGATGCGGCCGCGGCAGAA TCCAGATGCTCAAGG	
ATG -> ACG	BamHI Mut	CAGATCCGCTAGGGATCCCCACAAACG TGGGAGGGCG	62
	β Globin Rev	AAGCTTATCGATGCGGCCGCGGCAGAA TCCAGATGCTCAAGG	
Optimized uORF	BamHI Opt	CAGATCCGCTAGGGATCCCCACAAATG GGGAGGGCGATAACCACTCGTTAGAAA GCGTGA	62
	β Globin Rev	AAGCTTATCGATGCGGCCGCGGCAGAA TCCAGATGCTCAAGG	
Frame Shift	eGFP internal	AGCACGACTTCTTCAAGTCCGCCATGCC	62
	β Globin Rev	AAGCTTATCGATGCGGCCGCGGCAGAA TCCAGATGCTCAAGG	

Table S4 Primers for reporter construct sequence verification.

Primer name	Primer sequence (5' -> 3')
5'UTR Rev	CATAGCAAACCCGCGGGTGC
SMN 5'UTR	AGAAGCCCCGGGCGGCGGAA
eGFP internal	AGCACGACTTCTTCAAGTCCGCCATGCC
β Glob Fwd ORF	CGGCATGGACGAGCTGTACAAGCTGCTGGTGGTCTACCCT TGGAC
pBI CMV4 Rev	TGGAGATATCGTCGACAAGC
mCherry seq Fwd	AGTGCCACCTGACGTCGGCAG
mCherry seq Rev	ATGTAACGCGGAACTCCATATATG

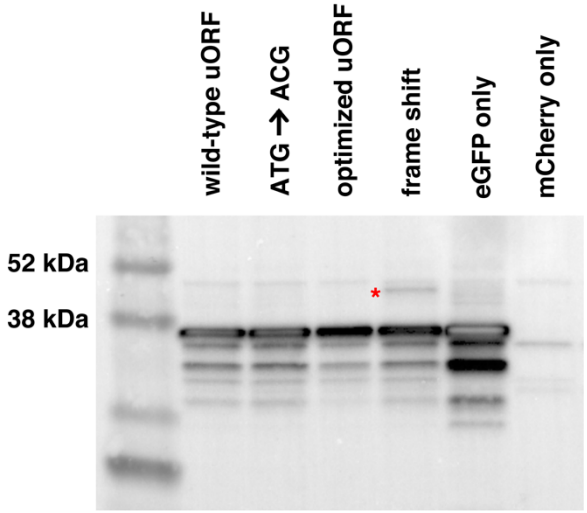

Figure S3 Translation that begins at the upstream start codon is rare (or slow). The wild-type eGFP fusion protein is 39 kDa. The protein encoded by the frame shift reporter has 53 additional amino acids (encoded by the 5'UTR) and is 45 kDa. This protein is indicated by the red asterisk. The signal from the higher molecular weight protein is visible only after the signal from the canonical protein is saturated.

Table S5 Primers for gene expression analysis by RT-qPCR.

RNA	Primer name	Primer sequences (5' -> 3')	Chemistry	T_a (ºC)
FL-SMN	FL-SMN qF	GCTTTGGGAAGTATGTTAATTTCA	Sybr Green	60
	FL-SMN qR	CTATGCCAGCATTTCTCCTTAATT		
SMNΔ7	SMNΔ7 qF	CCACCACCCCACTTACTATCA	Sybr Green	60
	SMNΔ7 qR	GCTCTATGCCAGCATTTCCATA		
Total SMN	Total SMN qF	GCGATGATTCTGACATTTGG	Sybr Green	60
	Total SMN qR	GGAAGCTGCAGTATTCTTCT		
GAPDH	GAPDH qF	CTCAACGACCACTTTGTCAAGCTC	Sybr Green	60
	GAPDH qR	TCTTACTCCTTGGAGGCCATGT		
MYC	MYC qF	TACCCTCTCAACGACAGCAGC	Sybr Green	60
	MYC qR	TCTTGTTCCTCCTCAGAGTCG		
Total hSMN	Tot-hSMN qF	TCAGTGCTGTATCATCCCAAATG	TaqMan	60
	Tot-hSMN qR	CAGGAGGATTCCGTGCTGTT		
	Probe	6-FAM-CGGCACAGG/ZEN/CCAGA GCGATG-IB-FQ		
mPolJ	mPolJ qF	GTGGTCTTCTTTGTTGATGGTG	TaqMan	60
	mPolJ qR	TTCGAGTCGTTCTTGCTCTTC		
	Probe	HEX-AAGCAGGCG/Zen/TTGGGA ACCTTAGT-IB-FQ		

Table S6 Primers for *SMN2* exon 7 inclusion RT-PCR.

Primer name	Primer sequences (5' -> 3')	T_a (ºC)
SMN PAGE Fwd	AGGTCTAAAATTCAATGGCCCA	60
SMN PAGE Rev	GTGTCATTTAGTGCTGCTCTATGC	

Table S7 Confirming Click-iT assay specificity to nascent RNA.

Before the 5-ethynyl uridine pulse, a group of fibroblasts were treated with actinomycin D to prevent transcription and serve as an experimental control. Those samples have higher RT-qPCR C_t values (less amplification of *SMN* and *GAPDH*) than samples not treated with actinomycin D. Values shown are mean plus or minus standard deviation. n = 3.

	Average C_t *SMN*	Average C_t *GAPDH*
NTC ASO	27.41 $\pm$ 0.46	25.94 $\pm$ 0.08
5'UTR ASO	26.49 $\pm$ 0.81	25.40 $\pm$ 0.62
Untreated	27.20 $\pm$ 0.73	25.99 $\pm$ 0.61
Actinomycin D	34.04 $\pm$ 0.60	29.99 $\pm$ 0.39
Carrier	25.47 $\pm$ 0.05	25.92 $\pm$ 0.21

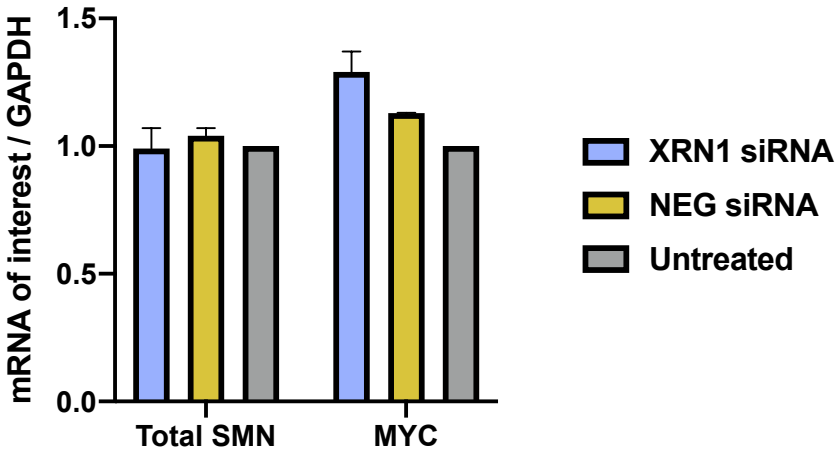

Figure S4 XRN1 knockdown does not affect *SMN* mRNA levels. GM03814 (carrier) fibroblasts were transfected with 100 nM XRN1 siRNA or negative control siRNA (NEG). RT-qPCR measured total *SMN* or *MYC* mRNA levels. Expression was normalized to *GAPDH* and calculated as a fold change relative to levels in untreated cells. Error bars show SEM. There was no statistical significance, as determined by *t* test between XRN1 and NEG values.

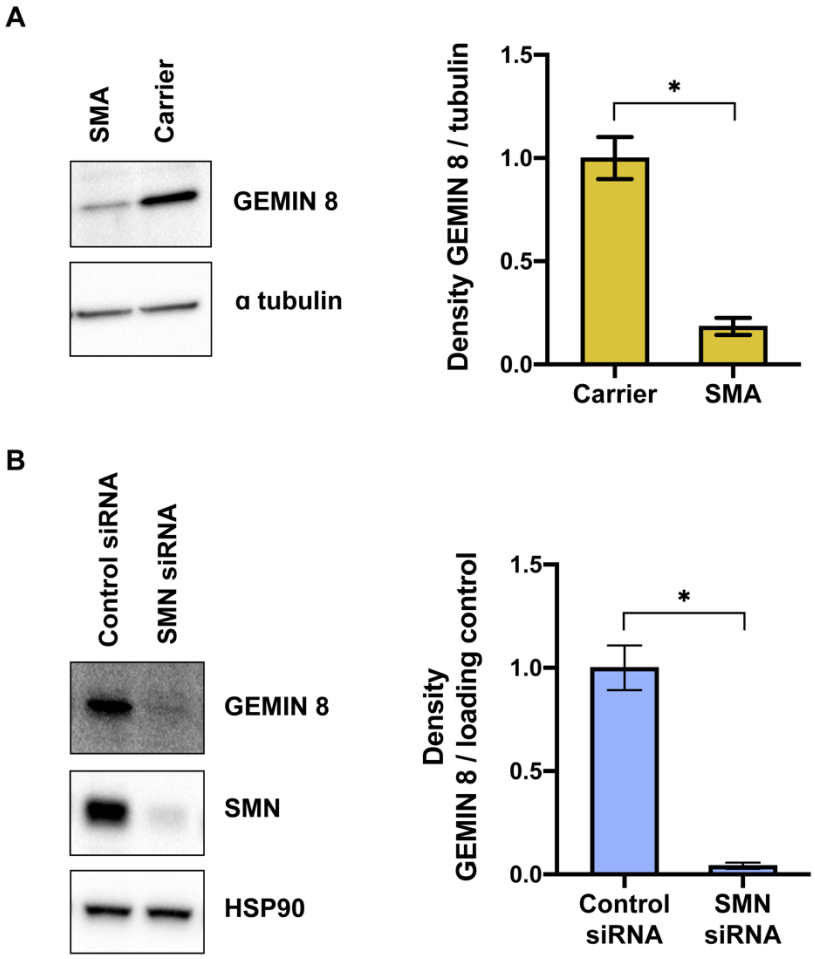

Figure S5 Confirmation that SMN and Gemin8 protein levels correlate in fibroblasts. A) Western blot to detect Gemin8 protein levels in SMA (Coriell GM00232 and GM03813) and carrier (Coriell GM03814) fibroblasts. Gemin8 signal was normalized to alpha tubulin and then calculated as a fold change relative to Gemin8 levels in carrier cells. B) Immunoblot of protein extracted from carrier cells 72 hours after transfection with either SMN or control siRNA. Gemin8 signal was normalized to a loading control (alpha tubulin or HSP90) and then calculated as a fold change relative to Gemin8 levels in cells transfected with control siRNA. Error bars show propagated error. Statistical significance determined by *t*-test between the normalized signal intensity values for the two sample groups. n = 2 per group; * $p < 0.05$.

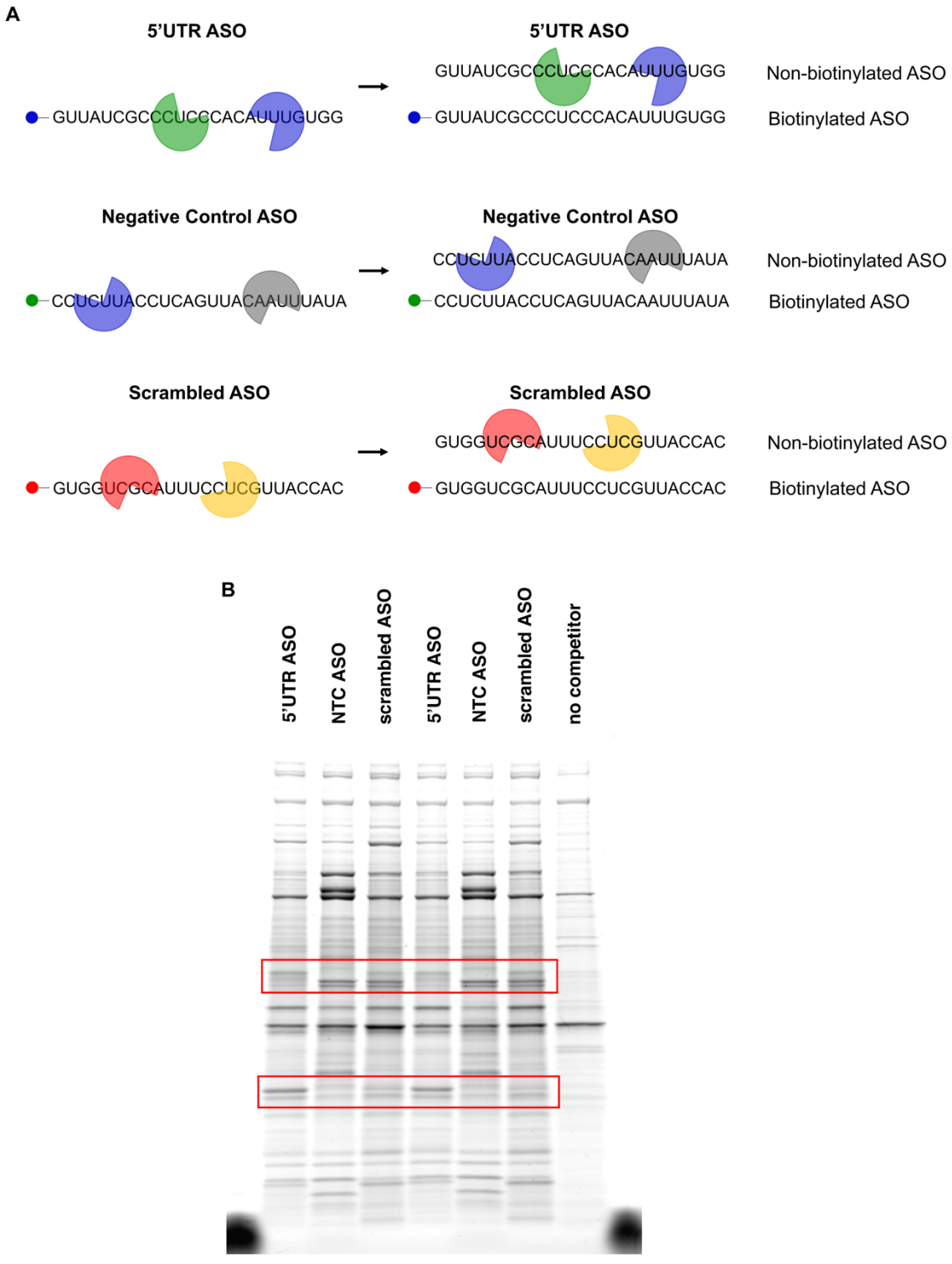
A
5'UTR ASO
GUUAUCGCCCUCCCACAUUUGUGG
5'UTR ASO
GUUAUCGCCCUCCCACAUUUGUGG
GUUAUCGCCCUCCCACAUUUGUGG
Non-biotinylated ASO
Biotinylated ASO
Negative Control ASO
CCUCUUACCUCAGUUACAAUUUAUA
Negative Control ASO
CCUCUUACCUCAGUUACAAUUUAUA
CCUCUUACCUCAGUUACAAUUUAUA
Non-biotinylated ASO
Biotinylated ASO
Scrambled ASO
GUGGUCGCAUUUCCUCGUUACCAC
Scrambled ASO
GUGGUCGCAUUUCCUCGUUACCAC
GUGGUCGCAUUUCCUCGUUACCAC
Non-biotinylated ASO
Biotinylated ASO
B
5'UTR ASO
NTC ASO
scrambled ASO
5'UTR ASO
NTC ASO
scrambled ASO
no competitor

Figure S6 Identification of proteins that bind to the 5'UTR 2'MOE ASO.

A) Magnetic beads were coated with 5' biotinylated ASOs (depicted as sequences preceded by colored 'biotin' circles) and incubated with lysates to allow for protein binding. After binding and washing, the ASO-protein complexes were incubated with a competitor ASO. The competitor ASOs were the same sequences as the biotinylated ASOs. The proteins that were pulled-down by the biotinylated ASOs were allowed to bind to the competitor ASOs. Without biotin, the competitor ASOs did not stick to the beads, which enabled them (and their bound proteins) to be collected in the supernatant. B) 20% of each sample was run on a 4-20% gel. The gel was stained with SYPRO Ruby Protein Gel Stain and imaged. Bands of interest (boxed in red) that were present in the 5'UTR ASO lanes but absent in other lanes were excised for mass spectrometry.

Table S8 Protein hits identified by mass spectrometry. A detailed description of the data contained in this table is provided on the following page.

				Abundance Ratios				Abundance Ratio P-Values			
				replicates 1+2		replicates 3+4		replicates 1+2		replicates 3+4	
Gene Symbol	MW [kDa]	# Unique Peptides	Coverage [%]	NTC / 5'UTR	Scram / 5'UTR	NTC / 5'UTR	Scram / 5'UTR	NTC / 5'UTR	Scram / 5'UTR	NTC / 5'UTR	Scram / 5'UTR
*HMGB1	24.9	15	73	0.15	0.44	0.05	0.12	4.2E-02	5.2E-01	4.6E-03	2.2E-02
*HMGB2	24	14	69	0.10	0.42	0.04	0.13	5.6E-02	7.0E-01	1.2E-02	9.7E-02
*PYM1	22.6	14	69	0.08	0.36	0.03	0.57	3.2E-04	3.6E-02	4.6E-05	2.9E-01
*HMGB3	23	17	65	0.18	0.38	0.06	0.20	6.7E-03	9.7E-02	5.0E-04	9.1E-03
*EIF6	26.6	9	57	0.36	0.46	0.14	0.74	3.9E-01	6.1E-01	4.5E-02	9.8E-01
*ALYREF	26.9	10	54	0.03	0.15	0.01	#1.038	2.4E-04	7.7E-03	6.1E-05	1.0E+00
MRPL15	33.4	11	51	0.01	0.28	0.13	0.42	9.2E-05	5.8E-02	7.4E-03	2.3E-01
RPL8	28	10	42	0.15	0.29	0.85	0.84	9.2E-02	3.4E-01	1.0E+00	1.0E+00
*SYF2	28.7	8	36	0.23	0.20	0.36	0.52	3.9E-04	2.5E-04	2.9E-03	2.8E-02
MRPL46	31.7	7	36	0.33	0.31	0.13	0.96	7.4E-02	6.2E-02	4.5E-03	1.0E+00
*BCDIN3D	33.2	7	32	0.21	0.42	0.17	0.68	8.5E-03	1.1E-01	4.4E-03	7.0E-01
CCDC59	28.7	7	30	0.01	0.01	0.14	0.01	6.9E-05		1.7E-03	
*SRSF7	27.4	7	30	0.06	0.14	0.08	0.55	3.4E-04	3.2E-03	6.9E-04	3.5E-01
RPS2	31.3	6	28	0.86	0.75	0.66	0.78	9.9E-01	9.1E-01	7.2E-01	9.4E-01
RCN1	38.9	7	24	0.72	0.94	0.57	0.90	9.8E-01	1.0E+00	8.7E-01	1.0E+00

Table S8 Protein hits identified by mass spectrometry (continued from previous page). This table provides data for 14 proteins that met the filtering criteria described below. Proteins are sorted based on highest to lowest percent coverage. The proteins of particular interest are denoted with an asterisk. Although we excised proteins from a narrow window of the gel, mass spectrometry yielded proteins with a wide range of molecular weights. This could be due to pieces of degraded proteins that migrated quickly through the gel, peptides that align to multiple proteins, or proteins that are particularly sticky and do not wash off the column between runs. Thus, for data filtration, we first excluded protein hits based on size. For the lower band, 394 proteins were identified by mass spectrometry that have a molecular weight appropriate for the excised piece of gel (between 20 and 40 kDa). We further narrowed down this list by calculating the abundance ratio of each protein in the scrambled or non-targeting control ASO sample relative to the 5'UTR ASO sample. Only 22 of the 394 proteins had an abundance ratio less than one across all comparisons, indicating preferential binding to the 5'UTR ASO. Of these, only 14 had more than five peptides per protein. A subset of these proteins is of particular interest (denoted with an asterisk) based on their abundance ratios, the number of peptides that map to the protein, and their molecular function(s). ALYREF is in a different color because it did not meet the filtering criteria (it has one abundance ratio greater than 1, denoted by #). It was appended to this table due to the congruency between its biological function and that of our 5'UTR ASO.

Table S9 Summary of RNA-seq data filtering. For each sample, there were 3.5 to 4.3 million total surviving read pairs after adaptor clipping and quality trimming. After reference mapping of those reads, the data were filtered as summarized in this table.

Total number of annotated genes:	**20,455**	
Total number of genes after removal of small RNAs	**20,342**	
Number of "expressed genes" (all samples in ≥ 1 group have a cross sample normalized TPM ≥ 2.5):	**7,204**	
Genes with 1.5 < fold change < -1.5:	**1706**	**934 up**
		772 down
Genes with 1.5 < fold change < -1.5 and p-value < 0.05:	**1529**	**830 up**
		699 down

Table S10 Top 5 canonical pathways predicted by Ingenuity Pathway Analysis to be affected by 5'UTR ASO treatment. Differentially expressed genes between samples treated with the 5'UTR ASO and NTC ASO are enriched in the following pathways. The ratio column provides the number of genes with differential expression in our dataset out of the total number of genes in that pathway. The last column lists the 5 most up-regulated (green) and 5 most down-regulated (red) differentially expressed genes in that pathway. The highlighted pathways are discussed in the text.

Pathways	p-value	Ratio	Differentially expressed genes in pathway
Hepatic fibrosis / hepatic stellate cell activation	1.95×10^{-7}	32 / 186	IL6, IGF2, CXCL8, MMP9, ICAM1, PDGFRA, IGFBP3, COL1A2, COL3A1, IGFBP5
Hepatic fibrosis signaling pathway	2.40×10^{-7}	50 / 368	SPP1, CXCL8, ICAM1, NFKBIE, RAC3, PIK3R2, PDGFRA, COL1A2, PDCD4, COL3A1
Virus entry via endocytic pathways	7.08×10^{-7}	22 / 107	ACTC1, RAC3, ACTA2, HLA-B, TFRC, PIK3R2, RALA, AP1S1, RRAS, ITGA6
Glucocorticoid receptor signaling	1.41×10^{-6}	45 / 336	KRT18, IL6, CXCL8, ICAM1, MAP3K14, POLR2J2, PIK3R2, TAF10, RALA, SERPINE1
NRF2-mediated oxidative stress response	2.63×10^{-6}	30 / 189	ACTC1, EPHX1, MAFF, TXNRD1, ACTA2, PIK3R2, DNAJB4, RALA, RRAS, ATF4

Table S11 iPSC lines used in Figure 3.4.

iPSC line name	Gender	Age at biopsy	Reprogramming method	Genotype	Disease
SMA A4	F	109 days	STEMCCA Lentivirus Reprogramming	Homozygous *SMN1* deletion, 2 copies *SMN2*	SMA Type 1
RS 1.2	M	74 days	STEMCCA Lentivirus Reprogramming		Age-matched control
IPS-OXSMA-03 (Clone 03 03)	M	49 years	CytoTune Sendai Reprogramming	Homozygous *SMN1* deletion, 3 copies *SMN2*	SMA Type 2
IPS-OXSMA-02 (Clone 02 04)	M	30 years	CytoTune Sendai Reprogramming	Homozygous *SMN1* deletion, 4 copies *SMN2*	SMA Type 3
OX1 (Clone 841-03-01)	M	36 years	CytoTune Sendai Reprogramming		Age-matched control